Oxidation of hemoglobin in the lung parenchyma facilitates the differentiation of pneumococci into encapsulated bacteria

Babek Alibayov[1], Anna Scasny[1], Ana G. Jop Vidal[1] Landon Murin[1], Sandy Wong[1, 2], Kristin S. Edwards[3], Zehava Eichembaun[4], Tracy Punshon[5], Brian P. Jackson[5], Marie-T. Hopp[6,7], Larry S. McDaniel[1,2], Brian J. Akerley[1,2], Diana Imhof[6], and Jorge E. Vidal[1,2,#],

[1]Department of Cell and Molecular Biology, [2]Center for Immunology and Microbial Research, [3]Department of Pharmacology and Toxicology, School of Medicine, University of Mississippi Medical Center, Jackson, MS. [4]Department of Biology, Georgia State University, Atlanta GA. [5]Dartmouth College, Hanover New Hampshire. [6]Pharmaceutical Biochemistry and Bioanalytics, Pharmaceutical Institute, University of Bonn, D-53121 Bonn, Germany. [7]Department of Chemistry, Institute for Integrated Natural Sciences, University of Koblenz, D-56070 Koblenz, Germany.

Running title: Differentiation of Spn in the lung parenchyma

#Address correspondence to:

Jorge E. Vidal, PhD

2500 North State Street, Jackson Mississippi 39216

Phone: (601) 984-1711, Fax: (601) 984-1708

Email jvidal@umc.edu,

Summary

Pneumococcal pneumonia causes cytotoxicity in the lung parenchyma but the underlying mechanism involves multiple factors contributing to cell death. Here, we discovered that hydrogen peroxide produced by *Streptococcus pneumoniae* (Spn-H_2O_2) plays a pivotal role by oxidizing hemoglobin, leading to its polymerization and subsequent release of labile heme. At physiologically relevant levels, heme selected a population of encapsulated pneumococci. In the absence of capsule and Spn-H_2O_2, host intracellular heme exhibited toxicity towards pneumococci, thus acting as an antibacterial mechanism. Further investigation revealed that heme-mediated toxicity required the ABC transporter GlnPQ. *In vivo* experiments demonstrated that pneumococci release H_2O_2 to cause cytotoxicity in bronchi and alveoli through the non-proteolytic degradation of intracellular proteins such as actin, tubulin and GAPDH. Overall, our findings uncover a mechanism of lung toxicity mediated by oxidative stress that favor the growth of encapsulated pneumococci suggesting a therapeutic potential by targeting oxidative reactions.

39 **Highlights**

40

41 - Oxidation of hemoglobin by *Streptococcus pneumoniae* facilitates differentiation to
42 encapsulated pneumococci *in vivo*
43 - Differentiated *S. pneumoniae* produces capsule and hydrogen peroxide (Spn-H_2O_2) as
44 defense mechanism against host heme-mediated toxicity.
45 - Spn-H_2O_2-induced lung toxicity causes the oxidation and non-proteolytic degradation of
46 intracellular proteins tubulin, actin, and GAPDH.
47 - The ABC transporter GlnPQ is a heme-binding complex that makes Spn susceptible to heme
48 toxicity.

49

50 **Graphical abstract**

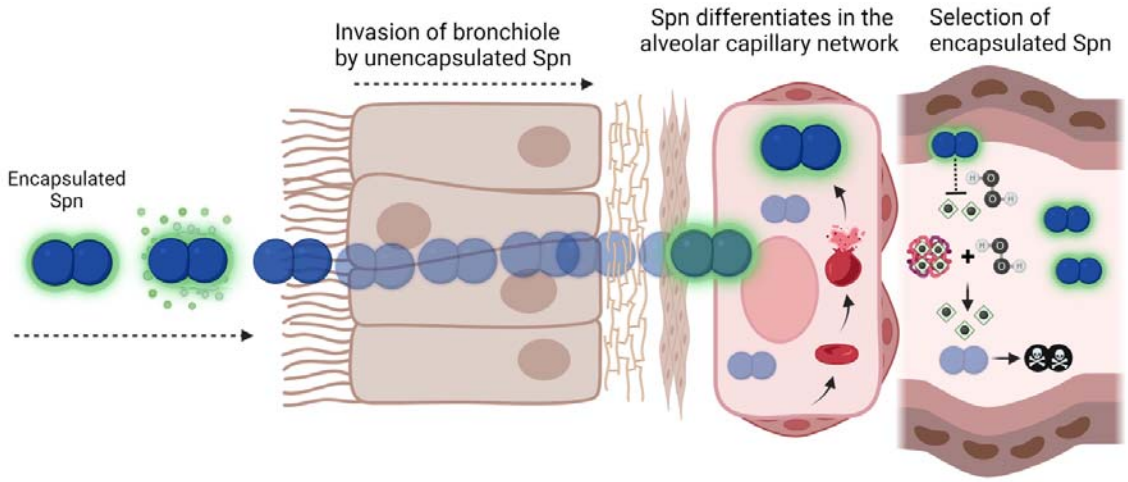

51

52

53

54

55

56

57

58

59

60

61

62

63

64

65

66 **Introduction**

67 *Streptococcus pneumoniae* (Spn) strains colonize the lungs causing pneumonia, a global
68 disease that kills more than a million individuals every year.[1] Pneumococcal pneumonia is an acute
69 bacterial infection of the pulmonary parenchyma and can lead to subsequent invasion of
70 pneumococci into the respiratory epithelium. [2,3] Invasion of bronchi and terminal bronchiole allows
71 pneumococci to reach respiratory bronchiole, alveolar ducts, and alveoli, where pneumococci have
72 access to the alveolar-capillary network, a large surface area containing ~300 billion of capillaries
73 and where the exchange of CO_2 by O_2 occurs. Once Spn gains access to the alveolus and causes
74 cytotoxicity, Spn may then migrate to the bloodstream to cause bacteremia and meningitis.[2]

75 Spn strains include more than 100 capsular types, the most prevalent of which are the
76 targets of pneumococcal vaccines that have saved millions since their licensure.[4] The capsular
77 polysaccharide is negatively charged and allows pneumococci to colonize the lungs by evading
78 entrapment by mucus secreted in the lumen of bronchi and terminal bronchioles.[2] The capsule is
79 also anti-phagocytic by blocking complement deposition and enhances intracellular survival in
80 cardiovascular endothelial cells.[2,5-7]

81 The synthesis of the pneumococcal capsule is linked to the glycolytic pathway.[8,9] Spn has a
82 fermentative metabolism to produce energy oxidizing glucose, in the presence of molecular oxygen
83 (O_2), to ultimately produce ATP. This metabolic pathway includes the oxidation of pyruvate by the
84 enzyme pyruvate oxidase (SpxB), releasing H_2O_2 as a byproduct.[10-12] In the absence of O_2, pyruvate is
85 converted to L-lactate, while in its presence, L-lactate is converted back to pyruvate, via lactate
86 oxidase (LctO) in a reaction which byproduct is also H_2O_2.[10,11] In cultures of Spn grown under a
87 mixture of gases with ~20% atmospheric O_2 (~150 mm Hg) and ~5% CO_2, nearly 85% of the pool of

88 H_2O_2 (Spn-H_2O_2) released occurs through the reaction catalyzed by SpxB whereas the remaining
89 ~15% is attributed to LctO.[13,14]

90 Besides components of the glycolytic pathway and atmospheric O_2, the alveolar-capillary
91 network is a source of erythrocytes and hemoglobin. We recently demonstrated that hemoglobin
92 enhances *in vitro* growth of Spn strains and upregulates expression of the *spxB* gene and genes
93 encoding the capsule locus.[15,16] Moreover, another recent study demonstrated that H_2O_2 produced
94 by the pneumococcus oxidizes oxy-hemoglobin (Fe^{2+}) from different mammals, including humans, to
95 produce the non-oxygen-binding form of hemoglobin known as met-hemoglobin (Fe^{3+}).[17,18] The
96 oxidation of hemoglobin by Spn produced potent oxidants, including labile heme[19] and a
97 hemoglobin-derived side chain tyrosyl radical.[20] These toxic products are important in the
98 pathophysiology of human diseases that are accompanied by intravascular hemolysis, such as sickle
99 cell disease (SCD), and in inflammatory conditions, such as sepsis.[21-23] In children with SCD,
100 hemoglobin (Hb)S is oxidized to met-hemoglobin resulting in an acute hemolytic vascular
101 inflammatory process inducing the polymerization of hemoglobin, and consequently acute lung
102 injury.[23,24] The oxidation of hemoglobin results in highly oxidizing ferryl hemoglobin ($^{\bullet}$Hb-Fe^{4+}), met-
103 hemoglobin (Hb-Fe^{3+}) and the release of toxic heme that disrupted the mitochondrial membrane
104 potential of lung epithelial cells and endothelial cells.[25,26]

105 To the best of our knowledge, oxidative reactions catalyzed by Spn-H_2O_2 and hemoglobin
106 have not been associated with the pathophysiology of pneumococcal pneumonia. Recent evidence
107 indicate that oxidation of hemoglobin does occur. Firstly, patients with acute bacterial respiratory
108 distress syndrome (ARDS) have elevated levels of cell-free hemoglobin in the lungs that correlates
109 with alveolar-capillary barrier dysfunction.[27] Secondly, a mouse model of pneumococcal pneumonia

110 demonstrated that Spn damages the alveolar-capillary barrier, thereby facilitating the translocation
111 of blood and fluids into the alveolar space.[28] Finally, the alveolar-capillary barrier dysfunction was
112 recapitulated in a mouse model of ARDS by intratracheal delivery of extracellular hemoglobin or
113 heme.[27]

114 In this study, we demonstrate that Spn-H_2O_2 oxidizes hemoglobin leading to the
115 differentiation of encapsulated pneumococci in the alveoli which allows for survival against heme-
116 mediated toxicity. We further show that both Spn-H_2O_2 and the capsule act synergistically to protect
117 pneumococci from heme toxicity. These results suggest that heme-mediated toxicity in
118 pneumococcal pneumonia targets encapsulated pneumococci and perhaps other encapsulated
119 bacteria for survival during infection.

120

121 **Results**

122 ***Streptococcus pneumoniae*-H_2O_2 reacts with heme from hemoglobin causing its degradation.** Since
123 heme degradation can occur by nonselective destruction of the double bonds in its protoporphyrin
124 IX ring caused by reactive oxygen species (Fig. 1A)[29-31], we investigated whether Spn-H_2O_2 released
125 in the supernatant degrades heme. Spn strains released into the supernatant >650 µM of H_2O_2 at 6
126 h post-inoculation in THY (Fig. 1B, and Fig. S1A). Isogenic Δ*spxB*Δ*lctO* mutant derivatives did not
127 produce detectable levels of H_2O_2 (Fig. 1B and Fig. S1A). THY-Hb^{3+} was then inoculated with TIGR4,
128 D39, EF3030, or their isogenic H_2O_2-defective strain, Δ*spxB*Δ*lctO*. Subsequently, we analyzed heme
129 levels in the supernatants using an in-gel heme staining approach (Fig. S1B), and a Quantichrom
130 assay. [32,33] A median concentration of 27.13 µM labile heme and heme-bound hemoglobin (total
131 heme) was observed in uninfected THY-Hb^{3+} containing 10 µM of Hb^{3+} (Fig. 1C, and 1D). Heme could

132 not be detected (Fig. 1C, Fig. S1C) or was significantly lower (Fig. 1D, and 1E) in cultures of TIGR4,
133 D39 or EF3030, incubated for up to 6 h. In contrast, THY-Hb^{3+} cultures of TIGR4Δ*spxB*Δ*lctO,*
134 D39Δ*spxB*Δ*lctO*, or EF3030Δ*spxB*Δ*lctO* yielded 16.82 µM, 19.76 µM, or 19.78 µM of total heme at 6
135 h post-inoculation, respectively (Fig. 1D and 1E). We demonstrated peroxidase activity of Fe^{3+}-heme
136 as Spn-H_2O_2 was not detected 2 or 4 h post-inoculation of THY+Hb-Fe^{3+} cultures (Fig. 1F). As a result,
137 H_2O_2 produced in Spn cultures oxidized hemoglobin leading to the subsequent degradation of both,
138 labile and heme-bound hemoglobin.

139 The treatment of hemoglobin A_0 (HbA_0) with hydrogen peroxide has resulted in the
140 crosslinking of globins.[34,35] To explore whether the non-rate limiting Spn-H_2O_2 produced in
141 supernatants causes the aggregation of globins, we conducted Western blot analysis. Notably, using
142 either a polyclonal anti-hemoglobin antibody, a monoclonal anti-alpha or anti-beta chain antibody
143 (Fig. S1D), we found that α globin, and β globin, were absent in THY-Hb^{3+} cultures containing 10 µM
144 hemoglobin (Fig. 1G) when oxidation had occurred (Fig. S1E) or cultures with 20 µM hemoglobin
145 (Fig. S1D). In THY-Hb^{3+} cultures of H_2O_2-deficient mutants, however, hemoglobin monomers and
146 dimers were detected at similar level as that in the uninfected control (Fig. 1G, 1H, and S1D). The
147 aggregation of globins was visually evident.

148 Structural changes, such as amino acid oxidation, have been reported in the reaction of H_2O_2
149 with HbA_0, including oxidation of β-globin methionine 55 to methionine sulfoxide (MetO), and other
150 non-heme containing proteins.[35-37] We conducted untargeted metabolomics to analyze the primary
151 metabolism of molecules released, or produced by pneumococci, during the oxidation of
152 hemoglobin. TIGR4 or TIGR4Δ*spxB*Δ*lctO*, was cultured for two h in THY or in THY-Hb^{3+} and
153 supernatants harvested from these conditions were analyzed. Partial least squares discrimination

154 analysis (PLSDA) demonstrated that the groups were separable (Fig. 1J). Area under the curve (AUC)
155 analysis revealed that metabolites in THY-Hb^{3+} culture supernatants of TIGR4 producing H_2O_2 were
156 the most biologically different (component 2=10%; AUC=0.9542) (Fig. 1K). An overview of
157 differentiated metabolites at minimum 2-fold change and FDR $p<0.05$ is displayed in the heatmap
158 (Fig. 1I). A clear distinction of metabolites was obtained when Spn-H_2O_2 was present (Fig. 1I and
159 Table S1). Metabolites that increased in the supernatant where hemoglobin oxidation occurred
160 included creatinine, isoleucine, leucine, tyrosine, and tyrosyl, whereas those whose concentration
161 decreased were aspartic acid, guanine, and oxoproline (Table S1). Creatinine levels increased in
162 cultures containing hemoglobin with both H_2O_2-producing and H_2O_2-deficient pneumococci.
163 Metabolites that increased due to the presence of H_2O_2 included typical oxidative stress markers,[38]
164 such as MetO, oleamide, and putrescine. Metabolites that were downregulated included
165 methionine, oxidized to MetO[38], and pyruvic acid, the substrate of SpxB (Table S1). Therefore, the
166 oxidation of hemoglobin by Spn-H_2O_2 has a significant impact on the primary metabolism.
167
168 **Incubation of *S. pneumoniae* with hemoglobin produces thick pneumococcal aggregates and**
169 **selects for encapsulated pneumococci.** We demonstrated that hemoglobin induces formation of
170 Spn biofilms.[15,16] We next investigated if hemoglobin localizes on pneumococci. To assess this, Spn
171 was inoculated in THY-Hb^{3+} and the capsule, hemoglobin and the DNA were stained and analyzed by
172 confocal microscopy.
173 A projection of z-stacks and their three-dimensional (3D) reconstruction, revealed
174 hemoglobin-positive Spn bacteria (Spn-Hb^+) as soon as 2 h post-inoculation; Spn-Hb^+ increased in
175 abundance over time (Fig. 2A, Fig. S2A, S2B, and Video S1). Notably, the majority of Spn-Hb^+

176 bacteria did not stain with DAPI. A second population of pneumococci, those expressing capsule,
177 and that stained with DAPI was observed (Fig. 2A, left panels, arrows). In these encapsulated
178 pneumococci, the capsule signal began to fade 4 h post-inoculation (Fig. 2A, middle panels, arrows).
179 After 6 h of incubation, the capsule had already been replaced by signal of hemoglobin in individual
180 pneumococcal cells (Fig. 2A, right panel, arrows; Fig. S2B). Structures that resemble polymers of
181 hemoglobin were observed in Spn cultures (Fig. S2C and S2D, arrows) particularly after a gentle
182 washed (Fig. 2H, Fig. S3A). Hemoglobin signal was specific since Spn-Hb^{+} pneumococci were absent
183 in preparations where the anti-hemoglobin antibody was omitted (Fig. S2E). Planktonic
184 pneumococci incubated for 6 h in THY-Hb^{3+} showed a similar population of Spn-Hb^{+} bacteria and
185 encapsulated pneumococci (Fig. 2B and Fig. S2F).

186 Spn-Hb^{+} bacteria were also observed in preparations stained with monoclonal antibodies,
187 either with an anti-alpha chain hemoglobin (Fig. 2C, 2D and 2F) or an anti-beta chain hemoglobin
188 (Fig. S2G). To confirm that Spn-Hb^{+} had lost DNA, we performed colocalization studies between Spn-
189 Hb^{+} and the DNA stained with Toto-1. A Pearson's correlation coefficient <0.268 confirmed limited
190 co-localization indicating these Spn-Hb^{+} pneumococci had lost their DNA (Fig. S2G). XY and XZ optical
191 sections and 3D reconstructions of z-stacks of these preparations revealed a dome of pneumococci
192 of ~3 µm thick lacking Spn-Hb^{+} bacteria [Figs. 2C (arrow), 2D (arrow), 2F, Fig. S2H, and Video S2].
193 Quantitative analysis of the fluorescence intensity confirmed that the bacterial dome contained
194 significantly more live pneumococci (i.e., stained with Toto-1) than Spn-Hb^{+} bacteria (Fig. 2E, and
195 Fig. S2I). Middle optical sections of the biofilm structure contained a mixture of both Spn-Hb^{+} and
196 live pneumococci, although the population of Spn-Hb^{+} bacteria was significantly more abundant (Fig.
197 S2H and Fig. S2I).

198

199 **H_2O_2-mediated oxidation of hemoglobin facilitates the selection of encapsulated pneumococci.**
200 Since selection of Spn-Hb$^+$ bacteria and encapsulated pneumococci occurs concurrently with
201 oxidation of hemoglobin, we investigated if its oxidation contributes to these phenotypes. To assess
202 this, we compared THY-Hb^3 cultures of Δ*spxB*Δ*lctO* mutants against their H_2O_2-producing
203 counterparts. The capsule, hemoglobin, and the DNA were stained and analyzed by confocal
204 microscopy and the density was investigated. In experiments inoculated with H_2O_2-deficient
205 Δ*spxB*Δ*lctO* strains we observed a significant decrease in both Spn-Hb$^+$ bacteria and encapsulated
206 pneumococci (Fig. 2H and not shown). Planktonic Δ*spxB*Δ*lctO* harvested from these cultures
207 showed a reduced population of Δ*spxB*Δ*lctO*-Hb$^+$ pneumococci (Fig. 2I, and S3B, yellow arrows) and
208 an increased population of bacteria with a DAPI signal (Fig. 2I, and S3B, white arrows).

209 Hemoglobin polymers resembling net-like structures (Fig. 2J, white arrows), Spn-Hb$^+$ bacteria
210 (Fig. 2J, yellow arrows) and encapsulated pneumococci (Fig. 2J, encircled) were also observed when
211 TIGR4 or EF3030 (Fig. S3C) were inoculated into cultures of human alveolar A549 cells and incubated
212 with DMEM-Hb^{3+} for 6 h. Hemoglobin was oxidized (Fig. 2K), and H_2O_2 was produced in DMEM- Hb^{3+}
213 cultures (Fig. S3D). Overall, the ultra-structure of these biofilms includes Spn-Hb$^+$ bacteria,
214 hemoglobin polymers embedded into aggregates of live pneumococci and Spn-Hb$^+$ bacteria of ~12
215 µm, and encapsulated pneumococci protruding out from the biofilm matrix (Fig. S2J).

216

217 **Heme released by the oxidation of hemoglobin causes intoxication in Spn-Hb$^+$ pneumococci.** We
218 then investigated the mechanism that intoxicates Spn-Hb$^+$ bacteria. We first compared the density
219 of pneumococci when incubated with or without hemoglobin. Cultures of Spn strains that lack

220 production of H_2O_2 have a fitness advantage compared with the WT strain[39-41] and as such in the
221 absence of hemoglobin the density of Spn WT was significantly lower than that of their
222 corresponding Δ*spxB*Δ*lctO* strain (Fig. 2O). In contrast to the differences in biofilm ultrastructure,
223 when incubated in THY-Hb^{3+}, the density of Spn WT strains and their corresponding Δ*spxB*Δ*lctO*
224 mutant was similar (Fig. 2P and no shown).

225 We reason that if heme is released during hemoglobin oxidation this can be toxic for
226 pneumococci. [42,43] We therefore conducted Western blot analysis of the peptidoglycan and cytosol
227 purified from THY-Hb^{3+} cultures of Spn and assessed for the presence of hemoglobin, or heme.
228 Neither hemoglobin monomers nor dimers were observed in peptidoglycan, or cytosolic,
229 preparations of TIGR4 or TIGR4Ω*spxB-lctO*, but they were present in those fractions purified from
230 cultures of TIGR4Δ*spxB*Δ*lctO* (Fig. 2L and Fig. S3E). The loading control PfbA, a ~67 kDa protein
231 anchored on the cell surface[44], or cytosolic signal of Ply, were observed in the corresponding
232 fractions (Fig. 2L and Fig. S3E). Heme was also quantified in the peptidoglycan. Heme signal in the
233 peptidoglycan of all Spn strains was detected although that in the peptidoglycan of
234 TIGR4Δ*spxB*Δ*lctO* was significantly higher than that of in the peptidoglycan of H_2O_2-producing Spn
235 strains (Fig. 2N). Thus, heme released during hemoglobin oxidation is located in the cell wall of H_2O_2-
236 producing Spn strains.

237 Because H_2O_2 is secreted and hemoglobin oxidation occurs in the extracellular milieu, we
238 reasoned that inoculating Spn in the top compartment of a transwell system device with a ~0.4 μm
239 membrane (Fig. 2Q), added with THY-Hb^{3+}, may intoxicate pneumococci. These intoxicated
240 pneumococci could then pass through the transwell membrane. A coverslip installed at the bottom,

241 and planktonic bacteria in the top compartment were collected, fixed, stained with fluorescence and
242 analyzed by confocal microscopy.

243 A middle XY and YZ confocal optical section and the projection of z-stacks of planktonic
244 TIGR4 pneumococci showed both encapsulated pneumococci (Fig. 2R, white arrows) and Spn-Hb^+
245 bacteria (Fig. 2R, yellow arrows). Notably, polymerized hemoglobin was produced and detected
246 both on the bottom substrate (Fig. 2S, left panel) and attached to Spn-Hb^+ bacteria (Fig. 2S, middle
247 panel). Spn-Hb^+ bacteria, but no encapsulated pneumococci, were observed in the bottom of the
248 well confirming that intoxicated pneumococci were able to traverse the ~0.4 µm transwell
249 membrane (Fig. 2S, right panel). Neither polymerized Hb nor Spn-Hb^+ like-bacteria were observed in
250 the bottom of transwell experiments inoculated with TIGR4Δ*spxB*Δ*lctO* or D39Δ*spxB*Δ*lctO* (not
251 shown).

252

253 **Both H_2O_2 and the capsule protect pneumococci from heme toxicity.** We next investigated heme
254 susceptibility of Spn strains. Dose-response studies found that the minimum bactericidal
255 concentration (MBC) of heme that killed 99.97% of TIGR4 bacteria, compared with untreated
256 control, was 10 µM (Fig. 3A and Fig. S4A), whereas the MBC for D39 (Fig. 3E) and EF3030 was 15 µM
257 (Fig. 3G). Culture supernatants were harvested, sterilized, and used for spectroscopic analysis which
258 showed significant degradation of heme when TIGR4 survived a challenge with 5 µM or 7.5 µM
259 heme (Fig. 3C, and Fig. S4C) whereas an intact heme peak was observed in supernatants collected
260 from a lethal challenge with 12.5 µM heme (Fig. 3D). These findings suggested that pneumococci are
261 resistant to levels of heme above the concentration of labile heme in plasma or the lungs ~0.2 µM[45-
262 47] and that Spn-H_2O_2 protects pneumococci from heme toxicity.

263 To directly assess this above, we performed heme-susceptibility studies in cultures lacking
264 H_2O_2 by either challenging Δ*spxB*Δ*lctO* strains with heme or treating WT pneumococci with catalase
265 and heme. Remarkably, the MBC of heme for TIGR4Δ*spxB*Δ*lctO* was 1.25 µM (Fig. 3B and Fig. S4B),
266 and that of D39Δ*spxB*Δ*lctO* was 2.5 µM (Fig. 3F). A microplate assay incubated for 24 h resulted in a
267 >3-fold lower minimum inhibitory concentration (MIC) for Spn strains lacking H_2O_2 compared with
268 the corresponding WT strain, including another reference strain, EF3030 (Fig. 3G, Table S2).
269 Spectroscopy analysis showed an intact heme curve in supernatants from heme-challenged
270 TIGR4Δ*spxB*Δ*lctO* (Fig. 3C). We next treated TIGR4 with catalase and this treatment rendered
271 encapsulated pneumococci susceptible to 5.0 µM heme (Fig. 3J).
272 Besides lacking H_2O_2 production, TIGR4Δ*spxB*Δ*lctO* has a defect for capsule production[9]. We
273 therefore conducted experiments to investigate whether the capsule and H_2O_2 confer synergistic
274 protection against heme toxicity. To address this, a TIGR4 capsule knockout strain (TIGR4Δ*cps*), or a
275 D39-derivative capsule mutant, R6, were challenged with heme. Unlike the WT strains, which had an
276 MBC>10 µM, the MBC of heme for TIGR4Δ*cps* and R6 was 5 µM (Fig. 3K and 3L). TIGR4Δ*cps* and R6
277 produce WT levels of H_2O_2 (Fig. 1B and Fig. S1A). We then challenged TIGR4Δ*cps* or R6 with heme
278 and H_2O_2 in these cultures was scavenged with catalase. The treatment with catalase significantly
279 reduced the MBC of TIGR4Δ*cps* or R6 to 1.25 µM or 0.625 µM heme, respectively (Fig. 3K and Fig.
280 3L). To study heme toxicity at the structural level by confocal microscopy, we prepared a TIGR4Δ*cps*
281 expressing GFP (TIGR4Δ*cps*^{GFP}). When these TIGR4Δ*cps*^{GFP} bacteria were exposed to 1.25 µM heme,
282 and subsequently treated with catalase, our confocal micrographs revealed that they were sparsely
283 distributed (Fig. 3M, white arrows). Additionally, we observed a loss of DNA staining, which was
284 replaced by a signal from hemoglobin when we stained the bacteria with the anti-hemoglobin

285 polyclonal antibody (Fig. 3M). Altogether, these *in vitro* experiments demonstrated that Spn strains
286 are protected by both the capsule and H_2O_2 against heme (Fig. 3N, top panel) because the lack of
287 either increased heme susceptibility (Fig. 3N, middle panel). Additionally, the absence of both
288 capsule and H_2O_2 resulted in heme susceptibility at heme levels below 1.5 µM (Fig. 3N, bottom
289 panel).
290
291 **H_2O_2 contributes to toxicity and histopathological damage in the lung.** To evaluate the contribution
292 of H_2O_2-mediated oxidation of hemoglobin to pneumococcal disease, we utilized a mouse model of
293 pneumococcal pneumonia. The mouse model mimics the aspiration of Spn into the lower airways,
294 facilitating colonization in bronchi, bronchioles, and/or alveoli (Fig. 4A). Balb/c mice (N=8 per group)
295 were intranasally infected with an inoculum containing ~10^7 cfu of TIGR4, TIGR4Δ*spxB*Δ*lctO*,
296 TIGR4Ω*spxB-lctO*, D39 or D39Δ*spxB*Δ*lctO*. Two additional groups of Balb/c mice were infected with
297 ~10^8, or ~10^9 cfu of TIGR4Δ*spxB*Δ*lctO*. Since the capsule protects Spn from the innate immune
298 response[2,5-7], we quantified encapsulated bacteria in the inoculum before infecting mice. Confocal
299 micrographs of TIGR4, TIGR4Ω*spxB-lctO*, D39 and D39Δ*spxB*Δ*lctO* showed abundant encapsulated
300 (CPS^+) bacteria, whereas capsule signal in TIGR4Δ*spxB*Δ*lctO* bacteria and that from a
301 nonencapsulated TIGR4Δ*cps* control, was limited (Fig. 4B). We then quantified pneumococci that
302 expressed capsule from these micrographs (i.e., $DAPI^+/CPS^+$). Most TIGR4, TIGR4Ω*spxB-lctO,* D39,
303 and D39Δ*spxB*Δ*lctO* pneumococci (>84.1%) were encapsulated whereas the population of
304 encapsulated TIGR4Δ*spxB*Δ*lctO* was significantly lower ($p<0.001$), compared to TIGR4, at 28.8% (Fig.
305 4C). Thus, mutation of *spxB* and *lctO* only affected production of capsule in TIGR4 but not in D39.

306 We then proceeded to investigate mouse mortality. Mice infected with TIGR4, TIGR4Ω*spxB-*
307 *lctO* or D39 succumbed within 96 h post infection (Fig. 4D and Fig. S5A). Remarkably, mice infected
308 with either ~10^7, ~10^8, or ~10^9 cfu of TIGR4Δ*spxB*Δ*lctO* survived 96 h post-infection, while 30% of
309 those infected with D39Δ*spxB*Δ*lctO* survived (Fig. 4D, not shown and Fig. S5A). We calculated the
310 rate of death and found that mice inoculated with D39 succumbed 3.5 times faster than those in the
311 D39Δ*spxB*Δ*lctO* group (Fig. S5A). We also monitored signs of stress and weight loss to evaluate the
312 severity of the infection. Animals infected with TIGR4, or TIGR4Ω*spxB-lctO*, showed ruffled fur, and
313 lethargy as soon as 24 h post-infection and had significantly lost 15.3%, or 18.78%, respectively, of
314 their body weight at the time of euthanasia (Fig. 4E). Mice infected with TIGR4Δ*spxB*Δ*lctO* presented
315 ruffled fur within 24 h, but they recovered a normal appearance within 48 h post-infection and had
316 only lost 1.51% of their body weight at the time of euthanasia (Fig. 4E).
317 Gross pathology of lungs from mice infected with TIGR4, or TIGR4Ω*spxB-lctO*, showed
318 hemorrhage with sub lobar focal lesions (Fig. 4F, arrowheads) while those from mice infected with
319 TIGR4Δ*spxB*Δ*lctO* appeared normal (Fig. 4F). Accordingly, colonization of lungs of mice infected with
320 TIGR4 reached a median density of 2.3×10^7 cfu/g, that of TIGR4Ω*spxB-lctO* was 1.4×10^8 cfu/g at the
321 time of the euthanasia (Fig. 4G), whereas pneumococci in mice infected with TIGR4Δ*spxB*Δ*lctO* had
322 been completely cleared from the lungs at 96 h post-infection (Fig. 4G). Mice had been transiently
323 colonized with TIGR4Δ*spxB*Δ*lctO* for 48 h post-infection, pneumococci were recovered from lungs at
324 a median density of 6.2×10^3 cfu/g (not shown). Pneumococci in the blood of mice infected with
325 TIGR4, or TIGR4Ω*spxB-lctO,* yielded a density of 3.4×10^6, or 2.8×10^6, cfu/ml, respectively with
326 abundant encapsulated pneumococci observed in fresh collected blood (Fig. 4H, Fig. S5D). In

327 contrast, pneumococci were not isolated from blood of those infected with TIGR4Δ*spxB*Δ*lctO* at 48
328 or 96 h post-infection (Fig. 4H and not shown).

329 To investigate if the rapid clearance of TIGR4Δ*spxB*Δ*lctO* from the lung was due to a
330 decreased adhesion, we infected *in vitro* cultured human (A549), or mouse (MLE-12), alveolar type I
331 pneumocytes with TIGR4 or TIGR4Δ*spxB*Δ*lctO* and investigated the density by culture and confocal
332 microscopy. The density of TIGR4 and TIGR4Δ*spxB*Δ*lctO* adhered to human or mouse alveolar
333 pneumocytes was similar (Fig. 4I and 4J) and strains were observed attached to pneumocytes by
334 confocal microscopy (Fig. 4K). Thus, the clearance of TIGR4Δ*spxB*Δ*lctO* from the mice lungs was not
335 due to an impaired adhesion to alveolar type I pneumocytes.

336 We then performed a histopathological assessment of the lungs of mice. Mice infected with
337 TIGR4, or D39, showed detachment of bronchiolar epithelium, indicating a cytotoxic event involving
338 the ciliated columnar pseudostratified epithelium [Fig. 4L, and Fig. S5B, Fig. S5C]. Alveoli of mcie
339 infected with TIGR4, or D39, were fibrotic with abundant erythrocytes and additional areas of
340 intracellular pneumococci within non-viable pneumocytes were observed (Fig. 4L, arrowhead and
341 Fig. S5B, Fig. S5C). The alveolar artery of the mice infected with TIGR4, or D39, showed abundant
342 endothelial cytotoxicity, associated with cytotoxicity of the alveoli surrounding the artery. In
343 contrast, the bronchioles of the uninfected mice and the mice infected with Δ*spxB*Δ*lctO* showed
344 normal bronchiolar epithelium (Fig. 4L and Fig. S5B, Fig. S5C). These bronchioles contained normal
345 smooth muscle (Figure 4L and Fig. S5B, Fig. S5C). TIGR4Δ*spxB*Δ*lctO* caused minimal acute
346 hemorrhage in the bronchiole, whereas D39Δ*spxB*Δ*lctO* caused areas with inflammatory infiltrate.
347 Alveoli of mice infected with TIGR4Δ*spxB*Δ*lctO* showed no fibrosis or cytotoxicity, and bacteria were
348 not identified, whereas D39Δ*spxB*Δ*lctO* caused alveolar fibrosis without cytotoxicity (Fig. 4L and Fig.

349 S5B, Fig. S5C). Histopathological scores demonstrated significant bronchiolar hypertrophy,
350 bronchiolar cellular exudate, and alveolar inflammatory cell infiltrate in lung of mice infected with
351 TIGR4, or TIGR4Ω*spxB-lctO*, compared to TIGR4Δ*spxB*Δ*lctO* (Fig. 4M). These findings show that
352 pneumococci producing Spn-H_2O_2 causes abundant cytotoxic damage in the lung parenchyma,
353 engaging all cellular types, including bronchial cells, alveolar cells, and endothelial cells of arteries
354 and veins.
355
356 **Oxidation of hemoglobin by Spn-H_2O_2 triggers capsule production in the lung**. To gain further
357 insight into the mechanisms of pathogenesis mediated by Spn-H_2O_2, lung sections of mice infected
358 with pneumococci were stained with fluorescence and analyzed by confocal microscopy. We
359 investigated the location of pneumococci in bronchioles, alveoli, and/or pulmonary arteries and
360 veins and the subcellular localization of bacteria. Notably, in the lumen of the respiratory bronchiole
361 of mice infected with TIGR4, or TIGR4Ω*spxB-lctO*, ~98% of pneumococci did not express the capsule
362 [Fig. 5A, 5C (l-CPS$^+$) and Fig. S6]. Moreover, 88.4% of pneumococci that had internalized into the
363 ciliated columnar respiratory epithelium of bronchi did not express capsule (Fig. 5A, 5C and Fig. S6).
364 Remarkably, encapsulated bacteria increased by 42.1% in pneumococci located inside bronchiole-
365 adjacent alveoli [Fig. 5A, arrows and 5C (a-CPS$^+$), Fig. S6]. When imaged in alveoli, 39.5%
366 pneumococci were encapsulated inside alveoli and only 12.1% encapsulated bacteria were observed
367 in the lumen [Fig. 5A and 5D (l-CPS$^+$)]. Presence of encapsulated pneumococci was at 27.3% when
368 bacteria had invaded the single squamous epithelium of pulmonary arteries and translocated to the
369 lumen of pulmonary arteries (Fig. 5A, 5E, and Fig. S6). In the lung of mice infected with D39,
370 encapsulated pneumococci were attached to bronchiole and in the alveolar epithelium but were

371 absent inside bronchiole (Fig. S7). Unlike mice infected with TIGR4, bacteria in the lumen of
372 bronchiole or alveoli could not be observed in lung specimens of mice infected with D39 (Fig. S7).

373 Regardless of colonization with encapsulated or nonencapsulated pneumococci, we
374 observed a rearrangement of N-acetyl-D-glucosamine(GlcNAc)- and Sialic acid-containing cell
375 membrane proteins in the bronchiole, alveoli, arteries, and veins. This rearrangement was
376 characterized by intracellular signal of WGA (Fig. 5A, 5B, and Fig. S6). In contrast, in lungs from
377 uninfected mice or mice infected with TIGR4Δ*spxB*Δ*lctO* the signal of choline-containing proteins
378 remained in the membrane (Fig. 5B). The rearrangement of GlcNAc- and sialic acid-containing cell
379 membrane proteins and the absence of nuclei in areas with abundant Spn colonization, indicate
380 cytotoxicity (Fig. 5A, and Fig. S6). TIGR4Δ*spxB*Δ*lctO* (i.e., $DAPI^+$ bacteria) were only observed in the
381 lumen of bronchiole (Fig. 5B), whereas D39Δ*spxB*Δ*lctO* (encapsulated) was localized arrested in foci
382 in bronchiole, inside the respiratory epithelium of bronchiole, in the lumen of alveoli, or inside
383 alveoli (Fig. S7, encircled).

384 High resolution laser ablation inductively coupled plasma time of flight mass spectrometry
385 (LA-ICP-TOFMS), performed on sections of lungs from infected mice, revealed a significant alteration
386 of Fe^+,Cu^+, Zn^+, Mn^+, Ca^+, Na^+, Mg^+, and K^+ in mice infected with TIGR4 or TIGR4Ω*spxB-lctO,*
387 compared to mice infected with TIGR4Δ*spxB*Δ*lctO* or the mock-infected control (Fig. 5H, Fig. S8A-G).
388 Higher concentrations of Fe^+ and Zn^+ were observed in animals infected with H_2O_2-producing
389 pneumococci, with Fe^+ localizing in areas of toxicity (Fig. S9A and S9C) whereas the increase of Zn^+
390 was observed around the pleura (Fig. S8B). While the infection had resolved in this mice, animals
391 infected with TIGR4Δ*spxB*Δ*lctO*, which produces pneumolysin, showed accumulation of iron (Fig. 5H,
392 arrow) in areas where abundant inflammatory infiltrate is observed (Fig. S9B). Compared with

393 uninfected control mice and those infected with TIGR4Δ*spxB*Δ*lctO*, levels of Cu^+, Mn^+, Ca^+, Na^+, Mg^+,
394 and K^+ were significantly reduced in the lungs of mice infected with H_2O_2-producing pneumococci.
395 Altogether, infection with Spn producing H_2O_2 causes an imbalance in the availability of important
396 bio-metals with an increase of iron in areas of abundant cytotoxicity.
397
398
399 **Increased reactive oxygen species and cytotoxicity in the lungs of mice infected with H_2O_2-**
400 **producing pneumococci.** Given that Spn-H_2O_2 contributes to lung cell toxicity we next investigated
401 its production *in vivo*. The H_2O_2 concentration in the lungs of uninfected mice and mice infected with
402 Δ*spxB*Δ*lctO* was significantly lower than that in the lungs of mice infected with TIGR4 (Fig. 5F). We
403 then modeled production of Spn-H_2O_2 in human alveolar A549 cells and quantified intracellular
404 reactive oxygen species (ROS). Signal of ROS per area of lung cells (1.14×10^4 μm^2) significantly
405 increased in alveolar cells infected with TIGR4, and in the control cells treated with menadione (100
406 μM)[48], compared with uninfected cells or those infected with Δ*spxB*Δ*lctO* (Fig. 5G, and Fig. S10A).
407 Middle optical confocal sections (xy, xz, and yz) revealed the presence of intracellular pneumococci
408 in human alveolar cells infected with either TIGR4 or Δ*spxB*Δ*lctO* further indicating that the increase
409 of ROS was in part due to release of H_2O_2 by intracellular pneumococci (Fig. S10B). Despite elevated
410 intracellular Spn-H_2O_2, gene expression studies did not reveal increased expression of antioxidant
411 response genes, including catalase, nuclear respiratory factor 1, and superoxide dismutase (Figs.
412 5M-O).
413 An increase of intracellular ROS results in the oxidation, and non-proteolytic degradation, of
414 tubulin, and this has been associated with heart failure[36,49]. We therefore performed Western blot

415 analysis of alveolar cells infected with pneumococci utilizing antibodies against β-tubulin, and other
416 cytosolic proteins such as catalase, β-actin, and GADPH. Signal of catalase, a cytosolic peroxidase,
417 remained intact after 16 h of incubation of human alveolar cells with TIGR4 or TIGR4Δ*spxB*Δ*lctO* (Fig.
418 5I). Remarkably, the levels of all other proteins decreased 16 h post-infection (Fig. 5I). Therefore,
419 catalase was used to normalize the levels of all other intracellular proteins. In alveolar cells infected
420 with TIGR4 16 h post-infection, signal of β-actin (Fig. 5J), β-tubulin (Fig. 5K) and GADPH (Fig. 5L)
421 significantly decreased compared with alveolar cells infected with the H_2O_2 deficient strain
422 TIGR4Δ*spxB*Δ*lctO* (Fig. 5I). Oxidation and non-proteolytic degradation of important cytoskeletal
423 proteins can lead to cell contraction. Consequently, both nuclei number and the area of the actin
424 cytoskeleton decreased in alveolar cells infected with TIGR4, compared to those infected with
425 Δ*spxB*Δ*lctO* (Fig. S10C and S10D).

426 Altogether, we demonstrated that Spn-H_2O_2 is produced *in vivo* by intracellular pneumococci
427 causes cytotoxicity by increasing ROS inside the cells, and causing oxidation and non-proteolytic
428 degradation of important cytoskeletal proteins.

429

430 **H_2O_2-induced polymerization of hemoglobin occurs *in vivo* in the lung.** We propose that *in vivo*
431 oxidation of hemoglobin favors the differentiation of Spn into encapsulated pneumococci.
432 Therefore, we investigated the oxidation of hemoglobin in the lungs of mice infected with
433 pneumococci. Abundant hemoglobin signal and erythrocytes were observed in bronchioles, and
434 alveoli from lung of mice infected with TIGR4 (Fig. 5P and Fig. S11). Polymerized hemoglobin, and
435 Spn-Hb^+ bacteria, were observed inside alveoli (Fig. 5P, Fig. S11), in the lumen of alveoli (Fig. 5P,
436 yellow arrows), and in the pulmonary artery (Fig. 5Q, yellow arrows, enlargement). Note that

437 neither the nuclei of type I and type II pneumocytes nor the nuclei of endothelial cells were
438 observed, confirming cytotoxicity. Spn-Hb$^+$ bacteria, non-encapsulated and encapsulated
439 pneumococci were present in alveoli and arteries (Fig. 5P and 5Q). Abundant leukocytes were
440 observed in both alveoli and arteries of mice infected with TIGR4 (Fig. 5P, and Fig. S11, arrowheads).
441 Notably, these leukocytes were characterized by hemoglobin on the membrane, and signal of both
442 encapsulated and non-encapsulated pneumococci, with some pneumococci found embedded within
443 polymerized hemoglobin (Fig. 5Q, enlargement, Fig. S11, and Video S3 and S4). In contrast, neither
444 non-encapsulated pneumococci nor Spn-Hb$^+$ bacteria were observed in bronchioles or alveoli of
445 mice infected with TIGR4Δ*spxB*Δ*lctO* although leukocytes were observed in the lumen of pulmonary
446 arteries (Fig. 5P). Erythrocytes were also observed in the alveoli of mice infected with
447 TIGR4Δ*spxB*Δ*lctO* but there was no signal of polymerized hemoglobin. Thus, *in vivo* oxidation of
448 hemoglobin causes its polymerization, creation of Spn-Hb$^+$ pneumococci, and triggers encapsulation
449 of Spn.
450
451 **Identification of a heme-binding protein involved in heme sensitivity.** To gain further insight into
452 the molecular mechanism of hemoglobin oxidation leading to selection of encapsulated
453 pneumococci and Spn-Hb$^+$ bacteria, we performed transposon insertion site sequencing analysis
454 using the High-throughput Insertion Tracking by Sequencing (HITS) method with a D39 transposon
455 mutant library. To identify genes involved in bacterial fitness during Hb-induced biofilm formation
456 we conducted pair-wise comparisons between each of two bacterial transposon mutant
457 populations, planktonic bacteria, or biofilms growing with or without Hb (10 µM). Both, planktonic
458 pneumococci and biofilm bacteria were separately analyzed, and genes required for fitness in each

459 condition are presented in Table S3. In general, genes encoding proteins located on, or with activity
460 in, the cell envelope (i.e., permeases of ABC transporters PiuC, AmiC, autolysins LytB, LytC or Pbp1A)
461 were essential to cope with the hostile environment of hemoglobin oxidation. In addition to those
462 genes, HITS identified insertions in the gene SPD_1098 (*glnP*), encoding the permease of an ABC
463 transporter (GlnPQ), that were enriched in D39 biofilms incubated with hemoglobin compared to
464 biofilms grown with no hemoglobin (Table S3). Because the oxidation of hemoglobin is toxic for
465 pneumococci but bacteria with a *glnP* mutation were enriched, we hypothesized that the SPD_1098
466 encoded product could be involved in heme-mediated toxicity. SPD_1098 is transcribed as an
467 operon including SPD_1099 (*glnQ*), the ATP binding cassette (ABC) (Fig. 6A).[50] GlnPQ has been
468 described as a glutamine, and/or glutamic acid transporter in pathogenic bacteria [51].

469 Since GlnPQ could function either as a heme transporter or a heme-binding protein, we
470 investigated the mechanism by which GlnPQ may be involved in hemoglobin-induced biofilms and
471 susceptibility to heme. To assess this, we constructed an insertional deletion in *glnP* within the
472 TIGR4 background resulting in TIGR4Δ*glnP*. Additionally, we complemented the *gnlP* in the
473 TIGR4Δ*glnP* to generate TIGR4Ω*glnP* (Fig. 6A). These TIGR4-derivative mutants grew at the same
474 rate of that of the WT within 6 h but, unlike the WT strain, TIGR4Δ*glnP* did not undergo autolysis
475 (Fig. 6B). We incubated TIGR4Δ*glnP* in THY-Hb^{3+} and investigated the density of biofilms. The density
476 of TIGR4Δ*glnP* was three orders of magnitude higher (median, $1.18x10^8$ cfu/ml) compared to that of
477 TIGR4 ($1.93x10^5$ cfu/ml) whereas biofilms of TIGR4Ω*glnP* significantly decreased ($1.24x10^6$ cfu/ml)
478 (Fig. 6C). Accordingly, confocal micrographs, and quantification of the fluorescence intensity of all
479 channels, of TIGR4Δ*glnP* grown in THY-Hb^{3+} showed an increased population of encapsulated
480 pneumococci and a decrease of Hb^+ bacteria compared to the same populations in biofilms of

481 TIGR4Ω*glnP* (Fig 6E and 6F). Oxidation of hemoglobin by TIGR4Δ*glnP* was similar to that caused by
482 TIGR4 after 2, 4 or 6 h of incubation (Fig. 6D), suggesting that the increase viability (i.e., density) of
483 TIGR4Δ*glnP* was due to a decrease susceptibility to heme toxicity.

484 We investigated the susceptibility of TIGR4Δ*glnP* to a sub-inhibitory concentration of heme
485 (10 µM) and compared the results to those obtained with TIGR4. Growth of TIGR4, or TIGR4Ω*glnP*,
486 was inhibited by ≥10 µM heme (Fig. 6G, Fig. S12A, and Fig. S12C), whereas TIGR4Δ*glnP* was resistant
487 to up to 20 µM heme (Fig. 6H and Fig. S12B). Because TIGR4Δ*glnP* did not show autolysis (Fig. 6B),
488 we assessed whether the absence of autolysis, rather than the absence of the GlnPQ transporter
489 rendered strain TIGR4Δ*glnP* resistant to heme. We therefore prepared a TIGR4Δ*lytA* mutant and
490 demonstrated that this autolysis defective mutant was similarly susceptible to heme as TIGR4 (Fig.
491 6G and Fig. S12D), indicating that heme resistance of TIGR4Δ*glnP* was not due to the loss of
492 autolysis.

493 Structural studies were then conducted to investigate binding of heme to GlnP. Several
494 earlier studies[52] demonstrated the suitability of protein-derived peptides as models for the
495 investigation of heme-binding motifs (HBMs). Predicted by the web application HeMoQuest (Paul
496 George et al., 2020), six GlnP-derived peptides (**1** – **6**) were synthesized in this study (Table S4) and
497 analyzed for their heme-binding potential by UV/vis spectroscopy. Heme binding was observed for
498 peptides **1** (TTKS**H**^{120}KISK), **3** (NQSK**Y**^{395}G**Y**^{397}KIKT), and **5** (SP**Y**^{547}KSLR) by a shift of the Soret band to
499 ~420 nm (Fig. 6I). The highest heme-binding affinities were determined for peptides **3** and **5** with K_D
500 values of 7.26 ± 2.34 µM and 3.59 ± 0.90 µM, respectively, displaying both motifs as promising,
501 moderate heme-binding sites. Peptide **1** exhibits only a very weak heme-binding affinity (K_D = 12.19
502 ± 1.18 µM), which renders this motif as rather unsuitable for heme binding on protein level. In

503 contrast, peptides **2**, **4**, and **6** did not bind heme and were therefore discarded as potential heme-
504 binding sites in the GlnPQ ABC transporter (Fig. S4).

505 To further confirm the heme-binding potential of the identified HBMs on protein level,
506 molecular docking studies were performed. In accordance with the experimental studies, heme
507 binding to motif **5** showed the best binding properties with a distance of 3.45 Å between the oxygen
508 of Y^{547} and the iron ion of heme (Fig. 6I and 6J). With a slightly closer distance between the
509 coordinating amino acid Y^{397} and heme (2.65 Å), motif **3** possesses similar heme-binding potential as
510 motif **5** (Fig. 6I and 6J). In line with the very low heme-binding affinity on peptide level, heme
511 docking to motif **1** was not possible, confirming that this motif should not be considered as a HBM in
512 further investigations (Fig. S12E and S12F).

513 We finally investigated the virulence of TIGR4Δ*glnP* using the mouse model of pneumonia.
514 We hypothesize that in the absence of GlnP, infection with TIGR4Δ*glnP* would have been more
515 virulent or at least similar than infection with the WT strain. However, while four days post-
516 inoculation the mice infected with TIGR4 had already died, animals infected with TIGR4Δ*glnP*
517 survived (Fig. 6K). Inoculated TIGR4Δ*glnP* bacteria expressed capsule and H_2O_2 at the same level as
518 WT (not shown) supporting previous evidence that the GlnPQ transporter is necessary for lung
519 pathogenesis.[50,53] Because we discovered that TIGR4Δ*glnP* had a defect in autolysis (Fig. 6B) and
520 autolysis might be important for bronchiole invasion, we assessed the virulence of TIGR4Δ*glnP* by
521 inoculating bacteria via intraperitoneal injection. Mice injected with TIGR4 and TIGR4Δ*glnP* died
522 within 72 h post-infection whereas >90% mice infected with TIGR4Δ*spxB*Δ*lctO* survived (Fig. 6L).
523 Accordingly, pneumococci were recovered from the blood of mice infected with TIGR4 and

524 TIGR4Δ*glnP* but not from the blood of mice infected with TIGR4Δ*spxB*Δ*lctO* (Fig. 6M). Altogether,
525 these data confirmed that GlnPQ is a heme-binding protein that contributes to heme toxicity in Spn.
526
527 **Discussion**
528 *S. pneumoniae* thrives in the lung's alveolar-capillary network, benefiting from oxygen,
529 carbohydrates, and iron from heme-hemoglobin utilized for their metabolism but producing H_2O_2
530 and unintended consequences for the host. Under laboratory culture conditions, Spn-H_2O_2 reacts
531 with Fe^{2+} generating a hydroxyl radical ($^{\bullet}OH^{-}$) that is lethal to bacterial species with an electron
532 transport chain.[39,54] Spn-H_2O_2 oxidizes hemoproteins such as hemoglobin and cytochrome C (Cyt*c*)
533 and this oxidation creates two other toxic products, labile heme and a tyrosyl radical
534 ($^{\bullet}Hb+Fe^{4+}$).[17,19,20] Here, we discovered that oxidative reactions driven by Spn-H_2O_2 contributes to
535 lung toxicity by oxidizing hemoglobin contributing to the degradation of cytosolic proteins, and
536 facilitating the differentiation of pneumococci into encapsulated bacteria. Accordingly, the
537 differentiation predominantly takes place within the alveoli and endothelial cells of pulmonary
538 arteries. These mechanisms represent novel points of intervention for a disease that kills millions
539 every year.
540 The oxidation of hemoglobin by Spn-H_2O_2 induced its aggregation, maintaining pneumococci
541 suspended in the lung tissue. *In vitro* studies have demonstrated that H_2O_2 crosslinks the α-globin[34]
542 or β-globin[35] and our studies found that Spn-H_2O_2 caused the aggregation of both α and β globin
543 chains. The attack of Spn-H_2O_2 to the goblins generated MetOH, a product of the oxidation of
544 methionine-55 in the β chain and that has been associated with the collapse of the globin.[35] Cell free
545 hemoglobin is bound by haptoglobin (Hp) that is taken up by macrophages via CD163 for its

546 recycling.[55] Oxidized hemoglobin has a reduced Hp biding and therefore a weaken interaction with
547 human macrophages via CD163.[34] In the lung of mice infected with Spn, oxidized hemoglobin bound
548 to a subset of Spn-Hb^+ bacteria that lacked capsule, suggesting that it protected Spn-Hb^+ from the
549 cellular immune response. The abundance of $CD45^+$ leukocytes surrounding Spn-Hb^+ bacteria in
550 bronchioles and alveoli of mice infected with Spn, at the time of severe pneumonia, supports this
551 hypothesis.

552 Pneumococci produce the toxin pneumolysin or Ply,[56-59] but its mechanism of cytotoxicity
553 cannot explain the intricate pathophysiology observed in the lung of those suffering from
554 pneumococcal pneumonia.[60,61] There is a strong scientific premise for Spn-H_2O_2 both in causing cell
555 death and in triggering pneumococcal disease in animal models.[9,58,62-65] Moreover, simultaneous
556 activation of apoptosis and pyroptosis markers occur, which supports a complex molecular
557 mechanism leading to lung cytotoxicity.[66-69] We discovered a loss in cellular structure within mouse
558 lung regions exhibiting significant alveolar and bronchial cytotoxicity, where intracellular
559 pneumococci were located. Signal of nuclear DNA from epithelial cells was absent, but nuclei of
560 infiltrated $CD45^+$ cells were present. *In vivo* cytotoxicity was partially attributed to Spn-H_2O_2 that
561 was produced by pneumococci in the mouse lungs. Spn-H_2O_2 was also delivered intracellularly to *in*
562 *vitro* cultured human alveolar cells. While Spn-H_2O_2 can oxidize intracellular proteins, LA-ICP-TOFMS
563 analysis revealed increased iron levels in areas of lung toxicity, suggesting a scenario where Fenton
564 reactions generate $^{\bullet}OH^-$ radicals, contributing to toxicity by causing toxic DNA damage.[54,70]

565 We made a fascinating discovery related to the mechanism of lung cell death that correlated
566 with the loss of the lung's cellular structure. Proteins of the cell cytoskeleton involved in structural
567 stability and protein trafficking, such as β-tubulin and β-actin, and cytosolic GAPDH from the

568 glycolytic pathway were degraded during infection of human alveolar cells, or bronchial cells[20], with
569 H_2O_2-producing pneumococci. Degradation of cytoskeletal proteins correlated with microtubule
570 collapse (catastrophe) and cell swelling due to loss of actin stress fibers (not shown and [20]).
571 Structural damage of microtubules has been observed in ventricular cardiomyocytes exposed to
572 H_2O_2 (100 µm).[36] Oxidation of cysteines 213, 295, and 305 in the α globin and cysteine 129 in the β
573 globin weakened tubulin-tubulin interaction, inhibiting microtubule polymerization and leading to
574 catastrophe. [36,71,72] Similarly, the catalytic cysteine residue (Cys152) of human GAPDH has
575 exceptional reactivity towards H_2O_2, forming a cysteine sulfenic acid that further react with
576 glutathione leading to S-glutathionylation.[73] S-glutathionylation of GAPDH leads to cell death.[74,75]
577 Pharmacological induction of H_2O_2-mediated oxidation of GAPDH proves promising for the
578 treatment of glycolysis-dependent tumors as it activates non-apoptotic cell death.[76] Survival in
579 animal models of pneumococcal sepsis, or pneumonia, is improved by the administration of
580 antioxidants or scavenging of extracellular plasma hemoglobin with haptoglobin, respectively[77,78],
581 and antioxidants have reduced the mortality of patients with pneumococcal sepsis[79].

582 Spn-H_2O_2 oxidation of hemoglobin causes the release of heme, its degradation, and the
583 creation of highly reactive tyrosyl radical.[20,30,31,80,81] As such, heme destruction is extremely toxic. For
584 example, intravascular hemolysis with the accumulation of labile heme during hemolytic diseases
585 such as malaria and SCD[23] has been linked to proinflammatory and prothrombotic complications,[82]
586 as well as cell death through PANoptosis.[83] Notably, labile heme is also an inhibitor of
587 phagocytosis[84-86]. Additionally, the oxidation of heme-carrying proteins such metmyoglobin,
588 cytochrome C (Cyt*c*), and methemoglobin (Hb-Fe^{3+}) results in generation of toxic tyrosyl radicals[20,87-
589 [90]. The tyrosyl radical created by the oxidation of hemoglobin by Spn-H_2O_2[20] contributes to the

590 severity of alveolar cytotoxicity observed in the current study, as it has been demonstrated to
591 contribute to as seen in the pathophysiology in SCD[25].

592 Data in this study, and evidence form earlier research, support a model in which
593 encapsulated Spn reach the bronchi and bronchioles and decapsulate[91] to enter the bronchiolar
594 epithelium. Nonencapsulated pneumococci traffics down to alveoli, where bacteria reach the
595 alveolar-capillary network, a surface area of 70 m^2 with ~300 million blood capillaries each with a
596 diameter <10 µm.[92]. Upon lysis of erythrocytes, hemoglobin is then oxidized by Spn-H_2O_2
597 stimulating the differentiation of pneumococci to encapsulated bacteria. Several lines of evidence
598 allow us to propose such a new mechanism. For example, *in vitro* studies found that oxidation of
599 hemoglobin killed a population of pneumococci with the formation of Spn-Hb^+ bacteria. Moreover,
600 pneumococci that did not produce H_2O_2 and capsule were extremely sensitive to heme, and ~10^9
601 bacteria were cleared from the lungs within 48 h. Genes in the capsule locus are upregulated when
602 Spn is incubated in blood-mimicking conditions, or with labile heme.[19,93] Collectively, our findings
603 unveil novel intervention strategies. By addressing oxidative reactions in pneumococcal pneumonia
604 or by stimulating the natural antioxidant response of lung cells through pharmacological
605 approaches, we may unlock promising therapeutic possibilities.

606

607 **Acknowledgements**

608 This study was supported in part by a grant from the National Institutes of Health (NIH;
609 5R21AI144571-03) to JEV, BJA, and ZE. BA was supported by a Fulbright scholarship awarded by the
610 US Department of State. Studies of confocal microscopy, histology, and Oroboros O2k
611 FluoRespirometry, were supported by grants from the National Institute of General Medical
612 Sciences (NIGMS) of the National Institutes of Health under Award Numbers P20GM121334 and

613 P20GM104357. JEV is also supported by a grant from NIGMS through the Molecular Center of
614 Health and Disease (1P20GM144041-01A1 7651). Laser ablation elemental imaging was performed
615 at the Dartmouth Biomedical National Elemental Imaging Resource (BNEIR) supported by NIGMS
616 R24GM141194. The content is solely the responsibility of the authors and does not necessarily
617 represent the official view of the NIH or the US Department of State. Financial support by the
618 University of Bonn (STEP 4 programme to DI) and the Deutsche Forschungsgemeinschaft (German
619 Research Foundation; project number 507218303, to MTH) as well as technical support by Dhruv C.
620 Rathod and Karina M. Grimmig (both: University of Bonn) is gratefully acknowledged. We thank
621 Andrew Camilli from the Department of Molecular Biology and Microbiology of Tufts University for
622 his generous gift of the D39 transposon library. Additionally, we extend our gratitude to Dr. Timothy
623 Allen from the Department of Pathology at the University of Mississippi Medical Center for his
624 assistance with the pathology score.

625

626 **References**

627 1. Wahl, B., O'Brien, K.L., Greenbaum, A., Majumder, A., Liu, L., Chu, Y., Luksic, I., Nair, H.,
628 McAllister, D.A., Campbell, H., et al. (2018). Burden of Streptococcus pneumoniae and
629 Haemophilus influenzae type b disease in children in the era of conjugate vaccines: global,
630 regional, and national estimates for 2000-15. Lancet Glob Health *6*, e744-e757.
631 10.1016/S2214-109X(18)30247-X.
632 2. Weiser, J.N., Ferreira, D.M., and Paton, J.C. (2018). Streptococcus pneumoniae: transmission,
633 colonization and invasion. Nat Rev Microbiol *16*, 355-367. 10.1038/s41579-018-0001-8.
634 3. Musher, D.M., and Thorner, A.R. (2014). Community-acquired pneumonia. N Engl J Med *371*,
635 1619-1628. 10.1056/NEJMra1312885.
636 4. Ganaie, F., Saad, J.S., McGee, L., van Tonder, A.J., Bentley, S.D., Lo, S.W., Gladstone, R.A.,
637 Turner, P., Keenan, J.D., Breiman, R.F., and Nahm, M.H. (2020). A New Pneumococcal
638 Capsule Type, 10D, is the 100th Serotype and Has a Large cps Fragment from an Oral
639 Streptococcus. mBio *11*. 10.1128/mBio.00937-20.
640 5. Brissac, T., Martinez, E., Kruckow, K.L., Riegler, A.N., Ganaie, F., Im, H., Bakshi, S., Arroyo-
641 Diaz, N.M., Spencer, B.L., Saad, J.S., et al. (2021). Capsule Promotes Intracellular Survival and

642 Vascular Endothelial Cell Translocation during Invasive Pneumococcal Disease. mBio *12*,
643 e0251621. 10.1128/mBio.02516-21.
644 6. Hyams, C., Camberlein, E., Cohen, J.M., Bax, K., and Brown, J.S. (2010). The Streptococcus
645 pneumoniae capsule inhibits complement activity and neutrophil phagocytosis by multiple
646 mechanisms. Infect Immun *78*, 704-715. 10.1128/IAI.00881-09.
647 7. Kim, J.O., Romero-Steiner, S., Sorensen, U.B., Blom, J., Carvalho, M., Barnard, S., Carlone, G.,
648 and Weiser, J.N. (1999). Relationship between cell surface carbohydrates and intrastrain
649 variation on opsonophagocytosis of Streptococcus pneumoniae. Infect Immun *67*, 2327-
650 2333. 10.1128/IAI.67.5.2327-2333.1999.
651 8. Geno, K.A., Gilbert, G.L., Song, J.Y., Skovsted, I.C., Klugman, K.P., Jones, C., Konradsen, H.B.,
652 and Nahm, M.H. (2015). Pneumococcal Capsules and Their Types: Past, Present, and Future.
653 Clin Microbiol Rev *28*, 871-899. 10.1128/CMR.00024-15.
654 9. Echlin, H., Frank, M.W., Iverson, A., Chang, T.C., Johnson, M.D., Rock, C.O., and Rosch, J.W.
655 (2016). Pyruvate Oxidase as a Critical Link between Metabolism and Capsule Biosynthesis in
656 Streptococcus pneumoniae. PLoS Pathog *12*, e1005951. 10.1371/journal.ppat.1005951.
657 10. Lisher, J.P., Tsui, H.T., Ramos-Montanez, S., Hentchel, K.L., Martin, J.E., Trinidad, J.C.,
658 Winkler, M.E., and Giedroc, D.P. (2017). Biological and Chemical Adaptation to Endogenous
659 Hydrogen Peroxide Production in Streptococcus pneumoniae D39. mSphere *2*.
660 10.1128/mSphere.00291-16.
661 11. Taniai, H., Iida, K., Seki, M., Saito, M., Shiota, S., Nakayama, H., and Yoshida, S. (2008).
662 Concerted action of lactate oxidase and pyruvate oxidase in aerobic growth of Streptococcus
663 pneumoniae: role of lactate as an energy source. J Bacteriol *190*, 3572-3579.
664 10.1128/JB.01882-07.
665 12. Tettelin, H., Nelson, K.E., Paulsen, I.T., Eisen, J.A., Read, T.D., Peterson, S., Heidelberg, J.,
666 DeBoy, R.T., Haft, D.H., Dodson, R.J., et al. (2001). Complete genome sequence of a virulent
667 isolate of Streptococcus pneumoniae. Science *293*, 498-506. 10.1126/science.1061217.
668 13. Pericone, C.D., Park, S., Imlay, J.A., and Weiser, J.N. (2003). Factors contributing to hydrogen
669 peroxide resistance in Streptococcus pneumoniae include pyruvate oxidase (SpxB) and
670 avoidance of the toxic effects of the fenton reaction. J Bacteriol *185*, 6815-6825.
671 10.1128/jb.185.23.6815-6825.2003.
672 14. Ramos-Montanez, S., Kazmierczak, K.M., Hentchel, K.L., and Winkler, M.E. (2010). Instability
673 of ackA (acetate kinase) mutations and their effects on acetyl phosphate and ATP amounts in
674 Streptococcus pneumoniae D39. J Bacteriol *192*, 6390-6400. 10.1128/JB.00995-10.
675 15. Akhter, F., Womack, E., Vidal, J.E., Le Breton, Y., McIver, K.S., Pawar, S., and Eichenbaum, Z.
676 (2021). Hemoglobin induces early and robust biofilm development in Streptococcus
677 pneumoniae by a pathway that involves comC but not the cognate comDE two-component
678 system. Infect Immun. 10.1128/IAI.00779-20.
679 16. Akhter, F., Womack, E., Vidal, J.E., Le Breton, Y., McIver, K.S., Pawar, S., and Eichenbaum, Z.
680 (2020). Hemoglobin stimulates vigorous growth of Streptococcus pneumoniae and shapes
681 the pathogen's global transcriptome. Sci Rep *10*, 15202. 10.1038/s41598-020-71910-1.
682 17. McDevitt, E., Khan, F., Scasny, A., Thompson, C.D., Eichenbaum, Z., McDaniel, L.S., and Vidal,
683 J.E. (2020). Hydrogen Peroxide Production by Streptococcus pneumoniae Results in Alpha-
684 hemolysis by Oxidation of Oxy-hemoglobin to Met-hemoglobin. mSphere *5*.
685 10.1128/mSphere.01117-20.

686 18. Kajfasz, J.K., Rivera-Ramos, I., Abranches, J., Martinez, A.R., Rosalen, P.L., Derr, A.M., Quivey,
687 R.G., and Lemos, J.A. (2010). Two Spx proteins modulate stress tolerance, survival, and
688 virulence in Streptococcus mutans. J Bacteriol *192*, 2546-2556. 10.1128/JB.00028-10.
689 19. Alibayov, B., Scasny, A., Khan, F., Creel, A., Smith, P., Vidal, A.G.J., Fitisemanu, F.M., Padilla-
690 Benavides, T., Weiser, J.N., and Vidal, J.E. (2022). Oxidative Reactions Catalyzed by Hydrogen
691 Peroxide Produced by Streptococcus pneumoniae and Other Streptococci Cause the Release
692 and Degradation of Heme from Hemoglobin. Infect Immun *90*, e0047122. 10.1128/iai.00471-
693 22.
694 20. Scasny, A., Alibayov, B., Khan, F., Rao, S.J., Murin, L., Jop Vidal, A.G., Smith, P., Wei, L.,
695 Edwards, K., Warncke, K., and Vidal, J.E. (2023). Oxidation of hemoproteins by Streptococcus
696 pneumoniae collapses the cell cytoskeleton and disrupts mitochondrial respiration leading to
697 cytotoxicity of human lung cells. bioRxiv. 10.1101/2023.06.07.544089.
698 21. Nader, E., Romana, M., and Connes, P. (2020). The Red Blood Cell-Inflammation Vicious
699 Circle in Sickle Cell Disease. Front Immunol *11*, 454. 10.3389/fimmu.2020.00454.
700 22. Buehler, P.W., Humar, R., and Schaer, D.J. (2020). Haptoglobin Therapeutics and
701 Compartmentalization of Cell-Free Hemoglobin Toxicity. Trends Mol Med *26*, 683-697.
702 10.1016/j.molmed.2020.02.004.
703 23. Kato, G.J., Steinberg, M.H., and Gladwin, M.T. (2017). Intravascular hemolysis and the
704 pathophysiology of sickle cell disease. J Clin Invest *127*, 750-760. 10.1172/JCI89741.
705 24. van Beers, E.J., Samsel, L., Mendelsohn, L., Saiyed, R., Fertrin, K.Y., Brantner, C.A., Daniels,
706 M.P., Nichols, J., McCoy, J.P., and Kato, G.J. (2014). Imaging flow cytometry for automated
707 detection of hypoxia-induced erythrocyte shape change in sickle cell disease. Am J Hematol
708 *89*, 598-603. 10.1002/ajh.23699.
709 25. Kassa, T., Jana, S., Strader, M.B., Meng, F., Jia, Y., Wilson, M.T., and Alayash, A.I. (2015). Sickle
710 Cell Hemoglobin in the Ferryl State Promotes betaCys-93 Oxidation and Mitochondrial
711 Dysfunction in Epithelial Lung Cells (E10). J Biol Chem *290*, 27939-27958.
712 10.1074/jbc.M115.651257.
713 26. Balla, J., Jacob, H.S., Balla, G., Nath, K., Eaton, J.W., and Vercellotti, G.M. (1993). Endothelial-
714 cell heme uptake from heme proteins: induction of sensitization and desensitization to
715 oxidant damage. Proc Natl Acad Sci U S A *90*, 9285-9289. 10.1073/pnas.90.20.9285.
716 27. Shaver, C.M., Upchurch, C.P., Janz, D.R., Grove, B.S., Putz, N.D., Wickersham, N.E., Dikalov,
717 S.I., Ware, L.B., and Bastarache, J.A. (2016). Cell-free hemoglobin: a novel mediator of acute
718 lung injury. Am J Physiol Lung Cell Mol Physiol *310*, L532-541. 10.1152/ajplung.00155.2015.
719 28. Gotts, J.E., Bernard, O., Chun, L., Croze, R.H., Ross, J.T., Nesseler, N., Wu, X., Abbott, J., Fang,
720 X., Calfee, C.S., and Matthay, M.A. (2019). Clinically relevant model of pneumococcal
721 pneumonia, ARDS, and nonpulmonary organ dysfunction in mice. Am J Physiol Lung Cell Mol
722 Physiol *317*, L717-L736. 10.1152/ajplung.00132.2019.
723 29. Maitra, D., Byun, J., Andreana, P.R., Abdulhamid, I., Diamond, M.P., Saed, G.M., Pennathur,
724 S., and Abu-Soud, H.M. (2011). Reaction of hemoglobin with HOCl: mechanism of heme
725 destruction and free iron release. Free Radic Biol Med *51*, 374-386.
726 10.1016/j.freeradbiomed.2011.04.011.
727 30. Nagababu, E., and Rifkind, J.M. (2004). Heme degradation by reactive oxygen species.
728 Antioxid Redox Signal *6*, 967-978. 10.1089/ars.2004.6.967.

729 31. Nagababu, E., and Rifkind, J.M. (1998). Formation of fluorescent heme degradation products
730 during the oxidation of hemoglobin by hydrogen peroxide. Biochem Biophys Res Commun
731 *247*, 592-596. 10.1006/bbrc.1998.8846.
732 32. Pamplona, A., Ferreira, A., Balla, J., Jeney, V., Balla, G., Epiphanio, S., Chora, A., Rodrigues,
733 C.D., Gregoire, I.P., Cunha-Rodrigues, M., et al. (2007). Heme oxygenase-1 and carbon
734 monoxide suppress the pathogenesis of experimental cerebral malaria. Nat Med *13*, 703-
735 710. 10.1038/nm1586.
736 33. Mingone, C.J., Gupte, S.A., Chow, J.L., Ahmad, M., Abraham, N.G., and Wolin, M.S. (2006).
737 Protoporphyrin IX generation from delta-aminolevulinic acid elicits pulmonary artery
738 relaxation and soluble guanylate cyclase activation. Am J Physiol Lung Cell Mol Physiol *291*,
739 L337-344. 10.1152/ajplung.00482.2005.
740 34. Vallelian, F., Pimenova, T., Pereira, C.P., Abraham, B., Mikolajczyk, M.G., Schoedon, G.,
741 Zenobi, R., Alayash, A.I., Buehler, P.W., and Schaer, D.J. (2008). The reaction of hydrogen
742 peroxide with hemoglobin induces extensive alpha-globin crosslinking and impairs the
743 interaction of hemoglobin with endogenous scavenger pathways. Free Radic Biol Med *45*,
744 1150-1158. 10.1016/j.freeradbiomed.2008.07.013.
745 35. Jia, Y., Buehler, P.W., Boykins, R.A., Venable, R.M., and Alayash, A.I. (2007). Structural basis
746 of peroxide-mediated changes in human hemoglobin: a novel oxidative pathway. J Biol Chem
747 *282*, 4894-4907. 10.1074/jbc.M609955200.
748 36. Goldblum, R.R., McClellan, M., White, K., Gonzalez, S.J., Thompson, B.R., Vang, H.X., Cohen,
749 H., Higgins, L., Markowski, T.W., Yang, T.Y., et al. (2021). Oxidative stress pathogenically
750 remodels the cardiac myocyte cytoskeleton via structural alterations to the microtubule
751 lattice. Dev Cell *56*, 2252-2266 e2256. 10.1016/j.devcel.2021.07.004.
752 37. Griffiths, S.W., King, J., and Cooney, C.L. (2002). The reactivity and oxidation pathway of
753 cysteine 232 in recombinant human alpha 1-antitrypsin. J Biol Chem *277*, 25486-25492.
754 10.1074/jbc.M203089200.
755 38. Moskovitz, J., and Smith, A. (2021). Methionine sulfoxide and the methionine sulfoxide
756 reductase system as modulators of signal transduction pathways: a review. Amino Acids *53*,
757 1011-1020. 10.1007/s00726-021-03020-9.
758 39. Wu, X., Gordon, O., Jiang, W., Antezana, B.S., Angulo-Zamudio, U.A., Del Rio, C., Moller, A.,
759 Brissac, T., Tierney, A.R.P., Warncke, K., et al. (2019). Interaction between Streptococcus
760 pneumoniae and Staphylococcus aureus Generates (.)OH Radicals That Rapidly Kill
761 Staphylococcus aureus Strains. J Bacteriol *201*. 10.1128/JB.00474-19.
762 40. Bryant, J.C., Dabbs, R.C., Oswalt, K.L., Brown, L.R., Rosch, J.W., Seo, K.S., Donaldson, J.R.,
763 McDaniel, L.S., and Thornton, J.A. (2016). Pyruvate oxidase of Streptococcus pneumoniae
764 contributes to pneumolysin release. BMC Microbiol *16*, 271. 10.1186/s12866-016-0881-6.
765 41. Echlin, H., Frank, M., Rock, C., and Rosch, J.W. (2020). Role of the pyruvate metabolic
766 network on carbohydrate metabolism and virulence in Streptococcus pneumoniae. Mol
767 Microbiol *114*, 536-552. 10.1111/mmi.14557.
768 42. Gozzelino, R., Jeney, V., and Soares, M.P. (2010). Mechanisms of cell protection by heme
769 oxygenase-1. Annu Rev Pharmacol Toxicol *50*, 323-354.
770 10.1146/annurev.pharmtox.010909.105600.

771 43. Gbotosho, O.T., Kapetanaki, M.G., and Kato, G.J. (2020). The Worst Things in Life are Free:
772 The Role of Free Heme in Sickle Cell Disease. Front Immunol *11*, 561917.
773 10.3389/fimmu.2020.561917.
774 44. Yamaguchi, M., Terao, Y., Mori, Y., Hamada, S., and Kawabata, S. (2008). PfbA, a novel
775 plasmin- and fibronectin-binding protein of Streptococcus pneumoniae, contributes to
776 fibronectin-dependent adhesion and antiphagocytosis. J Biol Chem *283*, 36272-36279.
777 10.1074/jbc.M807087200.
778 45. Adisa, O.A., Hu, Y., Ghosh, S., Aryee, D., Osunkwo, I., and Ofori-Acquah, S.F. (2013).
779 Association between plasma free haem and incidence of vaso-occlusive episodes and acute
780 chest syndrome in children with sickle cell disease. Br J Haematol *162*, 702-705.
781 10.1111/bjh.12445.
782 46. Reiter, C.D., Wang, X., Tanus-Santos, J.E., Hogg, N., Cannon, R.O., 3rd, Schechter, A.N., and
783 Gladwin, M.T. (2002). Cell-free hemoglobin limits nitric oxide bioavailability in sickle-cell
784 disease. Nat Med *8*, 1383-1389. 10.1038/nm1202-799.
785 47. Saltini, C., Mohammad, N., Xin, Y., Alvarado, R., Ghio, A.J., Moneypenny, C.G., Riva, A., Fu, D.,
786 Flagg, T., Saltini, G.F.A., et al. (2023). Lung microhaemorrhage drives oxidative/inflammatory
787 damage in alpha(1)-antitrypsin deficiency. ERJ Open Res *9*. 10.1183/23120541.00662-2022.
788 48. Criddle, D.N., Gillies, S., Baumgartner-Wilson, H.K., Jaffar, M., Chinje, E.C., Passmore, S.,
789 Chvanov, M., Barrow, S., Gerasimenko, O.V., Tepikin, A.V., et al. (2006). Menadione-induced
790 reactive oxygen species generation via redox cycling promotes apoptosis of murine
791 pancreatic acinar cells. J Biol Chem *281*, 40485-40492. 10.1074/jbc.M607704200.
792 49. Drum, B.M., Yuan, C., Li, L., Liu, Q., Wordeman, L., and Santana, L.F. (2016). Oxidative stress
793 decreases microtubule growth and stability in ventricular myocytes. J Mol Cell Cardiol *93*, 32-
794 43. 10.1016/j.yjmcc.2016.02.012.
795 50. Hartel, T., Klein, M., Koedel, U., Rohde, M., Petruschka, L., and Hammerschmidt, S. (2011).
796 Impact of glutamine transporters on pneumococcal fitness under infection-related
797 conditions. Infect Immun *79*, 44-58. 10.1128/IAI.00855-10.
798 51. Ploetz, E., Schuurman-Wolters, G.K., Zijlstra, N., Jager, A.W., Griffith, D.A., Guskov, A.,
799 Gouridis, G., Poolman, B., and Cordes, T. (2021). Structural and biophysical characterization
800 of the tandem substrate-binding domains of the ABC importer GlnPQ. Open Biol *11*, 200406.
801 10.1098/rsob.200406.
802 52. Wissbrock, A., Goradia, N.B., Kumar, A., Paul George, A.A., Kuhl, T., Bellstedt, P.,
803 Ramachandran, R., Hoffmann, P., Galler, K., Popp, J., et al. (2019). Structural insights into
804 heme binding to IL-36alpha proinflammatory cytokine. Sci Rep *9*, 16893. 10.1038/s41598-
805 019-53231-0.
806 53. Hendriksen, W.T., Kloosterman, T.G., Bootsma, H.J., Estevao, S., de Groot, R., Kuipers, O.P.,
807 and Hermans, P.W. (2008). Site-specific contributions of glutamine-dependent regulator
808 GlnR and GlnR-regulated genes to virulence of Streptococcus pneumoniae. Infect Immun *76*,
809 1230-1238. 10.1128/IAI.01004-07.
810 54. Imlay, J.A., Chin, S.M., and Linn, S. (1988). Toxic DNA damage by hydrogen peroxide through
811 the Fenton reaction in vivo and in vitro. Science *240*, 640-642. 10.1126/science.2834821.
812 55. Ginzburg, Y., An, X., Rivella, S., and Goldfarb, A. (2023). Normal and dysregulated crosstalk
813 between iron metabolism and erythropoiesis. Elife *12*. 10.7554/eLife.90189.

814 56. Nishimoto, A.T., Rosch, J.W., and Tuomanen, E.I. (2020). Pneumolysin: Pathogenesis and
815 Therapeutic Target. Front Microbiol *11*, 1543. 10.3389/fmicb.2020.01543.
816 57. Shak, J.R., Ludewick, H.P., Howery, K.E., Sakai, F., Yi, H., Harvey, R.M., Paton, J.C., Klugman,
817 K.P., and Vidal, J.E. (2013). Novel role for the Streptococcus pneumoniae toxin pneumolysin
818 in the assembly of biofilms. mBio *4*, e00655-00613. 10.1128/mBio.00655-13.
819 58. Rubins, J.B., Duane, P.G., Clawson, D., Charboneau, D., Young, J., and Niewoehner, D.E.
820 (1993). Toxicity of pneumolysin to pulmonary alveolar epithelial cells. Infect Immun *61*,
821 1352-1358. 10.1128/iai.61.4.1352-1358.1993.
822 59. Rubins, J.B., Duane, P.G., Charboneau, D., and Janoff, E.N. (1992). Toxicity of pneumolysin to
823 pulmonary endothelial cells in vitro. Infect Immun *60*, 1740-1746. 10.1128/iai.60.5.1740-
824 1746.1992.
825 60. van der Poll, T., and Opal, S.M. (2009). Pathogenesis, treatment, and prevention of
826 pneumococcal pneumonia. Lancet *374*, 1543-1556. 10.1016/S0140-6736(09)61114-4.
827 61. Gonzales, J., Chakraborty, T., Romero, M., Mraheil, M.A., Kutlar, A., Pace, B., and Lucas, R.
828 (2021). Streptococcus pneumoniae and Its Virulence Factors H(2)O(2) and Pneumolysin Are
829 Potent Mediators of the Acute Chest Syndrome in Sickle Cell Disease. Toxins (Basel) *13*.
830 10.3390/toxins13020157.
831 62. Shenoy, A.T., Brissac, T., Gilley, R.P., Kumar, N., Wang, Y., Gonzalez-Juarbe, N., Hinkle, W.S.,
832 Daugherty, S.C., Shetty, A.C., Ott, S., et al. (2017). Streptococcus pneumoniae in the heart
833 subvert the host response through biofilm-mediated resident macrophage killing. PLoS
834 pathogens *13*, e1006582. 10.1371/journal.ppat.1006582.
835 63. Brissac, T., Shenoy, A.T., Patterson, L.A., and Orihuela, C.J. (2017). Cell invasion and pyruvate
836 oxidase derived H2O2 are critical for Streptococcus pneumoniae mediated cardiomyocyte
837 killing. Infection and immunity. 10.1128/IAI.00569-17.
838 64. Ramos-Montanez, S., Tsui, H.C., Wayne, K.J., Morris, J.L., Peters, L.E., Zhang, F., Kazmierczak,
839 K.M., Sham, L.T., and Winkler, M.E. (2008). Polymorphism and regulation of the spxB
840 (pyruvate oxidase) virulence factor gene by a CBS-HotDog domain protein (SpxR) in serotype
841 2 Streptococcus pneumoniae. Mol Microbiol *67*, 729-746. 10.1111/j.1365-
842 2958.2007.06082.x.
843 65. Spellerberg, B., Cundell, D.R., Sandros, J., Pearce, B.J., Idanpaan-Heikkila, I., Rosenow, C., and
844 Masure, H.R. (1996). Pyruvate oxidase, as a determinant of virulence in Streptococcus
845 pneumoniae. Mol Microbiol *19*, 803-813. 10.1046/j.1365-2958.1996.425954.x.
846 66. Rai, P., Parrish, M., Tay, I.J., Li, N., Ackerman, S., He, F., Kwang, J., Chow, V.T., and Engelward,
847 B.P. (2015). Streptococcus pneumoniae secretes hydrogen peroxide leading to DNA damage
848 and apoptosis in lung cells. Proc Natl Acad Sci U S A *112*, E3421-3430.
849 10.1073/pnas.1424144112.
850 67. Surabhi, S., Jachmann, L.H., Shumba, P., Burchhardt, G., Hammerschmidt, S., and Siemens, N.
851 (2022). Hydrogen Peroxide Is Crucial for NLRP3 Inflammasome-Mediated IL-1beta Production
852 and Cell Death in Pneumococcal Infections of Bronchial Epithelial Cells. J Innate Immun *14*,
853 192-206. 10.1159/000517855.
854 68. Brissac, T., Shenoy, A.T., Patterson, L.A., and Orihuela, C.J. (2018). Cell Invasion and Pyruvate
855 Oxidase-Derived H(2)O(2) Are Critical for Streptococcus pneumoniae-Mediated
856 Cardiomyocyte Killing. Infect Immun *86*. 10.1128/IAI.00569-17.

857 69. Feldman, C., Anderson, R., Cockeran, R., Mitchell, T., Cole, P., and Wilson, R. (2002). The
858 effects of pneumolysin and hydrogen peroxide, alone and in combination, on human ciliated
859 epithelium in vitro. Respir Med *96*, 580-585. 10.1053/rmed.2002.1316.
860 70. Park, S., You, X., and Imlay, J.A. (2005). Substantial DNA damage from submicromolar
861 intracellular hydrogen peroxide detected in Hpx- mutants of Escherichia coli. Proc Natl Acad
862 Sci U S A *102*, 9317-9322. 10.1073/pnas.0502051102.
863 71. Landino, L.M., Hagedorn, T.D., Kim, S.B., and Hogan, K.M. (2011). Inhibition of tubulin
864 polymerization by hypochlorous acid and chloramines. Free Radic Biol Med *50*, 1000-1008.
865 10.1016/j.freeradbiomed.2011.01.018.
866 72. Clark, H.M., Hagedorn, T.D., and Landino, L.M. (2014). Hypothiocyanous acid oxidation of
867 tubulin cysteines inhibits microtubule polymerization. Arch Biochem Biophys *541*, 67-73.
868 10.1016/j.abb.2013.10.026.
869 73. Hildebrandt, T., Knuesting, J., Berndt, C., Morgan, B., and Scheibe, R. (2015). Cytosolic thiol
870 switches regulating basic cellular functions: GAPDH as an information hub? Biol Chem *396*,
871 523-537. 10.1515/hsz-2014-0295.
872 74. Magherini, F., Tani, C., Gamberi, T., Caselli, A., Bianchi, L., Bini, L., and Modesti, A. (2007).
873 Protein expression profiles in Saccharomyces cerevisiae during apoptosis induced by H2O2.
874 Proteomics *7*, 1434-1445. 10.1002/pmic.200600796.
875 75. Mustafa Rizvi, S.H., Shao, D., Tsukahara, Y., Pimentel, D.R., Weisbrod, R.M., Hamburg, N.M.,
876 McComb, M.E., Matsui, R., and Bachschmid, M.M. (2021). Oxidized GAPDH transfers S-
877 glutathionylation to a nuclear protein Sirtuin-1 leading to apoptosis. Free Radic Biol Med *174*,
878 73-83. 10.1016/j.freeradbiomed.2021.07.037.
879 76. Ma, E., Chen, P., Wilkins, H.M., Wang, T., Swerdlow, R.H., and Chen, Q. (2017).
880 Pharmacologic ascorbate induces neuroblastoma cell death by hydrogen peroxide mediated
881 DNA damage and reduction in cancer cell glycolysis. Free Radic Biol Med *113*, 36-47.
882 10.1016/j.freeradbiomed.2017.09.008.
883 77. Carlson, D., Maass, D.L., White, D.J., Tan, J., and Horton, J.W. (2006). Antioxidant vitamin
884 therapy alters sepsis-related apoptotic myocardial activity and inflammatory responses. Am J
885 Physiol Heart Circ Physiol *291*, H2779-2789. 10.1152/ajpheart.01258.2005.
886 78. Remy, K.E., Cortes-Puch, I., Solomon, S.B., Sun, J., Pockros, B.M., Feng, J., Lertora, J.J.,
887 Hantgan, R.R., Liu, X., Perlegas, A., et al. (2018). Haptoglobin improves shock, lung injury, and
888 survival in canine pneumonia. JCI Insight *3*. 10.1172/jci.insight.123013.
889 79. Janz, D.R., Bastarache, J.A., Peterson, J.F., Sills, G., Wickersham, N., May, A.K., Roberts, L.J.,
890 2nd, and Ware, L.B. (2013). Association between cell-free hemoglobin, acetaminophen, and
891 mortality in patients with sepsis: an observational study. Crit Care Med *41*, 784-790.
892 10.1097/CCM.0b013e3182741a54.
893 80. Nagababu, E., and Rifkind, J.M. (2000). Reaction of hydrogen peroxide with
894 ferrylhemoglobin: superoxide production and heme degradation. Biochemistry *39*, 12503-
895 12511. 10.1021/bi992170y.
896 81. Nagababu, E., and Rifkind, J.M. (2000). Heme degradation during autoxidation of
897 oxyhemoglobin. Biochem Biophys Res Commun *273*, 839-845. 10.1006/bbrc.2000.3025.
898 82. Hopp, M.T., and Imhof, D. (2021). Linking Labile Heme with Thrombosis. J Clin Med *10*.
899 10.3390/jcm10030427.

900 83. Sundaram, B., Pandian, N., Mall, R., Wang, Y., Sarkar, R., Kim, H.J., Malireddi, R.K.S., Karki, R.,
901 Janke, L.J., Vogel, P., and Kanneganti, T.D. (2023). NLRP12-PANoptosome activates
902 PANoptosis and pathology in response to heme and PAMPs. Cell. 10.1016/j.cell.2023.05.005.
903 84. Martins, R., Maier, J., Gorki, A.D., Huber, K.V., Sharif, O., Starkl, P., Saluzzo, S., Quattrone, F.,
904 Gawish, R., Lakovits, K., et al. (2016). Heme drives hemolysis-induced susceptibility to
905 infection via disruption of phagocyte functions. Nat Immunol *17*, 1361-1372.
906 10.1038/ni.3590.
907 85. Olonisakin, T.F., Suber, T., Gonzalez-Ferrer, S., Xiong, Z., Penaloza, H.F., van der Geest, R.,
908 Xiong, Y., Osei-Hwedieh, D.O., Tejero, J., Rosengart, M.R., et al. (2021). Stressed
909 erythrophagocytosis induces immunosuppression during sepsis through heme-mediated
910 STAT1 dysregulation. J Clin Invest *131*. 10.1172/JCI137468.
911 86. Sankar, S.B., Donegan, R.K., Shah, K.J., Reddi, A.R., and Wood, L.B. (2018). Heme and
912 hemoglobin suppress amyloid beta-mediated inflammatory activation of mouse astrocytes. J
913 Biol Chem *293*, 11358-11373. 10.1074/jbc.RA117.001050.
914 87. Gunther, M.R., Tschirret-Guth, R.A., Witkowska, H.E., Fann, Y.C., Barr, D.P., Ortiz De
915 Montellano, P.R., and Mason, R.P. (1998). Site-specific spin trapping of tyrosine radicals in
916 the oxidation of metmyoglobin by hydrogen peroxide. Biochem J *330 (Pt 3)*, 1293-1299.
917 10.1042/bj3301293.
918 88. Shumaev, K.B., Kosmachevskaya, O.V., Timoshin, A.A., Vanin, A.F., and Topunov, A.F. (2008).
919 Dinitrosyl iron complexes bind with hemoglobin as markers of oxidative stress. Methods
920 Enzymol *436*, 445-461. 10.1016/S0076-6879(08)36025-X.
921 89. Barr, D.P., Gunther, M.R., Deterding, L.J., Tomer, K.B., and Mason, R.P. (1996). ESR spin-
922 trapping of a protein-derived tyrosyl radical from the reaction of cytochrome c with
923 hydrogen peroxide. J Biol Chem *271*, 15498-15503. 10.1074/jbc.271.26.15498.
924 90. Qian, S.Y., Chen, Y.R., Deterding, L.J., Fann, Y.C., Chignell, C.F., Tomer, K.B., and Mason, R.P.
925 (2002). Identification of protein-derived tyrosyl radical in the reaction of cytochrome c and
926 hydrogen peroxide: characterization by ESR spin-trapping, HPLC and MS. Biochem J *363*, 281-
927 288. 10.1042/0264-6021:3630281.
928 91. Kietzman, C.C., Gao, G., Mann, B., Myers, L., and Tuomanen, E.I. (2016). Dynamic capsule
929 restructuring by the main pneumococcal autolysin LytA in response to the epithelium. Nat
930 Commun *7*, 10859. 10.1038/ncomms10859.
931 92. Cloutier, M.M. (2019). Respiratory physiology, 2nd edition. Edition (Elsevier).
932 93. Aprianto, R., Slager, J., Holsappel, S., and Veening, J.W. (2018). High-resolution analysis of
933 the pneumococcal transcriptome under a wide range of infection-relevant conditions.
934 Nucleic Acids Res *46*, 9990-10006. 10.1093/nar/gky750.

935

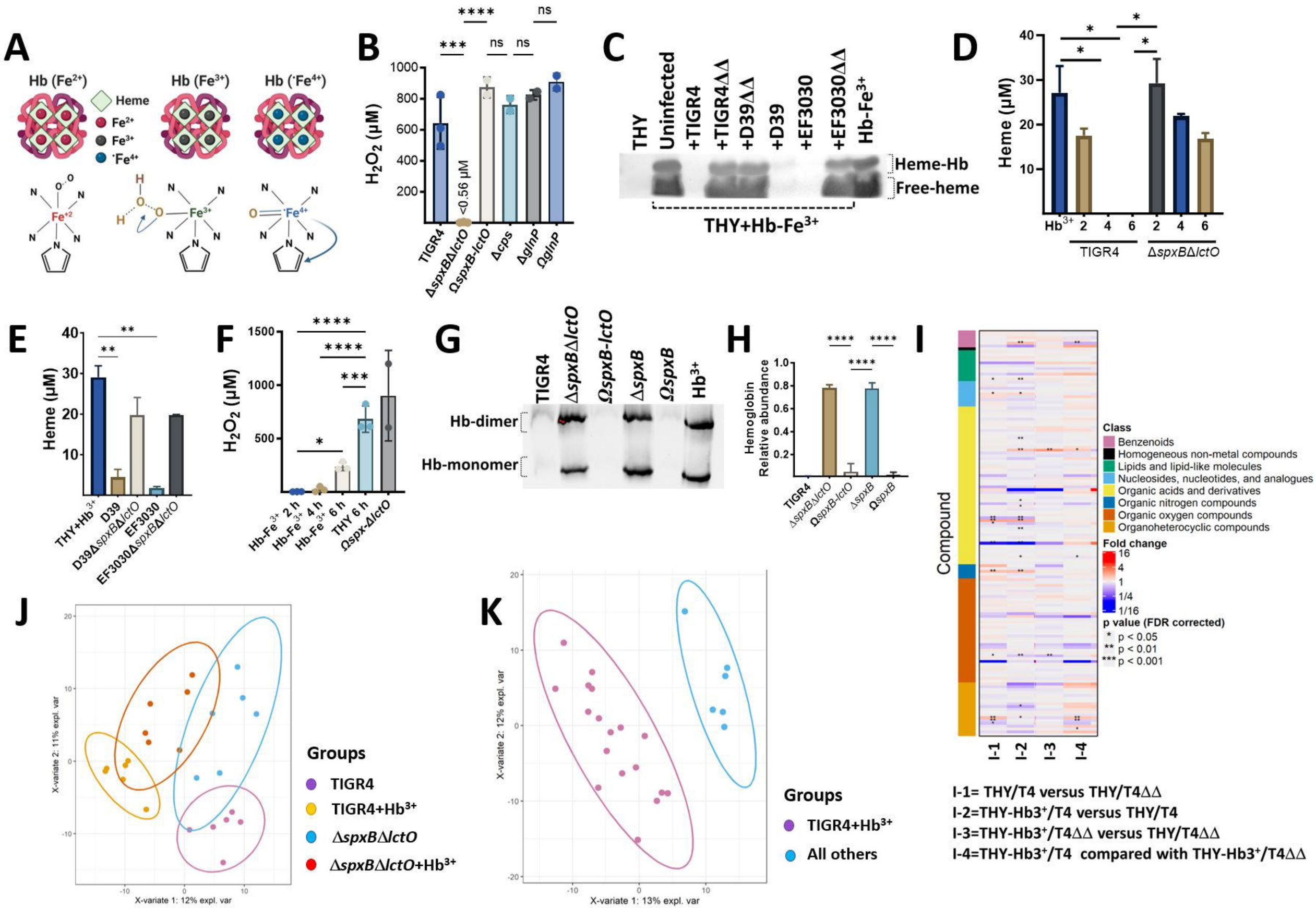
A
Hb (Fe2+)
Hb (Fe3+)
Hb (·Fe4+)
Heme
Fe2+
Fe3+
·Fe4+
B
H2O2 (µM)
<0.56 µM
TIGR4
ΔspxBΔlctO
ΩspxB-lctO
Δcps
ΔglnP
ΩglnP
C
THY
Uninfected
+TIGR4
+TIGR4ΔΔ
+D39ΔΔ
+D39
+EF3030
+EF3030ΔΔ
Hb-Fe3+
Heme-Hb
Free-heme
THY+Hb-Fe3+
D
Heme (µM)
Hb3+
TIGR4
ΔspxBΔlctO
E
Heme (µM)
THY+Hb3+
D39
D39ΔspxBΔlctO
EF3030
EF3030ΔspxBΔlctO
F
H2O2 (µM)
Hb-Fe3+ 2 h
Hb-Fe3+ 4 h
Hb-Fe3+ 6 h
THY 6 h
Ωspx-ΔlctO
G
TIGR4
ΔspxBΔlctO
ΩspxB-lctO
ΔspxB
ΩspxB
Hb3+
Hb-dimer
Hb-monomer
H
Hemoglobin Relative abundance
TIGR4
ΔspxBΔlctO
ΩspxB-lctO
ΔspxB
ΩspxB
I
Compound
Class
Benzenoids
Homogeneous non-metal compounds
Lipids and lipid-like molecules
Nucleosides, nucleotides, and analogues
Organic acids and derivatives
Organic nitrogen compounds
Organic oxygen compounds
Organoheterocyclic compounds
Fold change
16
4
1
1/4
1/16
p value (FDR corrected)
* p < 0.05
** p < 0.01
*** p < 0.001
I-1
I-2
I-3
I-4
J
X-variate 1: 12% expl. var
X-variate 2: 11% expl. var
Groups
TIGR4
TIGR4+Hb3+
ΔspxBΔlctO
ΔspxBΔlctO+Hb3+
K
X-variate 1: 13% expl. var
X-variate 2: 12% expl. var
Groups
TIGR4+Hb3+
All others
I-1= THY/T4 versus THY/T4ΔΔ
I-2=THY-Hb3+/T4 versus THY/T4
I-3=THY-Hb3+/T4ΔΔ versus THY/T4ΔΔ
I-4=THY-Hb3+/T4 compared with THY-Hb3+/T4ΔΔ

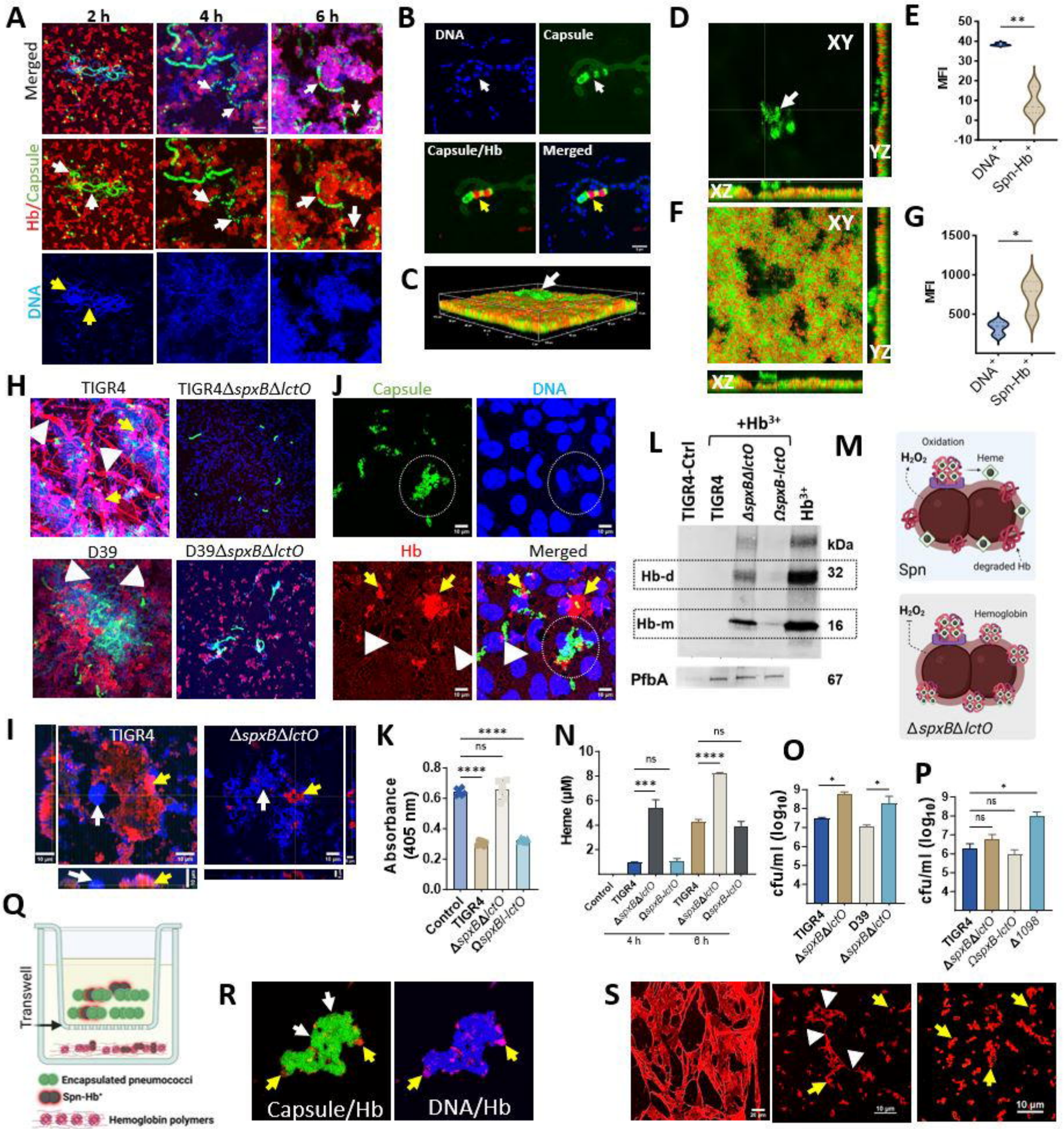
A
2 h
4 h
6 h
Merged
Hb/Capsule
DNA
B
DNA
Capsule
Capsule/Hb
Merged
C
D
XY
YZ
XZ
E
MFI
DNA+
Spn-Hb+
F
XY
YZ
XZ
G
MFI
DNA+
Spn-Hb+
H
TIGR4
TIGR4ΔspxBΔlctO
D39
D39ΔspxBΔlctO
J
Capsule
DNA
Hb
Merged
L
+Hb3+
TIGR4-Ctrl
TIGR4
ΔspxBΔlctO
ΩspxB-lctO
Hb3+
kDa
Hb-d
32
Hb-m
16
PfbA
67
M
Oxidation
H2O2
Heme
Spn
degraded Hb
H2O2
Hemoglobin
ΔspxBΔlctO
I
TIGR4
ΔspxBΔlctO
K
Absorbance (405 nm)
Control
TIGR4
ΔspxBΔlctO
ΩspxBl-lctO
N
Heme (μM)
Control
TIGR4
ΔspxBΔlctO
ΩspxB-lctO
4 h
6 h
O
cfu/ml (log10)
TIGR4
ΔspxBΔlctO
D39
ΔspxBΔlctO
P
cfu/ml (log10)
TIGR4
ΔspxBΔlctO
ΩspxB-lctO
Δ1098
Q
Transwell
Encapsulated pneumococci
Spn-Hb+
Hemoglobin polymers
R
Capsule/Hb
DNA/Hb
S
10 μm

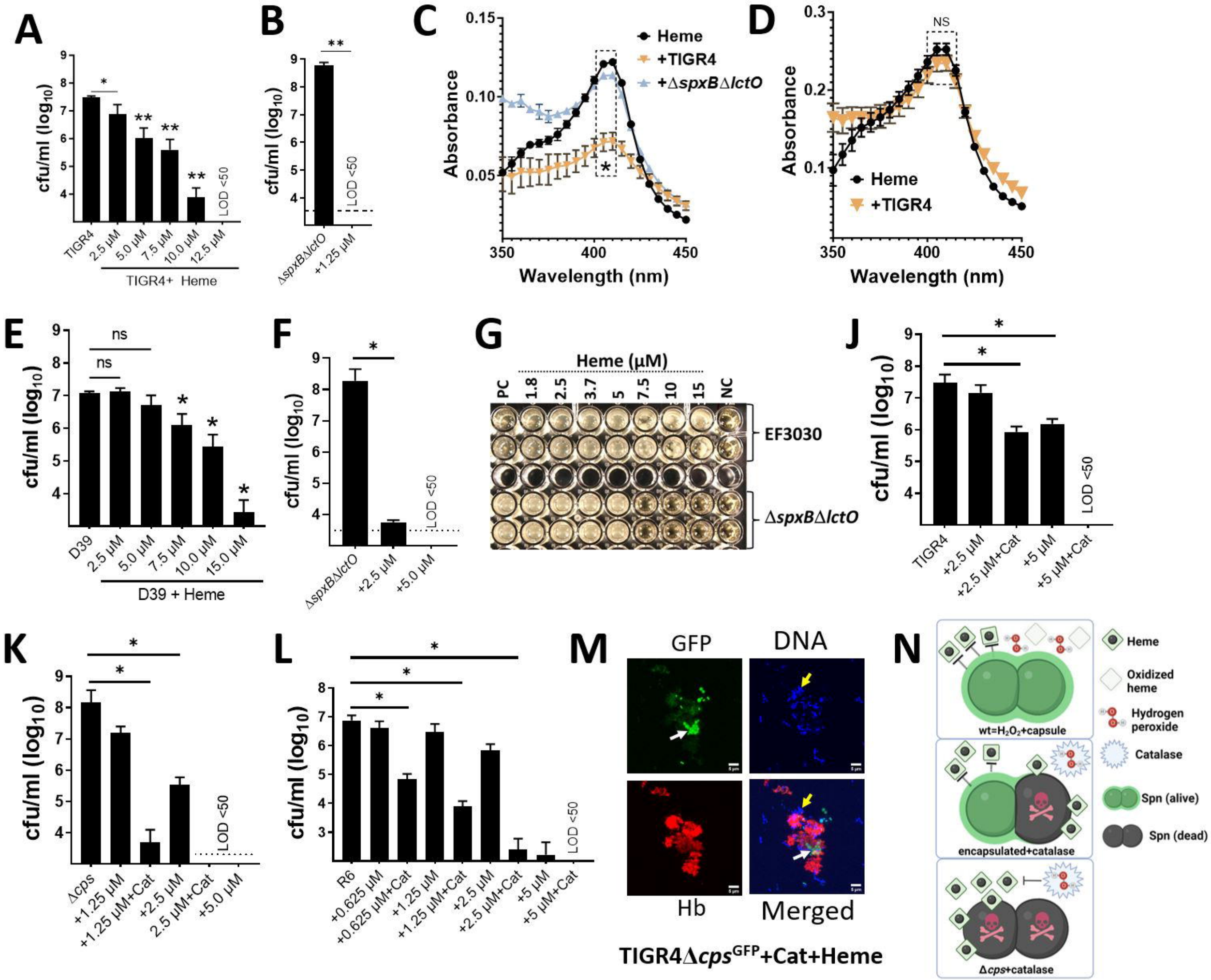
A
cfu/ml (log10)
TIGR4
2.5 µM
5.0 µM
7.5 µM
10.0 µM
12.5 µM
TIGR4+ Heme
LOD <50
B
ΔspxBΔlctO
+1.25 µM
C
Heme
+TIGR4
+ΔspxBΔlctO
Absorbance
Wavelength (nm)
D
NS
E
ns
D39
D39 + Heme
F
+2.5 µM
+5.0 µM
G
Heme (µM)
PC
1.8
2.5
3.7
5
7.5
10
15
NC
EF3030
ΔspxBΔlctO
J
TIGR4
+2.5 µM
+2.5 µM+Cat
+5 µM
+5 µM+Cat
K
Δcps
+1.25 µM
+1.25 µM+Cat
+2.5 µM
2.5 µM+Cat
+5.0 µM
L
R6
+0.625 µM
+0.625 µM+Cat
+1.25 µM
+1.25 µM+Cat
+2.5 µM
+2.5 µM+Cat
+5 µM
+5 µM+Cat
M
GFP
DNA
Hb
Merged
TIGR4ΔcpsGFP+Cat+Heme
N
wt=H2O2+capsule
encapsulated+catalase
Δcps+catalase
Heme
Oxidized heme
Hydrogen peroxide
Catalase
Spn (alive)
Spn (dead)

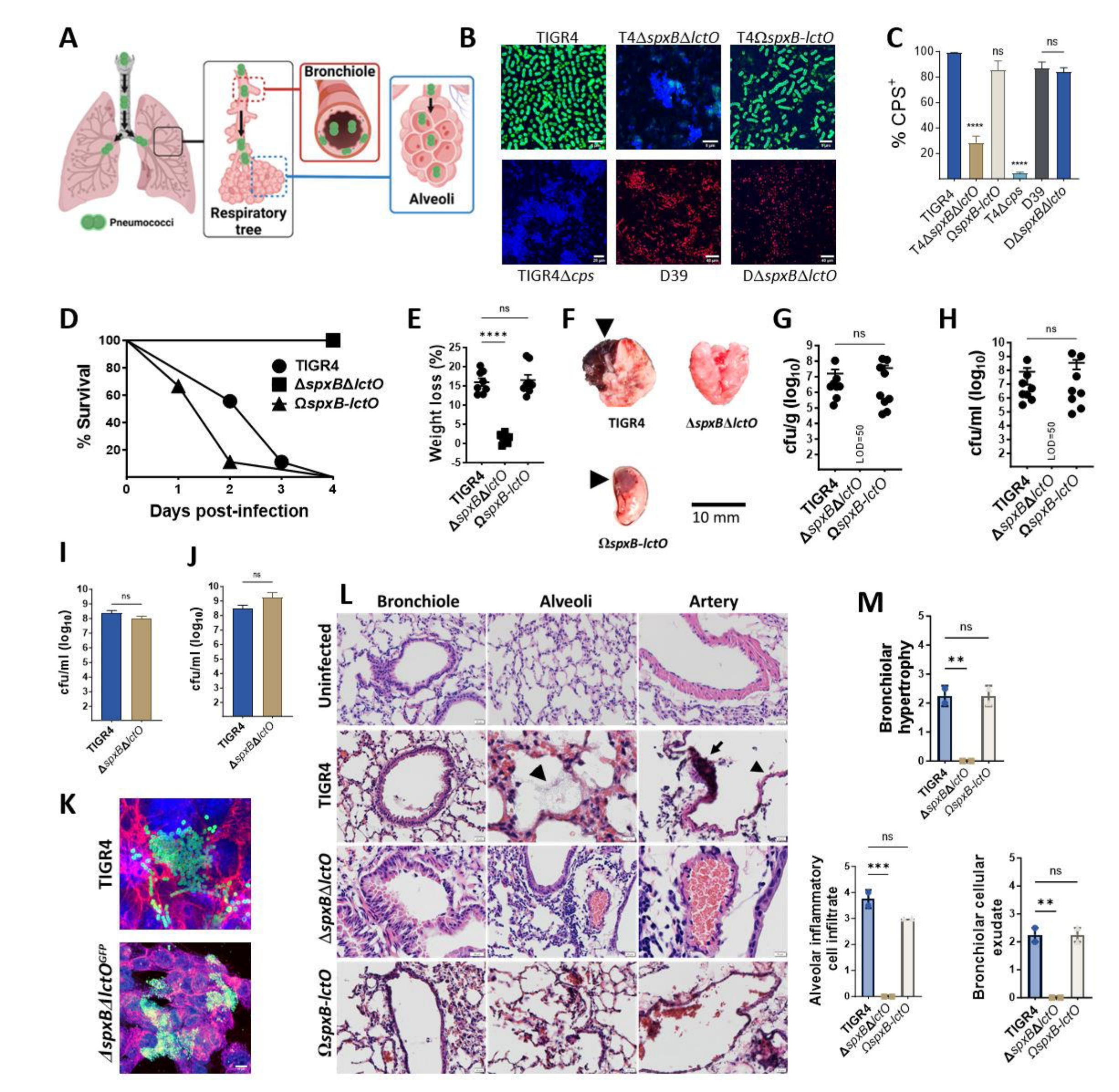
A
Bronchiole
Alveoli
Respiratory tree
Pneumococci
B
TIGR4
T4ΔspxBΔlctO
T4ΩspxB-lctO
TIGR4Δcps
D39
DΔspxBΔlctO
C
% CPS+
ns
****
TIGR4
T4ΔspxBΔlctO
ΩspxB-lctO
T4Δcps
D39
DΔspxBΔlcto
D
% Survival
Days post-infection
TIGR4
ΔspxBΔlctO
ΩspxB-lctO
E
Weight loss (%)
ns
****
F
TIGR4
ΔspxBΔlctO
ΩspxB-lctO
10 mm
G
cfu/g (log10)
ns
LOD=50
H
cfu/ml (log10)
ns
LOD=50
I
cfu/ml (log10)
ns
J
cfu/ml (log10)
ns
K
TIGR4
ΔspxBΔlctOGFP
L
Bronchiole
Alveoli
Artery
Uninfected
TIGR4
ΔspxBΔlctO
ΩspxB-lctO
M
Bronchiolar hypertrophy
ns
**
Alveolar inflammatory cell infiltrate
ns
***
Bronchiolar cellular exudate
ns
**

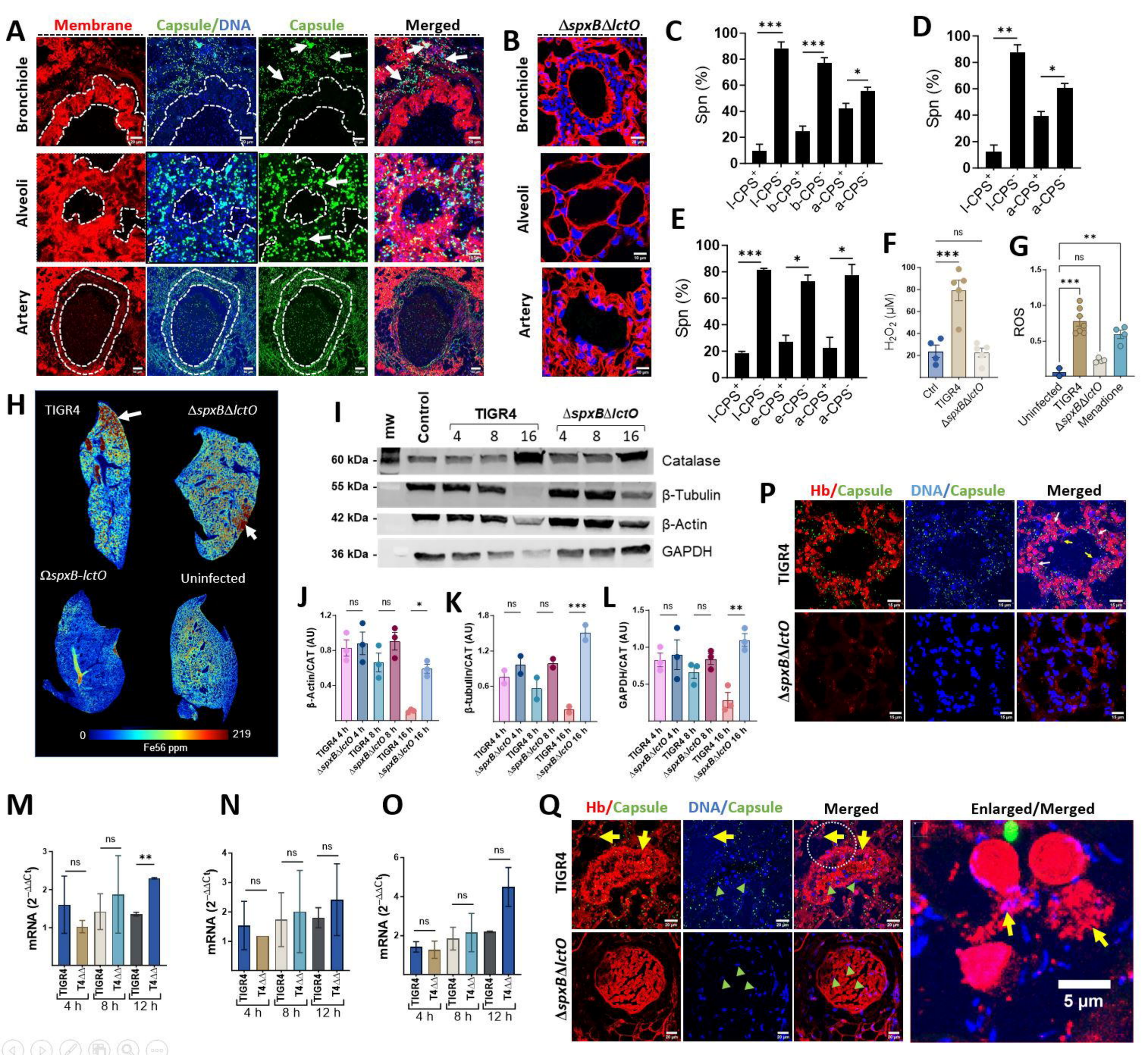
A
Membrane
Capsule/DNA
Capsule
Merged
Bronchiole
Alveoli
Artery
B
ΔspxBΔlctO
C
Spn (%)
I-CPS+
I-CPS-
b-CPS+
b-CPS-
a-CPS+
a-CPS-
D
E
e-CPS+
e-CPS-
F
H2O2 (μM)
Ctrl
TIGR4
ΔspxBΔlctO
G
ROS
Uninfected
Menadione
H
TIGR4
ΔspxBΔlctO
ΩspxB-lctO
Uninfected
0
219
Fe56 ppm
I
mw
Control
TIGR4
4
8
16
60 kDa
55 kDa
42 kDa
36 kDa
Catalase
β-Tubulin
β-Actin
GAPDH
J
β-Actin/CAT (AU)
K
β-tubulin/CAT (AU)
L
GAPDH/CAT (AU)
TIGR4 4 h
ΔspxBΔlctO 4 h
TIGR4 8 h
ΔspxBΔlctO 8 h
TIGR4 16 h
ΔspxBΔlctO 16 h
P
Hb/Capsule
DNA/Capsule
Merged
M
N
O
mRNA (2−ΔΔCt)
TIGR4
T4ΔΔ
4 h
8 h
12 h
Q
Enlarged/Merged
5 μm

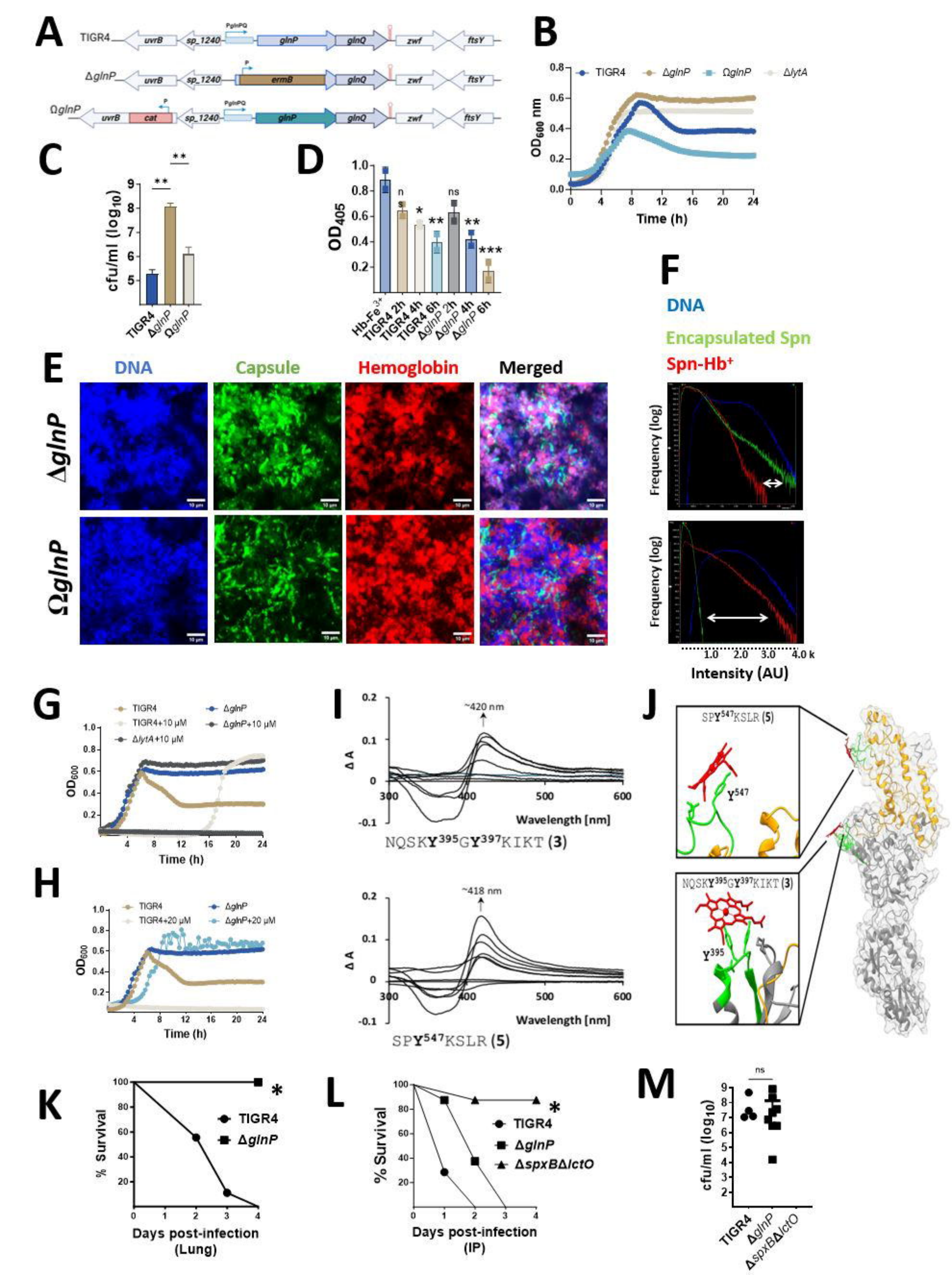
A
TIGR4
uvrB
sp_1240
PglnPQ
glnP
glnQ
zwf
ftsY
ΔglnP
ermB
ΩglnP
cat
B
TIGR4
ΔglnP
ΩglnP
ΔlytA
OD600 nm
Time (h)
C
cfu/ml (log10)
TIGR4
ΔglnP
ΩglnP
D
OD405
Hb-Fe3+
TIGR4 2h
TIGR4 4h
TIGR4 6h
ΔglnP 2h
ΔglnP 4h
ΔglnP 6h
E
DNA
Capsule
Hemoglobin
Merged
ΔglnP
ΩglnP
F
DNA
Encapsulated Spn
Spn-Hb+
Frequency (log)
Intensity (AU)
G
TIGR4
TIGR4+10 μM
ΔlytA+10 μM
ΔglnP
ΔglnP+10 μM
OD600
Time (h)
H
TIGR4
TIGR4+20 μM
ΔglnP
ΔglnP+20 μM
OD600
Time (h)
I
~420 nm
ΔA
Wavelength [nm]
NQSKY395GY397KIKT (3)
~418 nm
SPY547KSLR (5)
J
SPY547KSLR (5)
Y547
NQSKY395GY397KIKT (3)
Y395
K
% Survival
TIGR4
ΔglnP
Days post-infection (Lung)
L
% Survival
TIGR4
ΔglnP
ΔspxBΔlctO
Days post-infection (IP)
M
cfu/ml (log10)
ns
TIGR4
ΔglnP
ΔspxBΔlctO

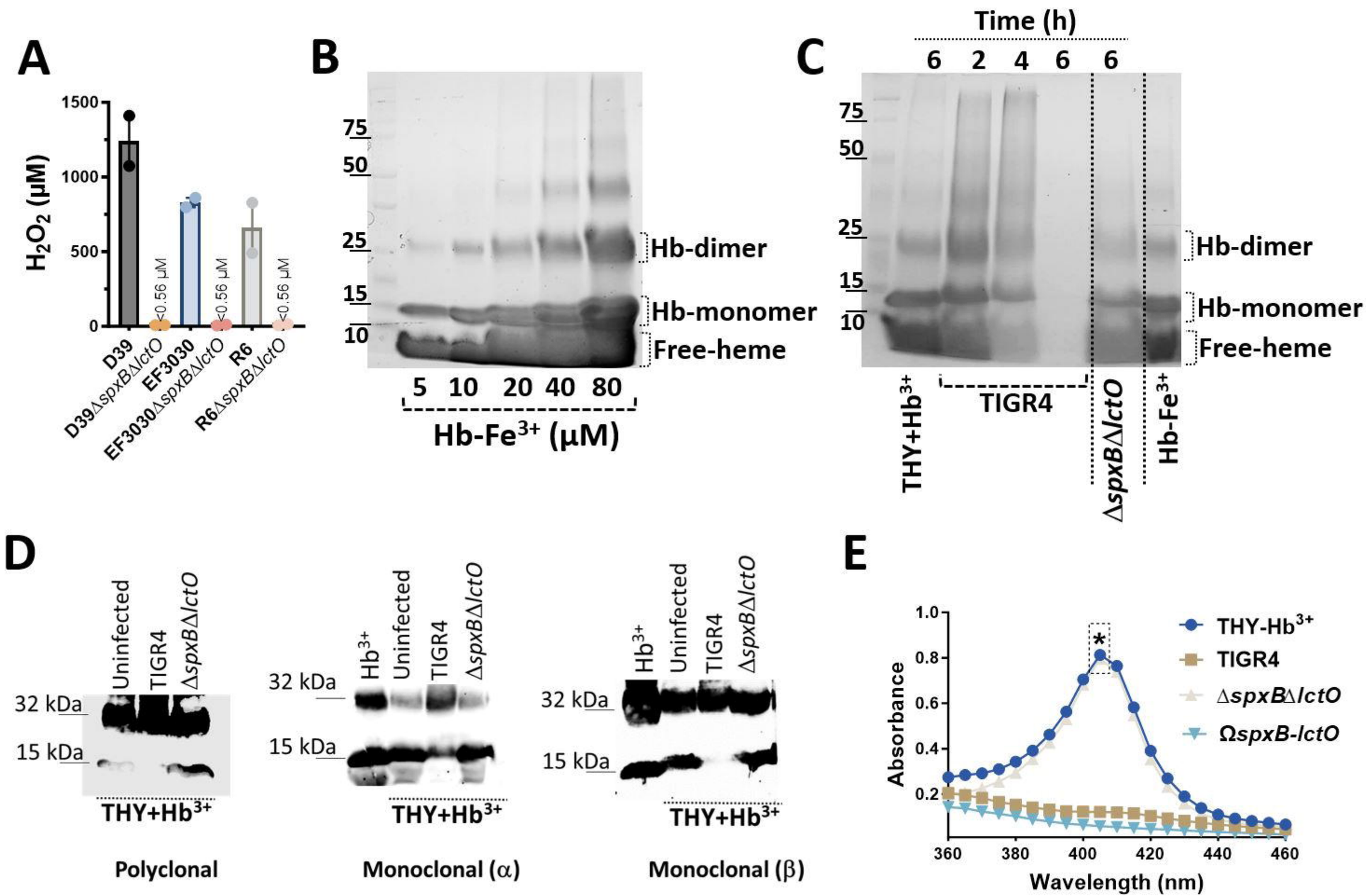
A
H_2O_2 (μM)
1500
1000
500
0
<0.56 μM
<0.56 μM
<0.56 μM
D39
D39ΔspxBΔlctO
EF3030
EF3030ΔspxBΔlctO
R6
R6ΔspxBΔlctO
B
75
50
25
15
10
Hb-dimer
Hb-monomer
Free-heme
5 10 20 40 80
Hb-Fe3+ (μM)
C
Time (h)
6 2 4 6 6
75
50
25
15
10
Hb-dimer
Hb-monomer
Free-heme
THY+Hb3+
TIGR4
ΔspxBΔlctO
Hb-Fe3+
D
Uninfected
TIGR4
ΔspxBΔlctO
32 kDa
15 kDa
THY+Hb3+
Polyclonal
Hb3+
Uninfected
TIGR4
ΔspxBΔlctO
32 kDa
15 kDa
THY+Hb3+
Monoclonal (α)
Hb3+
Uninfected
TIGR4
ΔspxBΔlctO
32 kDa
15 kDa
THY+Hb3+
Monoclonal (β)
E
Absorbance
1.0
0.8
0.6
0.4
0.2
*
THY-Hb3+
TIGR4
ΔspxBΔlctO
ΩspxB-lctO
360
380
400
420
440
460
Wavelength (nm)

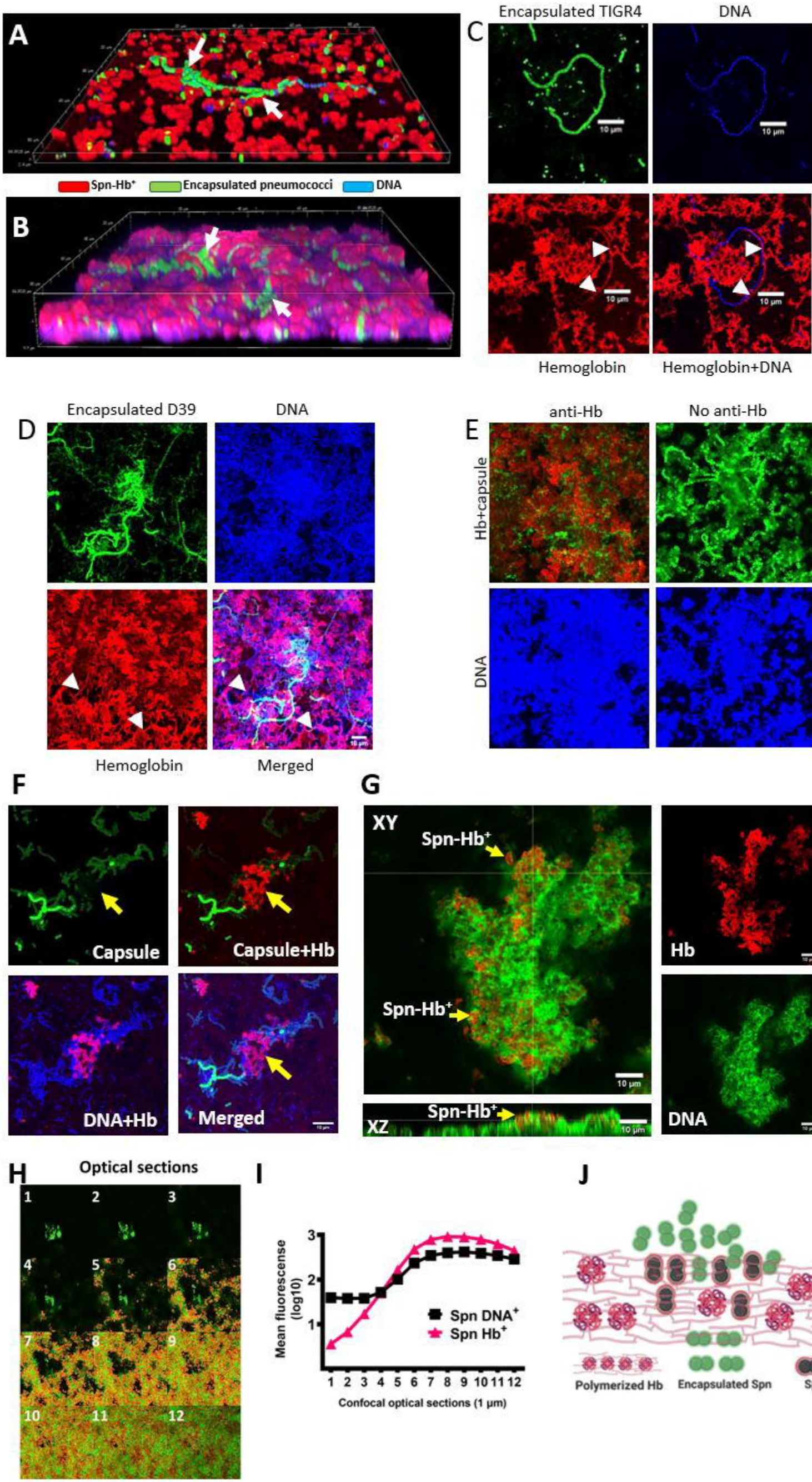
A
Spn-Hb+
Encapsulated pneumococci
DNA
B
C
Encapsulated TIGR4
DNA
10 µm
Hemoglobin
Hemoglobin+DNA
D
Encapsulated D39
DNA
Hemoglobin
Merged
E
anti-Hb
No anti-Hb
Hb+capsule
DNA
F
Capsule
Capsule+Hb
DNA+Hb
Merged
G
XY
Spn-Hb+
Hb
DNA
XZ
H
Optical sections
1
2
3
4
5
6
7
8
9
10
11
12
I
Mean fluorescense (log10)
Spn DNA+
Spn Hb+
Confocal optical sections (1 µm)
J
Polymerized Hb
Encapsulated Spn
Spn-Hb+

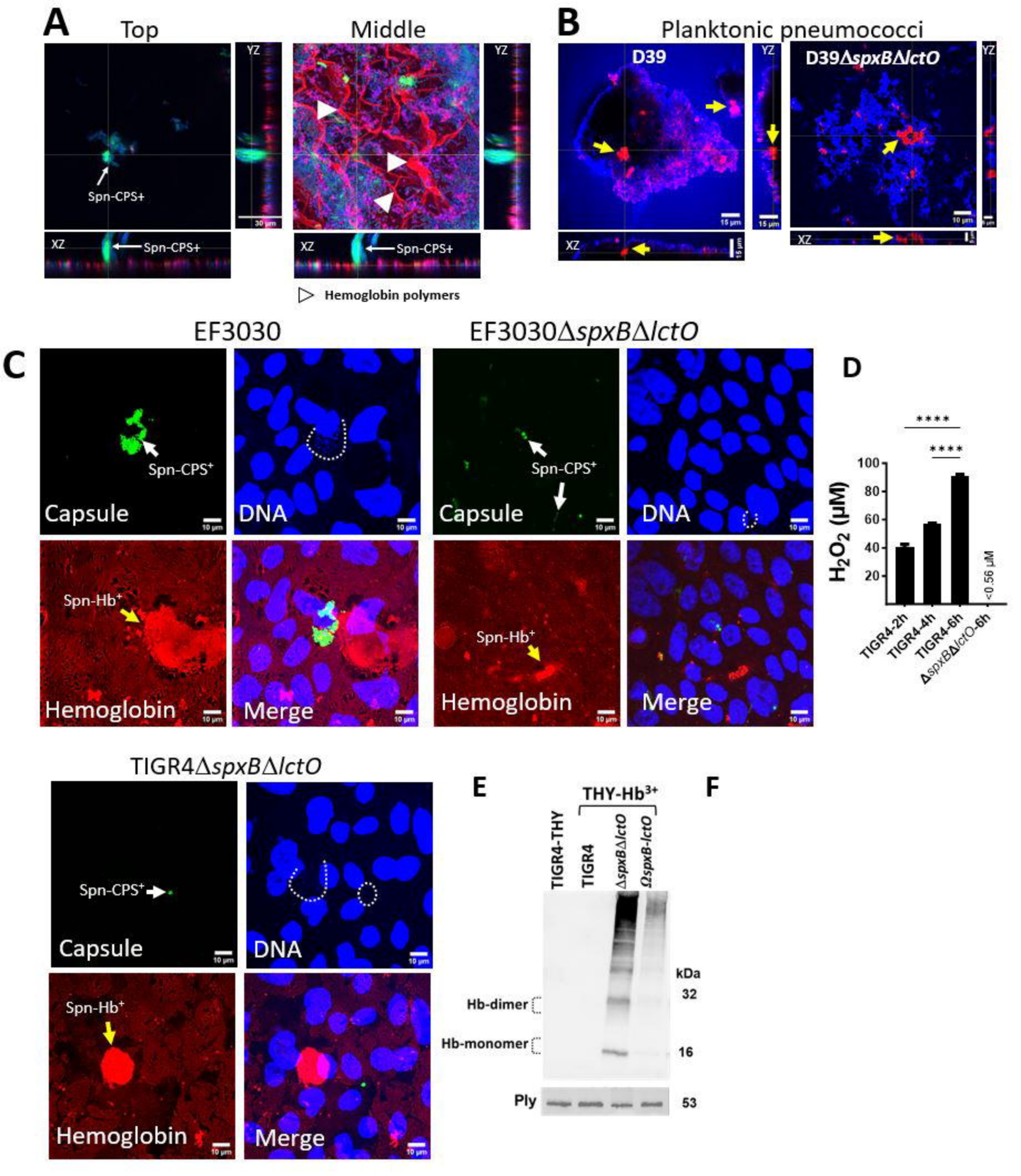
A
Top
Middle
YZ
XZ
Spn-CPS+
Hemoglobin polymers
B
Planktonic pneumococci
D39
D39ΔspxBΔlctO
C
EF3030
EF3030ΔspxBΔlctO
Spn-CPS+
Spn-Hb+
Capsule
DNA
Hemoglobin
Merge
D
****
****
H2O2 (μM)
100
80
60
40
20
<0.56 μM
TIGR4-2h
TIGR4-4h
TIGR4-6h
ΔspxBΔlctO-6h
TIGR4ΔspxBΔlctO
E
THY-Hb3+
TIGR4-THY
TIGR4
ΔspxBΔlctO
ΩspxB-lctO
kDa
Hb-dimer
Hb-monomer
32
16
Ply
53
F

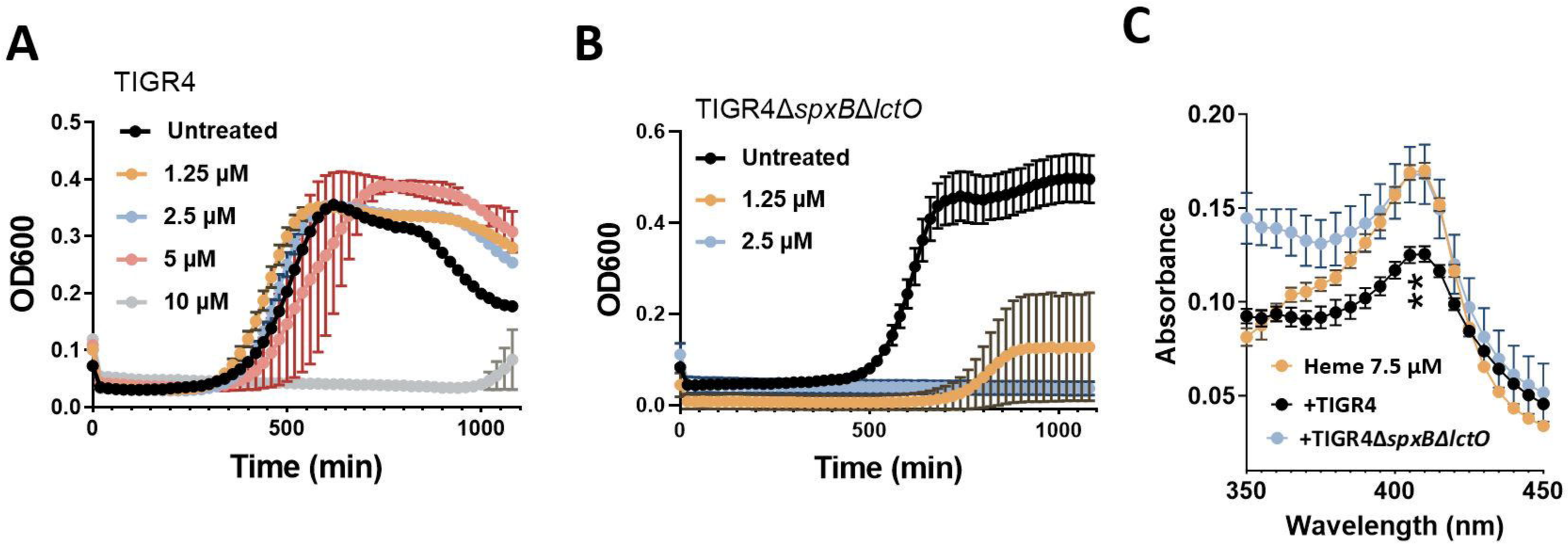
A
TIGR4
Untreated
1.25 μM
2.5 μM
5 μM
10 μM
OD600
Time (min)
B
TIGR4ΔspxBΔlctO
Untreated
1.25 μM
2.5 μM
OD600
Time (min)
C
Heme 7.5 μM
+TIGR4
+TIGR4ΔspxBΔlctO
Absorbance
Wavelength (nm)

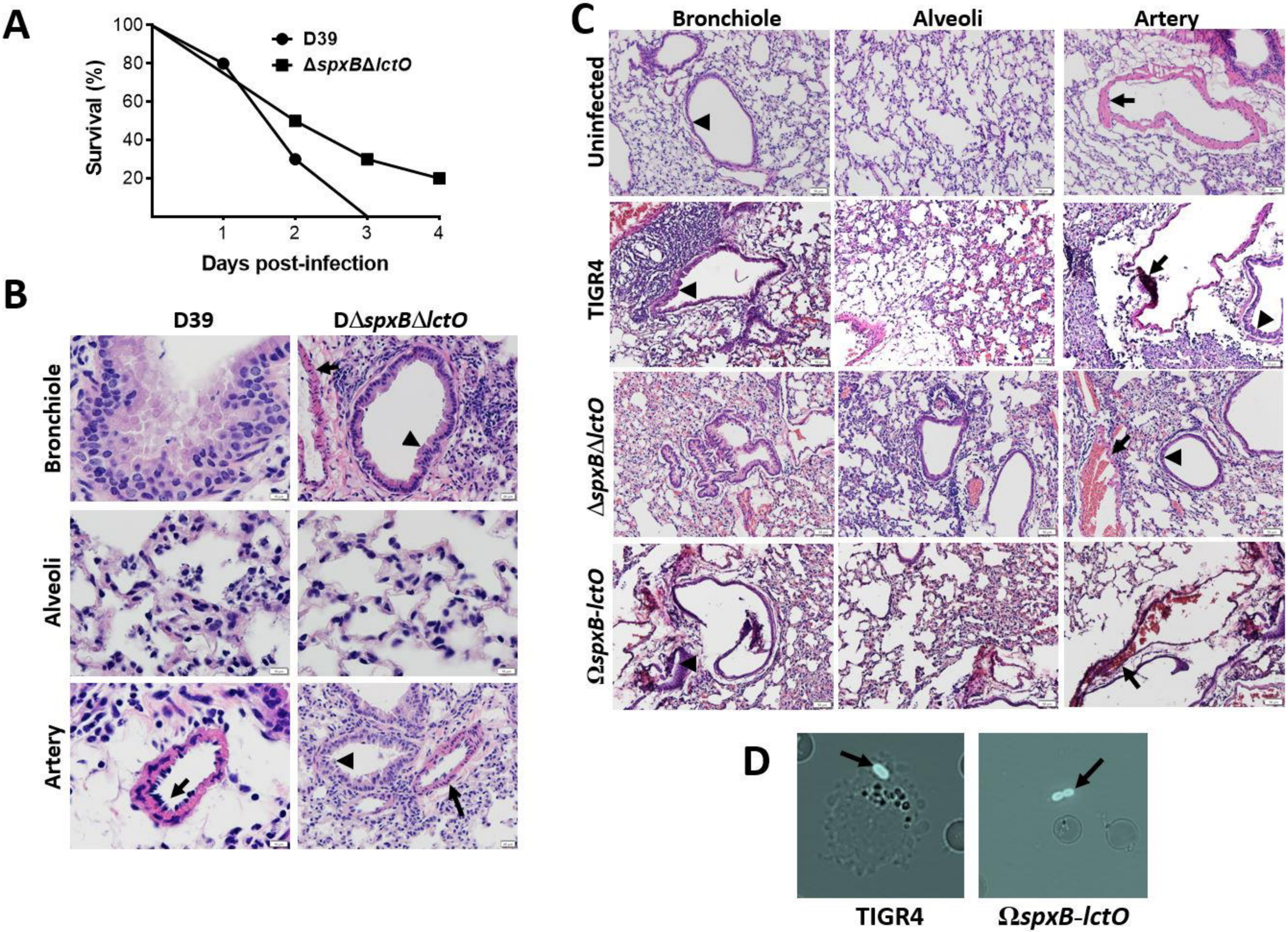
A
100
80
60
40
20
Survival (%)
D39
ΔspxBΔlctO
1
2
3
4
Days post-infection
B
D39
DΔspxBΔlctO
Bronchiole
Alveoli
Artery
C
Bronchiole
Alveoli
Artery
Uninfected
TIGR4
ΔspxBΔlctO
ΩspxB-lctO
D
TIGR4
ΩspxB-lctO

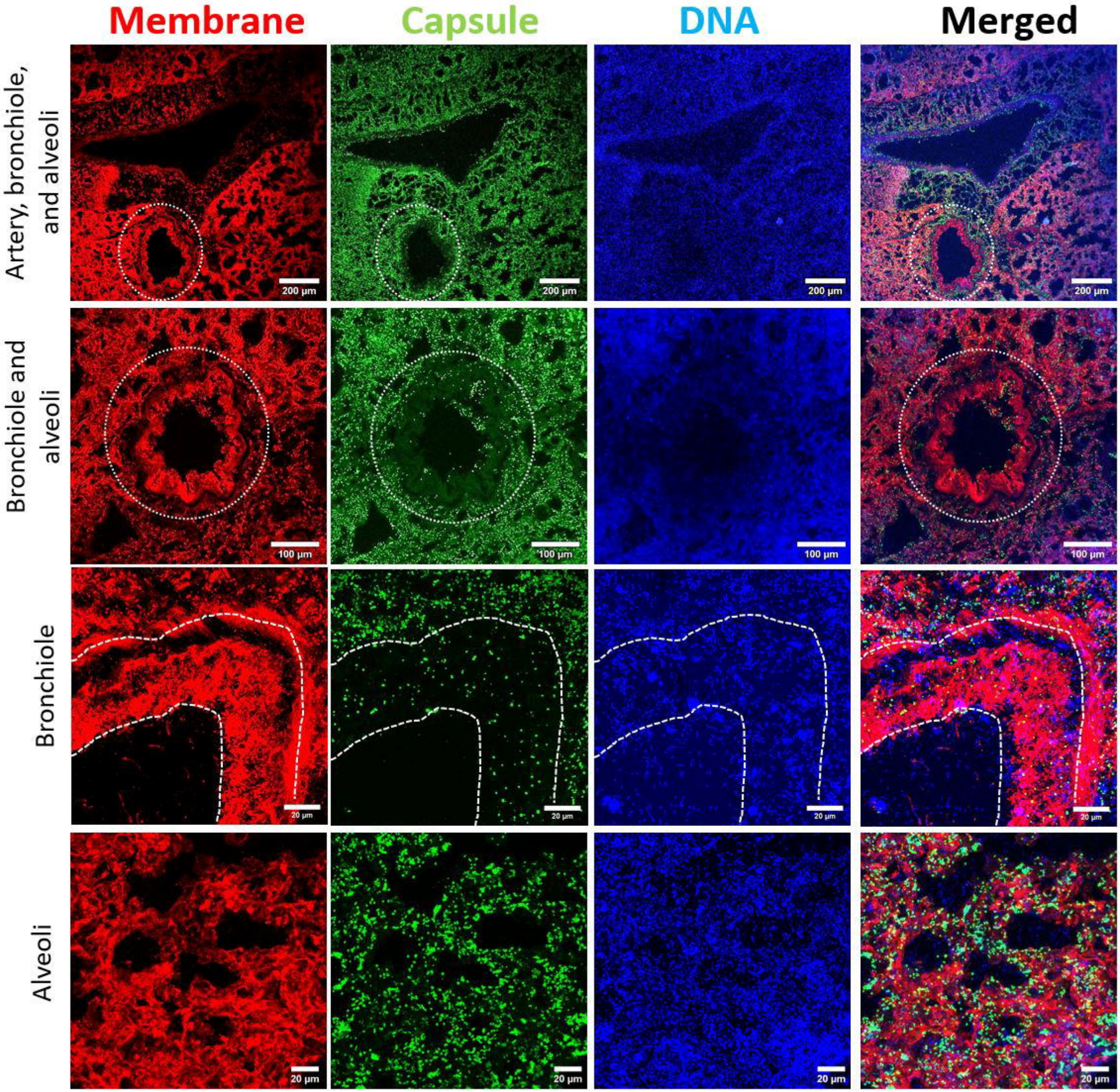
Membrane
Capsule
DNA
Merged
Artery, bronchiole, and alveoli
Bronchiole and alveoli
Bronchiole
Alveoli
200 µm
100 µm
20 µm

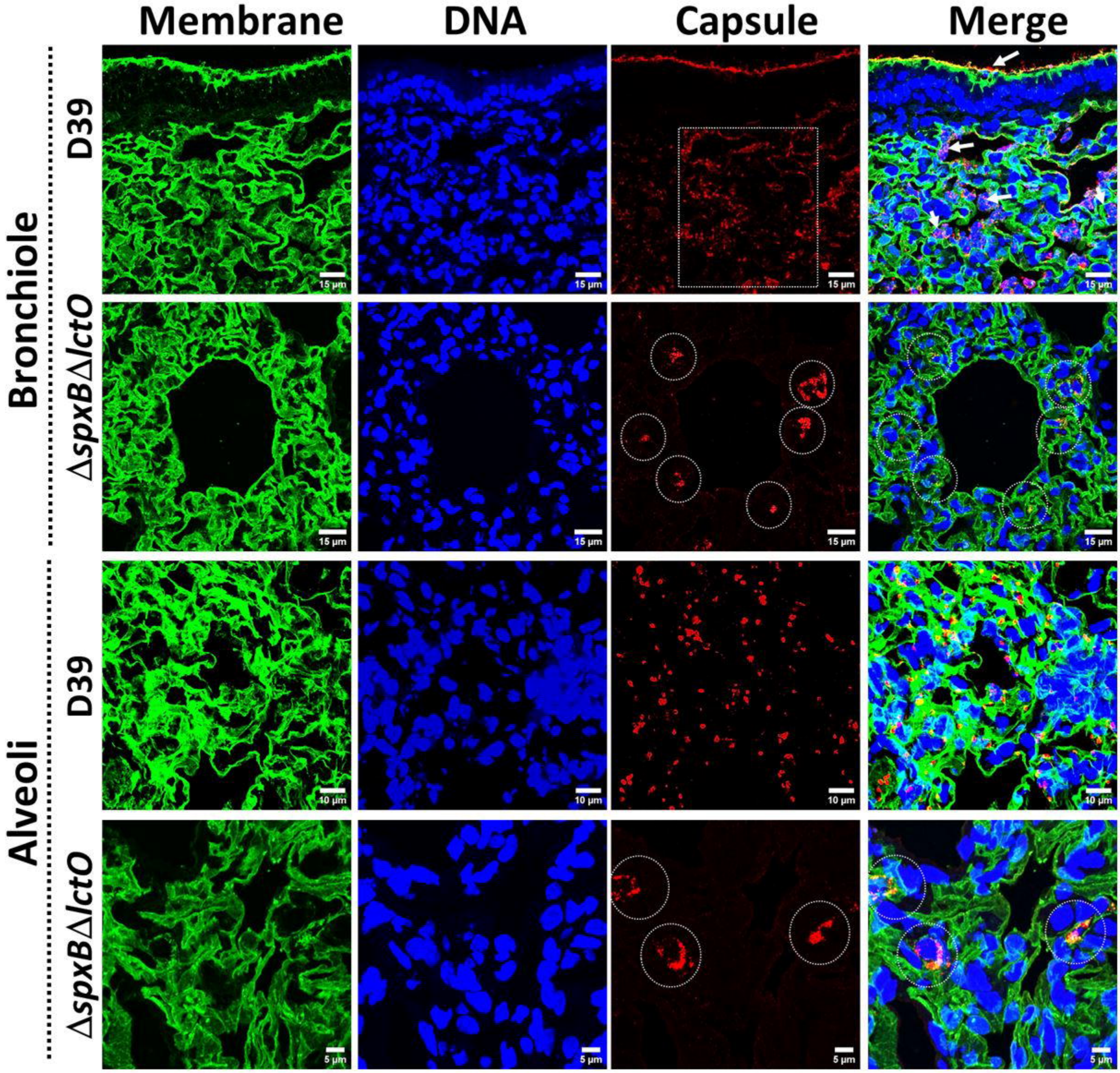
Membrane
DNA
Capsule
Merge
Bronchiole
D39
ΔspxBΔlctO
Alveoli
D39
ΔspxBΔlctO
15 µm
10 µm
5 µm

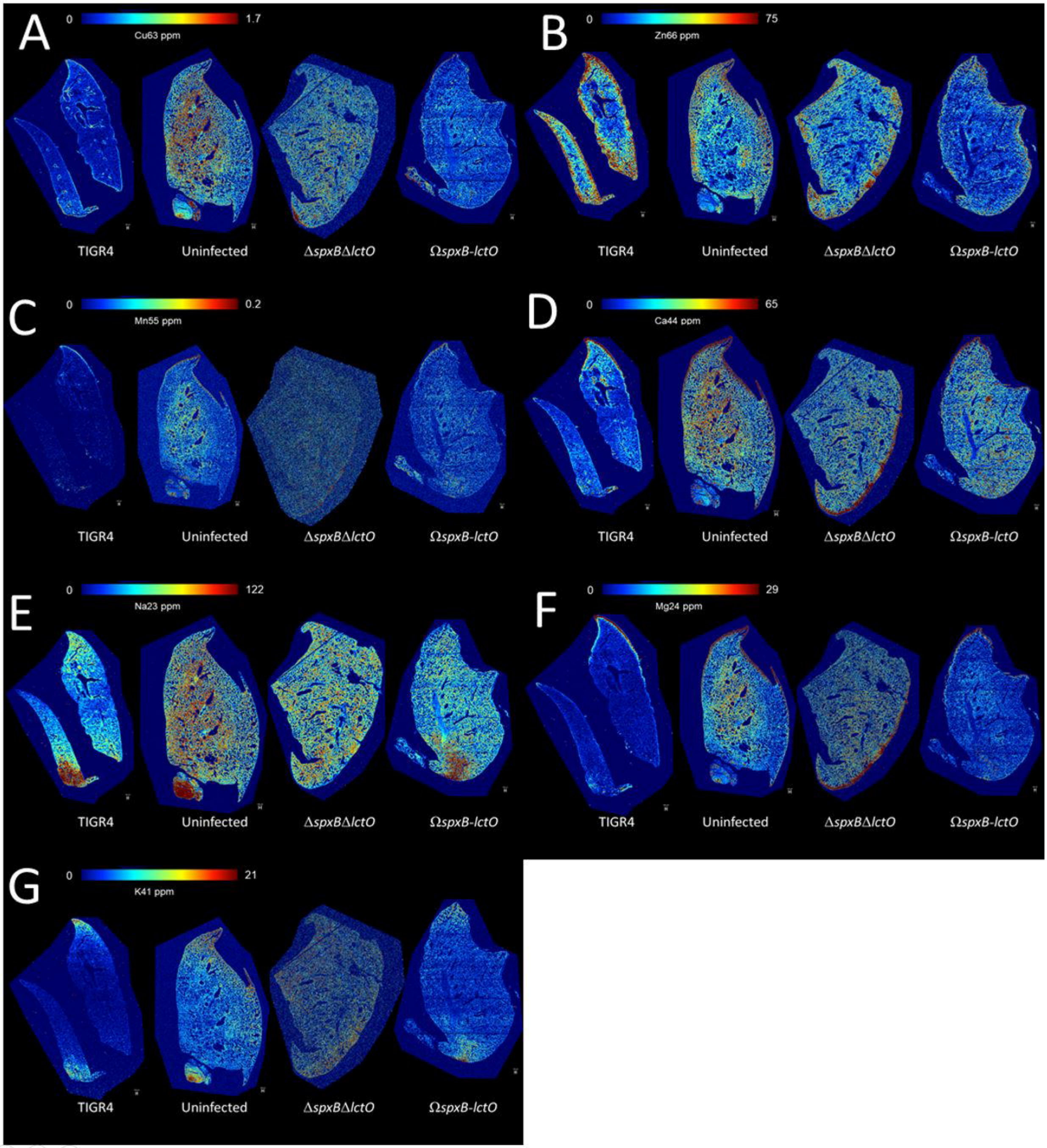
A
0
1.7
Cu63 ppm
TIGR4
Uninfected
ΔspxBΔlctO
ΩspxB-lctO
B
0
75
Zn66 ppm
TIGR4
Uninfected
ΔspxBΔlctO
ΩspxB-lctO
C
0
0.2
Mn55 ppm
TIGR4
Uninfected
ΔspxBΔlctO
ΩspxB-lctO
D
0
65
Ca44 ppm
TIGR4
Uninfected
ΔspxBΔlctO
ΩspxB-lctO
E
0
122
Na23 ppm
TIGR4
Uninfected
ΔspxBΔlctO
ΩspxB-lctO
F
0
29
Mg24 ppm
TIGR4
Uninfected
ΔspxBΔlctO
ΩspxB-lctO
G
0
21
K41 ppm
TIGR4
Uninfected
ΔspxBΔlctO
ΩspxB-lctO

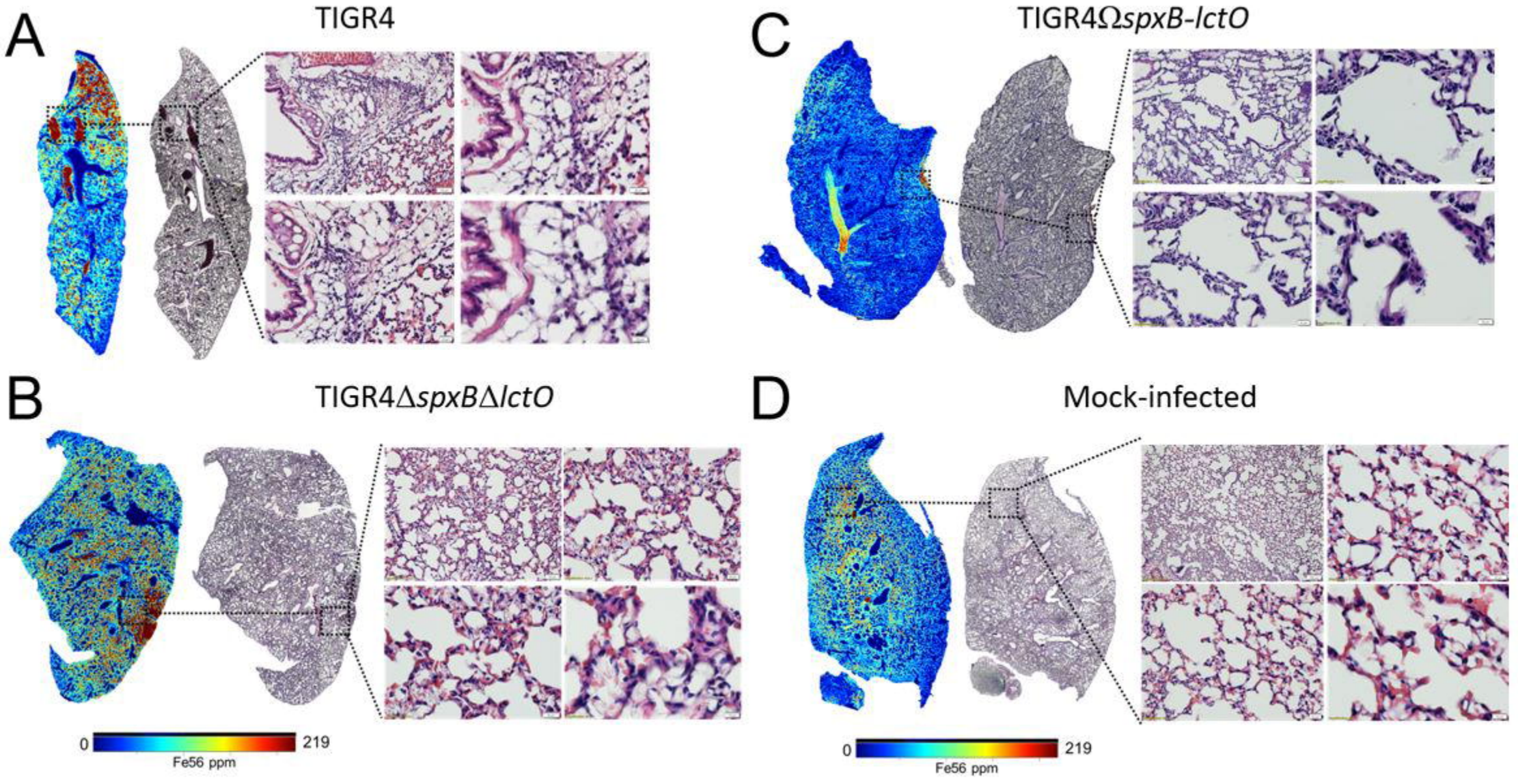
A
TIGR4
C
TIGR4Ω*spxB-lctO*
B
TIGR4Δ*spxB*Δ*lctO*
D
Mock-infected
0
219
Fe56 ppm
0
219
Fe56 ppm

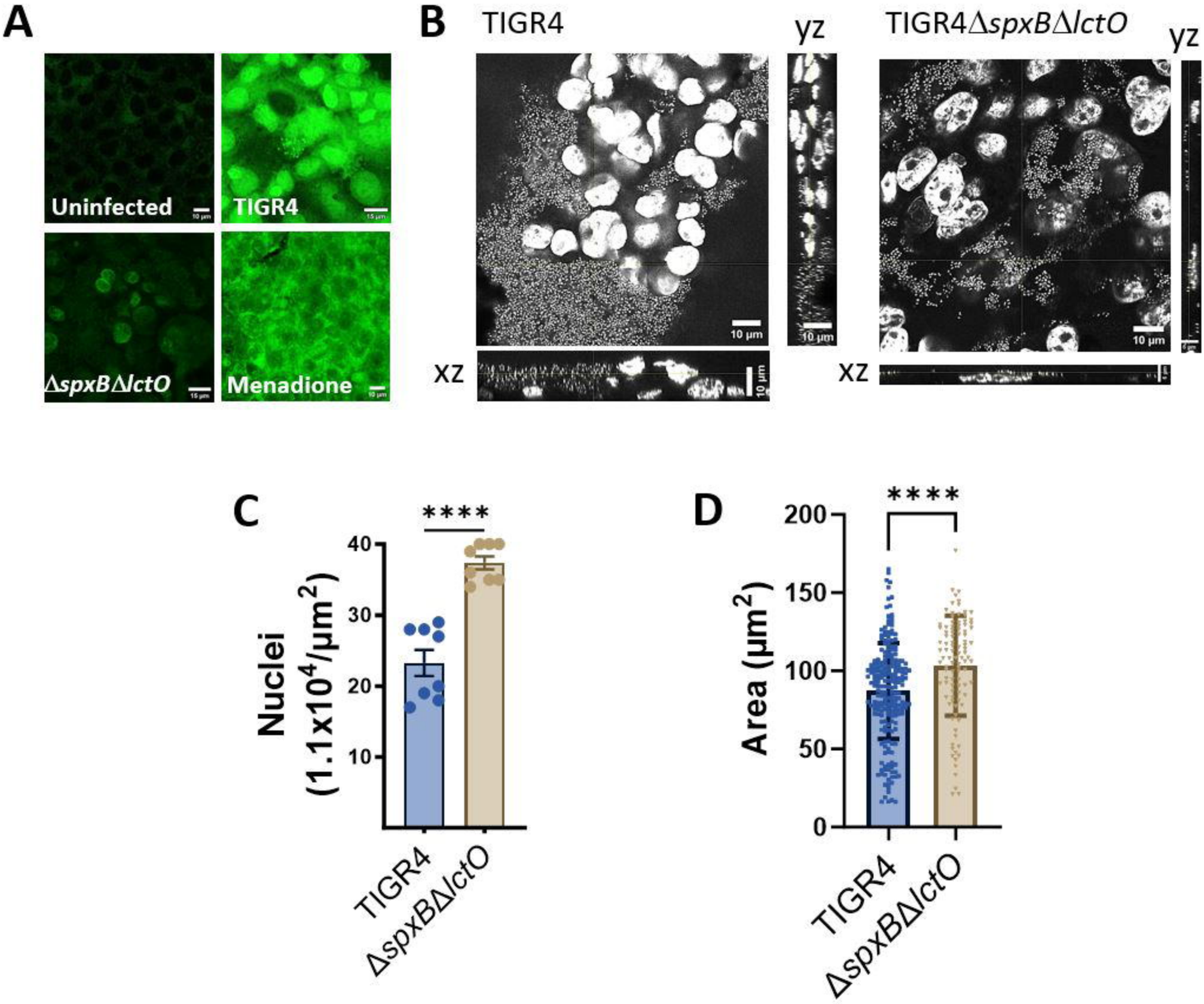
A
Uninfected
TIGR4
ΔspxBΔlctO
Menadione
B
TIGR4
yz
xz
10 µm
TIGR4ΔspxBΔlctO
yz
xz
10 µm
C
****
Nuclei
(1.1x10^4/µm^2)
40
30
20
10
TIGR4
ΔspxBΔlctO
D
****
Area (µm^2)
200
150
100
50
0
TIGR4
ΔspxBΔlctO

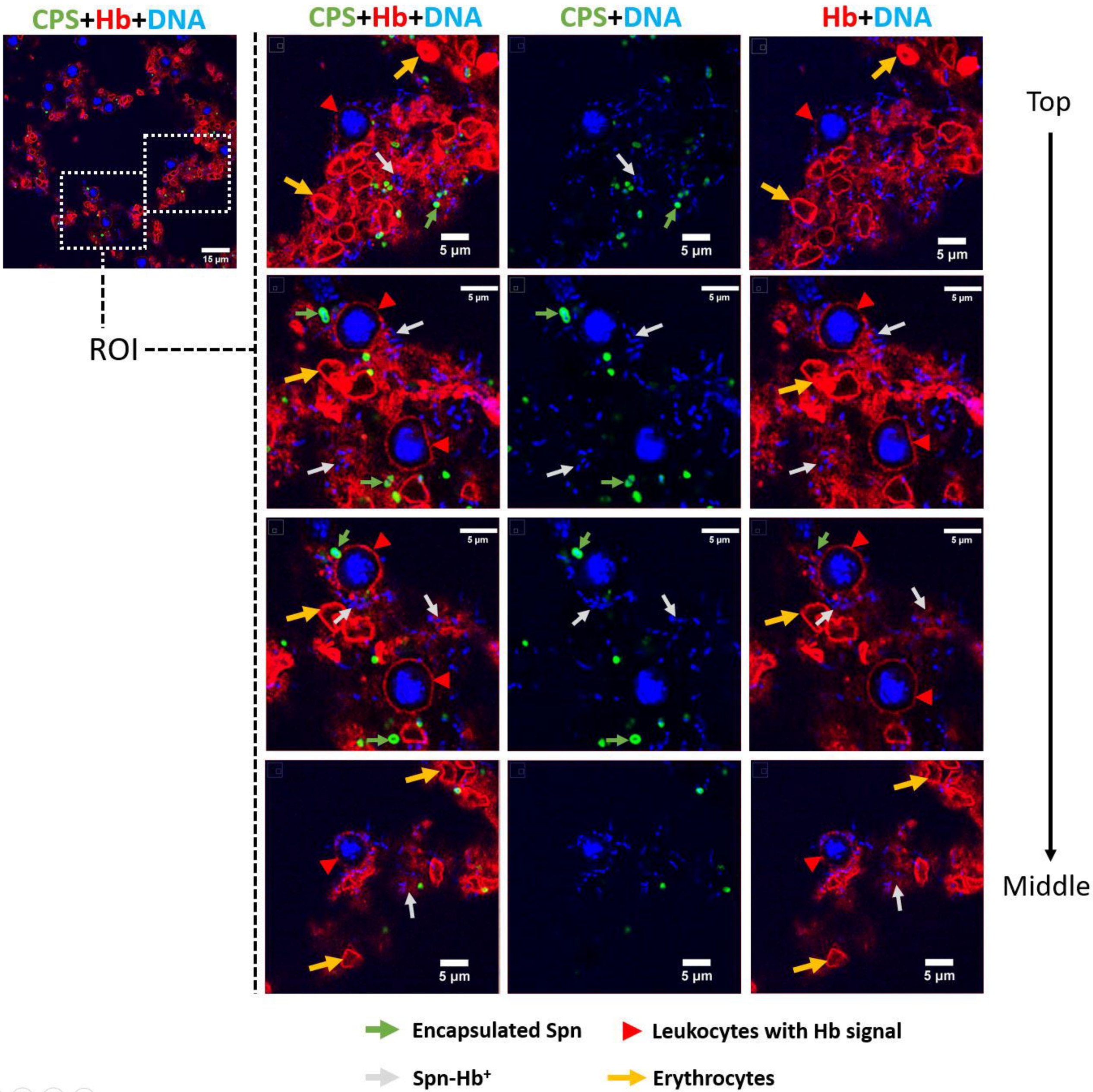
CPS+Hb+DNA
CPS+Hb+DNA
CPS+DNA
Hb+DNA
15 µm
5 µm
ROI
Top
Middle
Encapsulated Spn
Leukocytes with Hb signal
Spn-Hb+
Erythrocytes

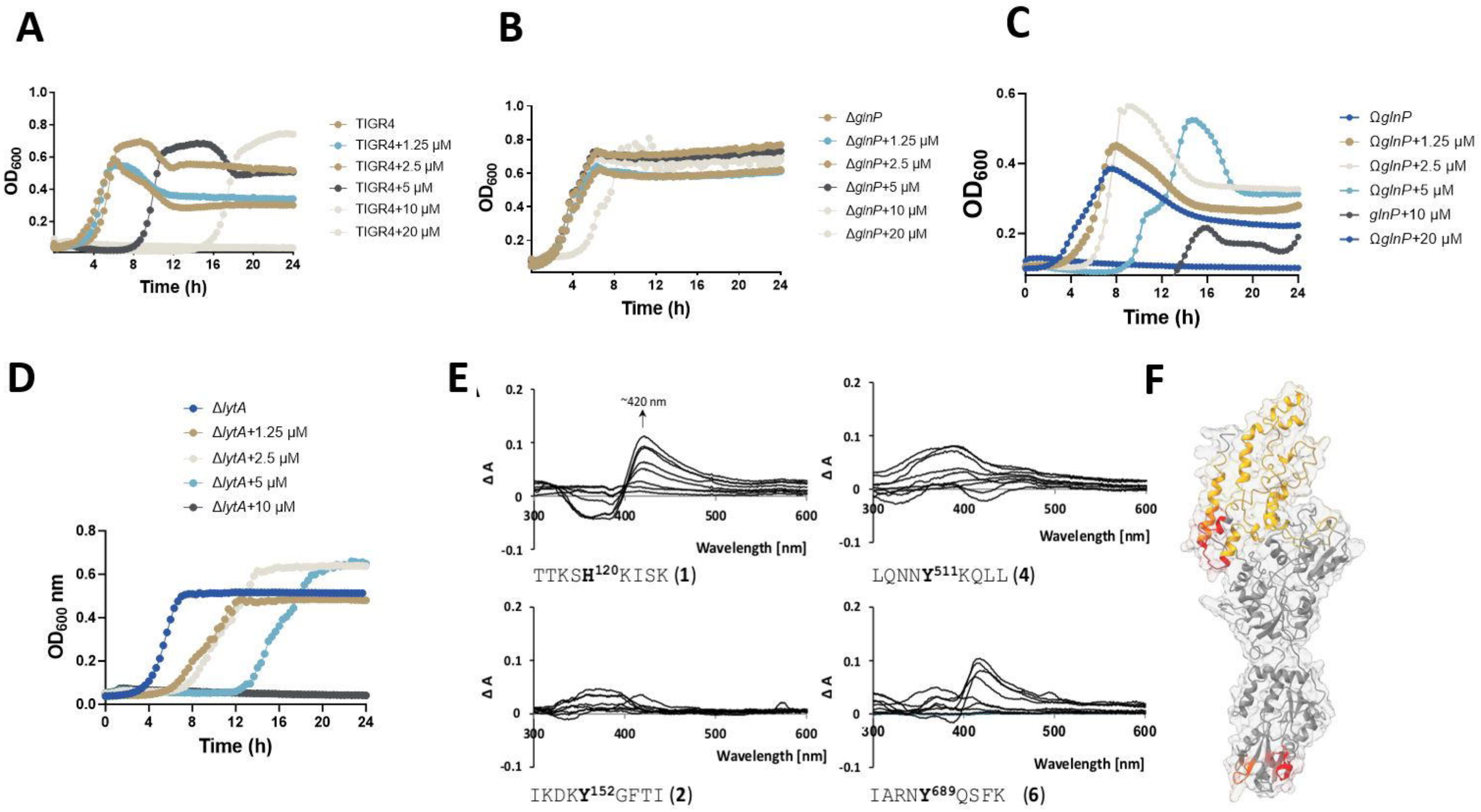
A
B
C
D
E
F
OD600
Time (h)
TIGR4
TIGR4+1.25 µM
TIGR4+2.5 µM
TIGR4+5 µM
TIGR4+10 µM
TIGR4+20 µM
ΔglnP
ΔglnP+1.25 µM
ΔglnP+2.5 µM
ΔglnP+5 µM
ΔglnP+10 µM
ΔglnP+20 µM
ΩglnP
ΩglnP+1.25 µM
ΩglnP+2.5 µM
ΩglnP+5 µM
glnP+10 µM
ΩglnP+20 µM
ΔlytA
ΔlytA+1.25 µM
ΔlytA+2.5 µM
ΔlytA+5 µM
ΔlytA+10 µM
OD600 nm
~420 nm
Δ A
Wavelength [nm]
TTKSH120KISK (1)
LQNNY511KQLL (4)
IKDKY152GFTI (2)
IARNY689QSFK (6)

Table S1. Metabolites differentially regulated in the supernatant of THY-Hb^{3+} cultures infected with TIGR4 compared to plain THY.

Molecule	Class	Adjusted *p*-value	Fold-change
THY-Hb^{3+}/TIGR4 compared with THY/TIGR4			
Aspartic acid	Organic acid	0.006	0.955886
Creatinine	Organic acid	0.003	1.616839
Guanine	Organoheterocyclic compounds	0.026	0.551192
Guanosine	Nucleosides, nucleotides, and analogues	0.026	1.301212
Isoleucine	Organic acids and derivatives	0.013	1.051325
Leucine	Organic acids and derivatives	0.013	1.079021
Methionine	Organic acids and derivatives	0.004	0.591517
Methionine sulfoxide	Organic acids and derivatives	0.004	2.001035
Nicotinamide	Organoheterocyclic compounds	0.031	0.899909
Oleamide NIST	Lipids and lipid-like molecules	0.006	1.119466
Oxoproline	Organic acids and derivatives	0.006	0.945675
Putrescine	Organic nitrogen compounds	0.004	1.683839
Pyruvic acid	Organic acids and derivatives	0.004	0.053013
Shikimic acid	Organic oxygen compounds	0.003	0.722413
Tyrosine	Organic acid	0.013	1.077018
Tyrosol	Benzenoids	0.004	1.614024
THY-Hb^{3+}/TIGR4Δ*spxB*Δ*lctO* compared with THY/TIGR4Δ*spxB*Δ*lctO*			
Creatinine	Organic acid	0.003	2.320286
Shikimic acid	Organic oxygen compounds	0.003	0.623841
THY-Hb^{3+}/TIGR4 compared with THY-Hb^{3+}/TIGR4Δ*spxB*Δ*lctO*			
Creatinine	Organic acids and derivatives	0.01	1.457524

Nicotinamide	Organoheterocyclic compounds	0.003	1.553198
Nicotinic acid	Organoheterocyclic compounds	0.003	0.753161
Tryptophan	Organoheterocyclic compounds	0.026	0.923314
Tyrosine	Organic acids and derivatives	0.013	0.88953
Tyrosol	Benzenoids	0.004	0.589645
THY/TIGR4 compared with THY/TIGR4Δ*spxB*Δ*lctO*			
Guanosine	Nucleosides, nucleotides, and analogues	0.026	1.204739
Methionine	Organic acids and derivatives	0.004	0.57766
Methionine sulfoxide	Organic acids and derivatives	0.004	2.064243
N-acetylornithine	Organic acids and derivatives	0.013	0.840103
Nicotinamide	Organoheterocyclic compounds	0.003	1.692531
Nicotinic acid	Organoheterocyclic compounds	0.003	0.762097
Oleamide NIST	Lipids and lipid-like molecules	0.017	1.082949
Orotic acid	Organoheterocyclic compounds	0.013	0.667873
Putrescine	Organic nitrogen compounds	0.004	1.622776
Pyruvic acid	Organic acids and derivatives	0.004	0.178594
Shikimic acid	Organic oxygen compounds	0.031	1.068225

Table S2. Minimum inhibitory concentration of heme for *Streptococcus pneumoniae* strains.

***Streptococcus pneumoniae* Strain**	**MIC (µM)***
D39	15
D39Δ*spxB*Δ*lctO*	5
D39Δ*spxB*	7
D39Δ*spbph*37	12.5
D39Δ*piu*Δ*pia*	12.5
EF3030	15
EF3030Δ*spxB*Δ*lctO*	5
EF3030Δ*spxB*	7.5

*A modified MIC assay in a 96-well microplate was performed to assess as recommended by the Clinical Laboratory Standards Institute (CLSI).

Table S3. Genes of *S. pneumoniae* strain D39 essential for growth in hemoglobin identified by HITS.

Gene name (gene ID)	Encoded protein	Sites	log2FC	p-value	Adj. p-value
Biofilms (Hb^-) compared to biofilms (Hb^+), Hb^+/Hb^-					
glnP (SPD_1098)	ABC transporter permease subunit	117	1.68	0	0
gidA (SPD_0129)	tRNA uridine 5-carboxymethylaminome	70	-1.2	0.0002	0.28313
tpx (SPD_1464)	Thiol peroxidase	23	1.43	0.0005	0.35392
cls (SPD_0185)	Cardiolipin synthetase	120	0.69	0.0007	0.4247
sufS (SPD_0764)	Cysteine desulfurase	56	1.7	0.0015	0.53087
sufB (SPD_0765)	SUF system FeS assembly protein	16	2.34	0.0015	0.53087
(SPD_1295)	Putative hemolysin	38	1.24	0.0024	0.67952
(SPD_0064)	GntR family transcriptional regulator,	46	1.15	0.0037	0.92435
malQ (SPD_1933)	4-alpha-glucanotransferase	74	0.79	0.0042	0.93881
ppc (SPD_0953)	Phosphoenolpyruvate carboxylase	179	-0.72	0.0041	0.93881
Planktonic pneumococci (Hb^-) compared to biofilms (Hb^+), Hb^+/Hb^-					
glnP (SPD_1098)	ABC transporter permease subunit	127	-1.38	0	0
pbp1A (SPD_0336)	Penicillin-binding protein 1A	143	-2.2	0	0
(SPD_1649)	piuC iron uptake ABC transporter permease	97	-1.11	0	0
amiC (SPD_1670)	Oligopeptide ABC transporter, permease protein AmiC	97	-1.11	0.0001	0.07078
pbp2A (SPD_1821)	Penicillin-binding protein Pbp2A	144	-0.73	0.0012	0.63705
Planktonic pneumococci (Hb^+) compared to biofilms- (Hb^+), Biofilm/Planktonic					

lytC (SPD_1403)	1,4-beta-N-acetylmuramidase, LytC	114	-1.09	0.0001	0.14157
pbp2A (SPD_1821)	Penicillin-binding protein 2A, Pbp2A	135	-0.71	0.0002	0.21235
pbp2A (SPD_1925)	Penicillin-binding protein 1B, Pbp1B	158	-0.53	0.0006	0.50964
cls (SPD_0185)	Cardiolipin synthetase	120	0.64	0.0013	0.61346
(SPV_1332)	Membrane protein, putative	81	0.97	0.0021	0.81079
(SPV_1672)	Membrane protein, putative	80	2.61	0.0025	0.88479
Planktonic pneumococci (Hb^-) compared to Planktonic pneumococci (Hb^+), Hb^+/Hb^-					
SPV_RS05135	UDP-N-acetylglucosamine 1-carboxyvinyltransferase, murA2	97	-1.97	0.001	1
amiC (SPD_1670)	Oligopeptide ABC transporter, permease protein AmiC,	97	-0.74	0.0031	1
(SPD_0361)	transcription regulator, putative	158	-0.7	0.004	1
pbp1A (SPD_0336)	Penicillin-binding protein 1A	143	-0.82	0.0044	1
dltA (SPD_2005)	D-alanine--D-alanyl carrier protein ligase	81	-0.63	0.01	1
mltG (SPD_1346)	Endolytic murein transglycosylase, MltG	100	-2.27	0.0101	1
lytB (SPD_0853)	Endo-beta-N-acetylglucosaminidase, LytB_1	155	0.66	0.011	1
sufB (SD_0766)	FeS assembly protein SufB	87	1.68	0.013	1
mtlA (SPD_0360)	PTS system, mannitol-specific IIBC components	131	-0.6	0.02	1
lytC (SPD_1403)	1,4-beta-N-acetylmuramidase, LytC	122	0.73	0.02	1
sufS (SPD_0764)	Cysteine desulfurase, SufS	58	1.48	0.027	1
ppc (SPD_0953)	Phosphoenolpyruvate carboxylase, SPD_0953	192	-0.73	0.028	1
guaB (SPD_2055)	Inosine-5'-monophosphate dehydrogenase	86	-0.98	0.035	1
dagA (SPD_0372)	D-alanine glycine permease	68	-0.84	0.036	1
ccpA (SPD_1797)	Catabolite control protein A, CcpA	66	-0.94	0.038	1

glnP (SPD_1098)	ABC transporter permease subunit	127	0.62	0.039	1
(SPD_0350)	Membrane protein, putative	36	-1.37	0.041	1
sufD (SPD_0763)	FeS assembly protein SufD	61	1.17	0.043	1
dltD (SPD_2002)	Undecaprenol-phosphate-poly D-alanine transfer protein	80	-0.62	0.047	1
glnA (SPD_0448)	Glutamine synthetase, type I	66	1.05	0.049	1

Table S4. Analytical characterization of the amino acid ABC transporter-derived peptides.

No.	Sequence	Position in the sequence of amino acid ABC transporter	Mw (Mw theor.) [g/mol]	HPLC t_R [min]	TLC R_f
1	TTKSHKISK	116 – 124	514.82[a] (1027.61)	14.22[c], 7.80[d]	0.60[g]
2	IKDKYGFTI	148 – 156	542.32[a] (1082.38)	29.04[e]	0.52[h], 0.40[i], 0.35[j]
3	NQSKYGYKIKT	391 – 401	443.58[b] (1327.73)	21.37[e], 11.16[f]	0.75[g]
4	LQNNYKQLL	507 – 515	566.83[a] (1131.64)	28.14[e]	0.42[h], 0.44[i], 0.48[j]
5	SPYKSLR	545 – 551	425.25[a] (848.45)	20.01[e]	0.38[h], 0.25[j]
6	IARNYQSFK	685 – 693	563.32[a] (1124.61)	21.96[e]	0.78[g], 0.38[h]

Mass peaks were detected as $[M+2H]^{2+}$ (a) and $[M+3H]^{3+}$ (b) by ESI-MS. HPLC conditions were as follows: Water with 0.1% TFA (eluent A), acetonitrile with 0.1% TFA (eluent B): 0% – 30% eluent B in 30 min (c), 5% – 55% eluent B in 50 min (d), 0% – 40% eluent B in 40 min (e), and 10% – 40% eluent B in 30 min (f). The following TLC systems were used: n-propanol/25% ammonia (3:7, v/v) (g), n-butanol/acetic acid/water (48:18:24, v/v) (h), n-propanol/25% ammonia (7:3, v/v) (i), and pyridine/ethyl acetate/acetic acid/water (5:5:1:3, v/v) (j). ABC, ATP-binding cassette; ESI-MS, electrospray ionization mass spectrometry. All peptides were >95 % HPLC pure.

Table S5. Primers used in this study.

Primer Name	Sequence (5′-3′)
Glnp up Fwd	TGCCAAAAGAACCACCTGAT
Glnp up Rev	TCTAAGTCTTATTCCCGGGTTTCTGCTTTGGCAATACCT
Glnp down Fwd	TCTAAATTTGGAAGCCGGCGAAACGCTTAGAAAAGAGG
Glnp down Rev	CCATCCTTGATTTGGCAGAT
Ery Fwd	CCCGGGAATAAGACTTAGA
Ery Rev	CGGCTTCCAAATTTACA
Glnp Fwd (screening)	TAAATACGAGCACCTGGTTACTG
Glnp Rev (screening)	GATTTCAATTTCAAACCTTGGTC
ΩGlnp up Fwd	AGGCTCACTTCAGGAACGTC
ΩGlnp up Rev	TAAGCCCCGAAAAGCAACACCGAGCAGTTGGTGGATAACA
ΩGlnp down Fwd	ACTTCTTGAACACTTGCCGAAGAATCCTCTCTCCATGTGCT
ΩGlnp down Rev	GCATAGGCGGTATCAGAAACA
Cam Fwd	GTGTTGCTTTTCGGGGCTTA
Cam Rev	TCGGCAAGTGTTCAAGAAGT
ΩGlnp Fwd	TGTCAAACCCAGATGCTCCA
ΩGlnp Rev	TTCACATTTGGCTCGCTACG
MK147 hlpA-Gfp Fwd	GATAAAAGGTGATGAGGGTAATGC
MK147 hlpA-Gfp Rev	TTCAATTCGACAAAACGAGAGTAA
ΩGlnp Fwd (plasmid)	AGCACGGGATCCGCAACCAAAGTGCAATCCTAGT
ΩGlnp Rev (plasmid)	ACTGTGTCTAGATGTTCTTCATATCCCCGTCCT
Nrf1 - TaqMan® Gene Expression Assay	Cat# 4331182
GAPDH - TaqMan® Gene Expression Assay	Cat# 4331182
Cat - TaqMan® Gene Expression Assay	Cat# 4331182
SOD1 - TaqMan® Gene Expression Assay	Cat# 4331182
HITS primers	
adap1	AGTTCTCCAGGTCTTGCGTTGCTCTTCCGATC*T
adap3	p-GATCGGAAGAGCACACGTCTGAACTCCAGTCAC
marout-nest 2	AGACCGGGGACTTATCAG
oljJD	GTGACTGGAGTTCAGACGT*G
MarPCR2-5N	AATGATACGGCGACCACCGAGATCTACACTCTTTCCCTACACGACGCTCTTCCGATCTNNNNNC CGGGGACTTATCAGCCAAC*C
BC#	CAAGCAGAAGACGGCATACGAGATxxxxxxGTGACTGGAGTTCAGACGTGTG

a * = phosphorothioate linkage, b p= 5’ phosphorylation, c xxxxxx = 6bp Illumina TruSeq barcode sequence

KEY RESOURCES TABLE

REAGENT OR RESOURCE	SOURCE	IDENTIFIER
Antibodies		
Rabbit anti-β Tubulin	Proteintech	Cat# 10068-1-AP
Mouse anti-β Actin	Proteintech	Cat# 66009-1-Ig
Mouse anti-GAPDH	Proteintech	Cat# 60004-1-Ig
Mouse anti-Catalase	Proteintech	Cat# 21260-1-AP
Mouse anti-Hemoglobin β, Alexa Fluor 546	Santa Cruz Biotechnology	Cat# sc-21757 AF546
Mouse anti-Hemoglobin β	Santa Cruz Biotechnology	Cat# sc-21757
Rabbit anti-Hemoglobin α	Santa Cruz Biotechnology	Cat# sc-21005
Mouse anti-ply	Santa Cruz Biotechnology	Cat# sc-80500
Goat anti-Hemoglobin	Invitrogen	Cat# PA-29342
Rabbit Anti-PfbA Serum	Kawabata lab	N/A
Rabbit anti-pneumococcal antisera type 4	Statens Serum Institut	Cat# 16747
Rabbit anti-pneumococcal antisera type 2	Statens Serum Institut	Cat# 76856
Rabbit anti-pneumococcal antisera type 19	Statens Serum Institut	Cat# 16911
Rabbit anti-pneumococcal antisera type 3	Statens Serum Institut	Cat# 76858
Rabbit anti-pneumococcal Omni antisera	Statens Serum Institut	Cat# 2438
Capsule 4, Alexa Fluor 488	This study	N/A
Capsule 4, Alexa Fluor 555	This study	N/A
Capsule 2, Alexa Fluor 555	This study	N/A
Capsule 3, Alexa Fluor 555	This study	N/A
Capsule 19, Alexa Fluor 555	This study	N/A
S. pneumoniae Capsule, Alexa Fluor 488	This study	N/A
Anti- Anti-WGA, Alexa Fluor 555	Invitrogen	Cat# W32464
Anti-WGA, Alexa Fluor 488	Invitrogen	Cat# W11261
Gout anti-mouse CD45	R&D systems, Bio-techne	Cat# AF114
Secondary Antibody, StarBright Blue 520 Goat anti-mouse IgG	Biorad	Cat# 12005866
Secondary Antibody, StarBright Blue 520 Goat anti-rabbit IgG	Biorad	Cat# 12005869
Secondary Antibody, Rabbit anti-mouse IgG (H+L) HRP	Jackson ImmunoResearch	Cat# 315-035-045
Secondary Antibody, Goat anti-rabbit IgG (H+L) HRP	Jackson ImmunoResearch	Cat# 111-035-045
Secondary Antibody, Donkey anti-goat IgG-HRP	Santa Cruz Biotechnology	Cat# sc-2020
Goat anti-mouse Ig, Human ads-FITC	SouthernBiotech	Cat# 1010-02
Bacterial strains		
TIGR4	Clinical isolate, serotype 4	Tettelin et al., 2001
P2422	TIGR4Δ*cps*; Kan^R	Zafar et al., 2016
SPJV29	TIGR4Δ*spxB*; Ery^R	McDevitt et al., 2020
SPJV41	TIGR4Δ*spxB*Δ*lctO*; Ery^R, Spc^R	McDevitt et al., 2020
	TIGR4Δ*spxB*Δ*lctO*Ω*gfp*; Ery^R, Spc^R, Cam^R	This study
SPJV44	TIGR4Δ*spxB*Δ*lctO*Ω*spxB-lctO*; Ery^R, Spc^R, Cam^R	Alibayov et al., 2022
SPJV52	TIGR4Δ*glnP*; Ery^R	This study
SPJV53	TIGR4Δ*glnP*Ω*glnP*; Cam^R	This study
EF3030	Clinical isolate, serotype 19F	Petersen et al., 2019

SPJV49	EF3030Δ*spxB*Δ*lctO*; Ery^R, Spc^R	McDevitt et al., 2020
D39	clinical isolate, serotype 2	Avery et al., 1944
SPJV45 (D39ΔspxBΔlctO)	D39Δ*spxB*Δ*lctO*; Ery^R, Spc^R	McDevitt et al., 2020
R6	D39 derivative serotype 2 (smooth or encapsulated) R6Δ*spxB*Δ*lctO*; Ery^R, Spc^R	Avery et al., 1944 McDevitt et al., 2020
BL21(DE3)	NEB	Cat# C2527H
Chemicals, peptides, and recombinant proteins		
Fetal Bovine Serum (FBS) Optima	R&D systems, Bio-techne	Cat# S12450
Gibco L-Glutamine 200 mM (100x)	Thermo Scientific	Cat# 25030081
Gibco MEM Non-Essential Amino Acids Solution (100X)	Thermo Scientific	Cat# 11140050
Gibco HEPES (1 M)	Thermo Scientific	Cat# 15630080
Gibco Penicillin-Streptomycin (10000 U/mL)	Thermo Scientific	Cat# 15140122
Dulbecco's Modified Eagle's Medium (DMEM)	Corning	Cat# 10013CV
Gibco Minimum Essential Medium (MEM)	Thermo Scientific	Cat# 11095080
Gibco Trypsin-EDTA (0.25%), phenol red	Thermo Scientific	Cat# 25200056
BBL Trypticase Soy Agar	BD	Cat# 211043
Bacto™ Todd Hewitt Broth	BD	Cat# 249240
Bacto™ Yeast Extract	BD	Cat# 212750
Blood Agar (TSA with Sheep Blood) Medium	Thermo Scientific	Cat# R01202
Horse Blood Defibrinated	Lampire Biological Laboratories, Inc.	Cat# 7233401
Sheep Blood Defibrinated	Quad FIVE	Cat# 610100
Bacto Tryptone	BD	Cat# 211705
Fixable Viability Stain 440UV	BD	Cat# 566332
Difco™ Skim Milk	BD	Cat# 232100
LB medium (Luria/Miller)	BD	Cat# 244610
LB agar (Luria/Miller)	BD	Cat# 244520
S.O.C medium	Invitrogen	Cat# 15544-034
Gentamicin solution	Sigma-Aldrich	Cat# G1397
Ampicillin sodium salt	Sigma-Aldrich	Cat# A9518
Erythromycin	Sigma-Aldrich	Cat# E6376
Kanamycin sulfate	Sigma-Aldrich	Cat# 60615
Chloramphenicol	Sigma-Aldrich	Cat# 857440
Kanamycin sulfate	Sigma-Aldrich	Cat# 60615
Spectinomycin sulfate	MP Biomedicals	Cat# 158993
Paraformaldehyde	Sigma-Aldrich	Cat# 158127
2-Mercaptoethanol	Sigma-Aldrich	Cat# M3148
Chelex-100	Biorad	Cat# 1421253
Mutanolysin from *Streptomyces globisporus* ATCC 21553	Sigma-Aldrich	Cat# M9901
Lysozyme from chicken egg white	Sigma-Aldrich	Cat# L6876
Sucrose, Crystal	Mallinckrodt Baker	Cat# MAL8360
Hemin	Sigma-Aldrich	Cat# H9039
Hemoglobin human	Sigma-Aldrich	Cat# H7379
Phosphate Buffered Saline (PBS) Tablets	Fisher BioReagents	Cat# BP2944100
Isoflurane Solution	Covetrus	Cat# 029404
Ketmine	Covetrus	Cat# 071173
Xylazine	Covetrus	Cat# 061035

Paraformaldehyde	MilliporeSigma	Cat# 158127
Hanks′ Balanced Salt solution (HBSS)	MilliporeSigma	Cat# H6648
Collagenase D from *Clostridium histolyticum*	Roche	Cat# 11088866001
DNase I	Roche	Cat# AMPD1
Glycerol (Molecular Biology)	Fisher BioReagents	Cat# BP229
Gentamicin solution (50 mg/mL)	MilliporeSigma	Cat# G1397
Dextrose (D-Glucose), Anhydrous	Fisher Chemical	Cat# D-16
cOmplete™, Mini, EDTA-free Protease Inhibitor Cocktail	Rosche	Cat# 11836170001
Iron (III) chloride hexahydrate	Sigma-Aldrich	Cat# 236489
Potassium hexacyanoferrate (III)	Sigma-Aldrich	Cat# 244023
Proteinase K from Tritirachium album	Sigma-Aldrich	Cat# P6556
ProLong™ Diamond Antifade Mountant	Invitrogen	Cat# P36970
Precision Plus Protein Dual Color Standards	Biorad	Cat# 1610374
Dimethyl Sulfoxide (DMSO)	Fisher BioReagents	Cat# BP231-100
Sodium Chloride 0.9%	B.Braun Medical	Cat# 3627632
SuperSignal™ West Pico PLUS Chemiluminescent Substrate	Thermo Scientific	Cat# 34577
12% Mini-PROTEAN® TGX Stain-Free™ Protein Gels	Biorad	Cat# 4568044
Turbo Transblot 5X buffer	Biorad	Cat# 10026938
10x Tris/Glycine/SDS	Biorad	Cat#1610732
Methanol (Certified ACS)	Fisher Chemical	Cat# A412
Ethanol, Absolute (200 Proof)	Fisher BioReagents	Cat# BP2818
Acetonitrile, Optima LC/MS Grade	Fisher Chemical	Cat# A955
Catalase from bovine liver	Sigma-Aldrich	Cat# C9322
TRIS EDTA Buffer	VWR	Cat# E112
Water, Ultra-Pure, Sterile, Molecular Biology Grade	Apex Bioresearch	Cat# 18-93
Apex Safe DNA Gel Stain	Apex Bioresearch	Cat# 20-278
1 kb DNA Ladder	NEB	Cat# N3232L
GeneRuler 100 bp DNA Ladder	Thermo Scientific	Cat# SM0242
Immersion oil Type B	Fisher Scientific	Cat# 16484
DAPI (4',6-Diamidino-2-Phenylindole, Dihydrochloride)	Invitrogen	Cat# D1306
T4 DNA Ligase	NEB	Cat# M0202L
CutSmart Buffer	NEB	Cat# B7204
BamHI	NEB	Cat# R0136S
XbaI	NEB	Cat# N3012S
NEBuffer™ 3.1	NEB	Cat# B7203S
Dephosphorylation of 5´-ends of DNA using CIP	NEB	Cat# M0290S
T4 DNA Polymerase	NEB	Cat# M0203S
Klenow Fragment	NEB	Cat# M0212L
λ DNA-HindIII Digest	NEB	Cat# R0145S
dNTP Mix (10 mM ea)	Thermo Scientific	Cat# 18427013
Bovine Serum Albumin Fraction V, protease-free	Roche	Cat# 03117332001
Non-fat dry milk, biotin free	LabScientific	Cat# M0841
Magnesium chloride hexahydrate	Sigma-Aldrich	Cat# M2670
Tween (Polysorbate) 20	Fisher Chemical	Cat# BP337-100
Glycerol (Molecular Biology)	Fisher BioReagents	Cat# BP229
Hydrogen Peroxide, 3% (Certified)	Fisher Chemical	Cat# H324
o-Dianisidine	Thermo Scientific Chemicals	Cat# A17150.22

Hematoxylin	Mercedes Scientific	Cat# MA1010
Eosin	Mercedes Scientific	Cat# MA1015
CellROX™ Green Reagent, for oxidative stress detection	Thermo Scientific	Cat# C10444
Sodium acetate solution	Sigma-Aldrich	Cat# 71196
RNAprotect	Qiagen	Cat# 76526
4x Laemmli Sample Buffer	Biorad	Cat# 1610747
CSP-1 (Competence-Stimulating Peptide-1)	AnaSpec Peptide Synthesis	Cat# AS-63779
CSP-2 (Competence-Stimulating Peptide-2)	AnaSpec Peptide Synthesis	Cat# AS-63877
Invitrogen™ Amplex™ UltraRed Reagent	Fisher Scientific	Cat# A36006
Superoxide Dismutase bovine	Sigma-Aldrich	Cat# S9697-15KU
Peroxidase from horseradish	Sigma-Aldrich	Cat# P8375-25KU
Fmoc Rink amide MBHA resin	Iris Biotech	Cat# BR-1305
HBTU	Iris Biotech	Cat# RL-1030
Trifluoracetic acid (TFA) for HPLC	Sigma-Aldrich	Cat# 302031
TFA for peptide cleavage	Solvay Fluor GmbH	Cat# AB 212435
Dichloromethane (DCM)	Fisher Scientific GmbH	Cat# AC610050040
Diethyl ether	VWR	Cat# 23809.363P
Dimethylformamide	VWR	Cat# ACRO354830010
Ethane-1,2-dithiol	Sigma-Aldrich	Cat# 800795
N-methylmorpholine	Sigma-Aldrich	Cat# 8.05894
Phenol	Sigma-Aldrich	Cat# 8.22296
Piperidine	Thermo Scientific	Cat# A12442
tert-Butanol	Fisher Scientific	Cat# 11394208
Thioanisole	Thermo Scientific	Cat# A14846.36
Fmoc-L-Thr(tBu)-OH	Orpegen	Cat# 03-1602
Fmoc-L-Lys(Boc)-OH	Orpegen	Cat# 03-1428
Fmoc-L-Ser(tBu)-OH	Orpegen	Cat# 03-1572
Fmoc-L-His(Trt)-OH	Orpegen	Cat# 03-1302
Fmoc-L-Ile-OH	Orpegen	Cat# 03-1360
Fmoc-L-Asp(OtBu)-OH	Orpegen	Cat# 03-2154
Fmoc-L-Tyr(tBu)-OH	Orpegen	Cat# 03-2662
Fmoc-L-Gly-OH	Orpegen	Cat# 03-0270
Fmoc-L-Phe-OH	Orpegen	Cat# 03-1510
Fmoc-L-Asn(Trt)-OH	Orpegen	Cat# 03-1122
Fmoc-L-Gln(Trt)-OH	Orpegen	Cat# 03-1212
Fmoc-L-Leu-OH	Orpegen	Cat# 03-1390
Fmoc-L-Pro-OH	Orpegen	Cat# 03-1540
Fmoc-L-Arg(Pbf)-OH	Orpegen	Cat# 03-1092
Fmoc-L-Ala-OH*H_2O	Orpegen	Cat# 03-1030
Ammonia, 25%	VWR	Cat# 1133.1000
Glacial acetic acid	VWR	Cat# A3701.1000PE
Ethyl acetate	VWR	Cat# 23882.310P
n-propanol	VWR	Cat# 1.01024
Pyridine	Carl Roth	Cat# CP07.2
HEPES	Carl Roth	Cat# HN77.5
Recombinant pneumolysin	Vidal lab	N/A
ABC transporter-derived peptides **1**-**6**, see Table S4	synthesized by Imhof lab (this study)	N/A

MarC9 transposase	labLampe et al, 1999	N/A
Critical commercial assays		
Amplex™ Red Hydrogen Peroxide/Peroxidase Assay Kit	Thermo Scientific	Cat# A22188
NEBuilder® HiFi DNA Assembly Master Mix	NEB	Cat# E2621S
PerfeCTa qPCR ToughMix	QuantoBio	Cat# 95112
PerfeCTa SYBR® Green FastMix	QuantoBio	Cat# 95072
Phusion™ Plus Green PCR Master Mix	Thermo Scientific	Cat# F632S
DreamTaq™ Hot Start Green PCR Master Mix	Thermo Scientific	Cat# K9021
Pierce™ BCA Protein Assay Kit	Thermo Scientific	Cat# 23227
Alexa Fluor™ 488 Protein Labeling Kit	Thermo Scientific	Cat# A10235
Alexa Fluor™ 555 Protein Labeling Kit	Thermo Scientific	Cat# A20174
QuantiChrom™ Heme Assay Kit	BioAssay Systems	Cat# DHIM-250
QuantiChrom™ Hemoglobin Assay Kit	BioAssay Systems	Cat# DIHB-250
QIAquick PCR Purification Kit	Qiagen	Cat# 28104
QIAamp DNA mini kit	Qiagen	Cat# 51306
Nextera DNA Flex Library Prep Kit	Illumina	Cat# 20018704
MiSeq Reagent Kit v2 (300-cycles)	Illumina	Cat# MS-102-2002
RNeasy Plus Kit	Qiagen	Cat# 74034
GeneJET Gel Extraction Kit	Thermo Scientific	Cat# K0691
iScript™ cDNA Synthesis Kit	Biorad	Cat# 1708890
Maxima H Minus First Strand cDNA Synthesis Kit	Thermo Scientific	Cat# K1651
DNA-free™ DNA Removal Kit	Thermo Scientific	Cat# AM1906
Deposited data		
Complete genome of selected *S. pneumoniae*	This study	NCBI: PRJNA1018957
TnSeq reads	This study	NCBI: PRJNA1029615
Experimental models: cell lines		
A549	ATCC	CCL-185
Detroit562	ATCC	CCL-138
MLE-12	ATCC	RL-2110
Experimental models: organisms/strains		
BALB/c mice, 4-weeks old, female	Charles River Laboratories	555NCIBALB/c
C57BL/6 mice, 4-weeks old, female	Charles River Laboratories	C57BL/6NCrl
Oligonucleotides		
see Table S5	This study	N/A
Recombinant DNA		
pPEPY-glnP (Purpose: insertion of indicated gene)	This study	N/A
PJIR750 (Purpose: amplify antibiotic marker gene)	This study	N/A
PJIR751(Purpose: amplify antibiotic marker gene)	This study	N/A
pPP2-glnP (Purpose: insertion of indicated gene)	This study	N/A
pMagellan6 (Purpose: source of transposon)	van Opijnen et al., 2009	N/A
Software and algorithms		
Prism	GraphPad	version 10.0.3
ImageJ	NIH	https://imagej.nih.gov/ij/
TnSeq insert comparison or tools		
Image Lab	Biorad	version 3.01
CFX Maestro	Biorad	version 2.3
The Read assembly and Annotation Pipeline Tool (RAPT)	NCBI	https://www.ncbi.nlm.nih

		.gov/rapt
Bacterial and Viral Bioinformatics Resource Center (BV-BRC)	BV-BRC	https://www.bv-brc.org/
Pathogenwatch	N/A	https://pathogen.watch/
Proksee	N/A	https://proksee.ca/
HeMoQuest	Paul George et al., 2020	http://131.220.139.55/SeqDHBM/
NIS-Elements Basic Research	Nikon	version 4.30.01
YASARA	YASARA Biosciences GmbH	version 21.8.27
C-I-Tasser	Zheng et al., 2021	https://zhanggroup.org/C-I-TASSER/
TRANSIT	DeJesus et al., 2015	https://github.com/mad-lab/transit

RESOURCE AVAILABILITY

Further information and requests for resources and reagents should be directed to and will be fulfilled by the Lead Contact, Jorge E. Vidal (jvidal@umc.edu).

Material and methods.

Ethics Statement. All experiments involving animals were performed with prior approval of and in accordance with protocol 1584 which was reviewed and approved by the UMMC Animal Care Committee. UMMC laboratory animal facilities have been fully accredited by the American Association for Accreditation of Laboratory Animal Care. Procedures were performed according to the institutional policies, Animal Welfare Act, NIH guidelines, and American Veterinary Medical Association guidelines on euthanasia.

Female 4-5-week-old Balb/c mice were obtained from Charles River Laboratories, Inc and allowed to acclimate for one week before the experimental challenge. At all times mice received food and water ad libitum.

Bacterial strains and growth conditions. All Spn strains used in this study are listed in the Star Table. Spn was cultured on BAP (Fisher Scientific) or BAP with 10 µg/ml gentamicin (Sigma-Aldrich) at 37°C for 24 h in a 5% CO_2 atmosphere. Colonies were inoculated into Todd-Hewitt-broth with 0.5% yeast extract (THY) (BD) and grown until exponential phase (OD_{600} 0.3, ~1 X 10^8 CFU/ ml). THY broth was utilized in all the experiments. Isogenic mutants were cultivated using appropriate antibiotics.

Cell culture lines. Low passage, A549 human type II alveolar epithelial cells (ATCC, CCL-185), and MLE-12 mouse lung type II epithelial cells (ATCC, CRL-2110), and Detroit 562 human pharyngeal epithelial cells (ATCC, CCL-138) were purchased from ATCC (American Type Culture Collection). The A549 and MLE-12 cells were cultured in Dulbecco's Modified Eagle's Medium (DMEM) (Corning) media with 2 mM L-glutamine (Gibco), 10% fetal bovine serum (FBS) (R&D systems, Bio-techne), 100 units/ml penicillin/streptomycin solution (Gibco). The Detroit 562 cells were cultured in Minimum Essential Medium (MEM) media supplemented with 2 mM L-glutamine (Gibco), 1x Non-Essential Amino Acids Solution (Gibco), 2 mM HEPES (Gibco), 10% fetal bovine serum (FBS) (R&D systems, Bio-techne), and 100 units/ml penicillin/streptomycin solution (Gibco). Cell passages were performed by trypsinization with Trypsin-EDTA (0.25%), phenol red (Gibco) and seeded in the experiment specific device. All experiments described hereafter were performed with cells that had been grown for 8-10 days in the specified device.

Preparation of inoculum for *in vitro* and for animal experiments. Inoculum for the *in vitro* studies was prepared essentially as previously described[1-3]. Briefly, an overnight BAP culture of the Spn strain was used to prepare a bacterial suspension in sterile phosphate buffered saline [(PBS), pH=7.4] (Fisher BioReagents). This fresh bacterial suspension was inoculated to a final OD_{600} of ~0.1 and the suspension contained ~5.15×10^8 cfu/ml. Aliquots of these suspensions were routinely diluted and plated to confirm bacterial counts (cfu/ml). Unless otherwise noted, all *in vitro* experiments described below were inoculated with fresh inocula, i.e., prepared right before the start of the experiment.

To prepare inoculant for mice studies, the Spn strain was inoculated in THY broth supplemented with 20% fetal bovine serum (FBS) (R&D systems, Bio-techne); this culture was grown for 4 h (i.e., early log phase) at 37°C in a 5% CO_2 atmosphere; the growth was monitored using a spectrophotometer Bio-Rad SmartSpec Plus. After this incubation time, the culture was centrifuged at 4500 g for 5 min and the pellet was resuspended in 10 ml PBS and washed once. The washed bacterial pellet was resuspended in PBS containing 10% (v/v) glycerol and stored at -80°C until it was used. Aliquots of inocula were thawed from each batch to obtain the density by dilution and platting. All inocula were used within two months.

Confocal microscopy studies. All micrographs obtained in these experiments and throughout this study were obtained with a Nikon C2 laser scanning confocal microscopy system.

(A) Studies of pneumococcal biofilms, and planktonic pneumococci, incubated with hemoglobin. Pneumococci were inoculated into 8-well glass slides (Thermo Fisher Scientific, Nunc Lab-Tek II CC2) that had been added with THY broth supplemented with 10 µM hemoglobin (Sigma-Aldrich) and incubated at 37°C in a 5% CO_2 atmosphere. At the end of the incubation time, planktonic pneumococci were removed, washed two times with PBS, and fixed with 4% paraformaldehyde (PFA) (Sigma-Aldrich) for 15 min at room temperature. Biofilms were washed two times with PBS and then fixed with PFA as above. Planktonic pneumococci, or biofilms, were then washed two times with PBS and with 2% bovine serum albumin (BSA) (Roche) for 30 min at room temperature. Planktonic bacteria were stained in suspension whereas biofilms were stained on the 8-well glass slides. Pneumococci were then stained for 1 h at room temperature with serotype-specific polyclonal antibody (Statens Serum Institute, Denmark) (40 µg/ml) that had been previously labeled with Alexa-488 (anti-S4-A488) (Thermo Scientific) or Alexa-555 (anti-S2-A555, or anti-S19-A555) (Molecular Probes) and with a mouse monoclonal anti-hemoglobin antibody labeled with Alexa-546 [(anti-Hb-A546), 20 µg/ml] (Santa Cruz Biotechnology). Stained planktonic bacteria or biofilms were finally washed three times with PBS. Planktonic

pneumococci dropped on microscope slides and stained biofilms were air dried and then mounted with ProLong Diamond Antifade mounting medium containing DAPI (Molecular Probes).

(B) Studies of hemoglobin polymerization and Spn-Hb$^+$ bacteria using a Transwell system. These experiments were performed using 6-well TC treated plates (Genesee Scientific, GenClone). We first installed a cover glass (Chemglass Life Sciences) in the bottom of the microplate and then a transwell system device (Corning Costar) with pore membrane of 0.4 µm- was installed in the well. The system was added with 1 ml of THY broth containing 10 µM hemoglobin, infected with Spn and incubated at 37°C in a 5% CO_2 atmosphere. At the end of the incubation, planktonic cells were removed from the transwell, and the cover glass that had been installed in the bottom, was removed and fixed with 2% PFA. The following staining procedure was done as indicated above or planktonic cells and biofilms; we stained the pneumococcal capsule, hemoglobin and DNA. Micrographs were obtained by a confocal microscope.

(C) Confocal microscopy studies of lung tissue. Deparaffinized sections of lung tissue ~5 µm mounted on microscope slides were washed three times with PBS and the preparations were blocked with 2% bovine serum albumin (BSA) for 1 h at room temperature. These preparations were then incubated for 1 h with serotype-specific polyclonal antibody (Statens Serum Institute, Denmark) (40 µg/ml) that had been previously labeled with Alexa-488 (anti-S4-A488) or Alexa-555 (anti-S2-A555) (Molecular Probes) and wheat germ agglutinin conjugated to Alexa-488 or Alexa-555 [(WGA), 5 µg/ml]. Some lung tissue specimens were stained with an anti-S4-A488 and a mouse monoclonal anti-hemoglobin antibody labeled with Alexa-546 [(anti-Hb-A546), 20 µg/ml] (Santa Cruz Biotechnology) for 1 h at room temperature. Stained tissues were finally washed three times with PBS, air dried and then mounted with ProLong Diamond Antifade mounting medium containing DAPI (Molecular Probes).

(D) Studies of pneumococci incubated with human alveolar cells in the presence of hemoglobin. Human A549 cells grown on an 8-well chamber (Thermo Fisher Scientific, Nunc Lab-Tek II CC2) were washed three times with PBS and then added with infection medium that had been supplemented with 10 µM hemoglobin. Pneumococci were infected and incubated at 37°C in a 5% CO_2 atmosphere. At the end of the incubation time, planktonic pneumococci that had been removed, and biofilms were washed, fixed with PFA and the capsule of pneumococci, DNA, and hemoglobin were stained essentially as detailed above.

Quantification of pneumococci expressing capsule. Aliquots of inocula prepared for animal studies, as detailed above, were thawed in ice and stained with a serotype-specific polyclonal antibody (40 µg/ml) for 1 h at room temperature.

Stained pneumococci were pelleted down by centrifugation at 21,130 x g for 5 min, washed two times with PBS and then fixed with 4% PFA that was incubated for 15 min at room temperature. Fixed bacteria were washed again two times with PBS, resuspended in PBS and air dried on a microscope slide. Preparations were mounted with ProLong Diamond Antifade mounting medium containing DAPI and micrographs were obtained by a confocal microscope. Capsule was quantified from confocal micrographs using ImageJ (NIH). The quantification process consisted of separating the DAPI channel (bacterial DNA) and the green channel (encapsulated pneumococci), quantifying the bacteria in the DAPI channel using the 'find maxima' function, then overlaying the green channel against the DAPI channel using the 'image calculator' function to confirm encapsulation before quantifying the green channel in the same manner. The 'prominence' setting was adjusted to filter out redundant counts, and the output was selected as 'single points'. Parameters were adjusted to reduce background noise. Absolute number of bacteria (encapsulated Spn/Spn) were obtained and utilized to calculate the percentage of pneumococci that expressed capsule.

Adhesion assay. Adhesion of pneumococci to A549 cells and MLE-12 cells was assessed as follows: Cells grown for 8-10 days on a 6-well microplate were washed three times with sterile PBS to remove the antibiotic and added with 1 ml of infection medium, which consisted of DMEM supplemented with 2 mM L-glutamine, HEPES buffer (100 mM) and 5% fetal bovine serum (FBS). Cells were infected with pneumococci and incubated for the indicated time points, after which infected cells were washed two times with PBS to remove unbound bacteria. Cells and pneumococci were detached by sonication (Branson Ultrasonic 2800) for 30 s and after homogenization in PBS, the suspensions were diluted and plated to obtain bacterial accounts.

Purification of the soluble fraction of human alveolar cells infected with pneumococci. A549 cells were infected as above and incubated for 4, 8, 12, 16 or 24 h at 37°C in 5% CO_2 atmosphere. Uninfected cells were used as a control. After incubation, cells were gently scrape off the 6-well microplate and washed twice with ice-cold PBS by centrifugation cycles of 300 x g for 5 min at 4°C. Washed cells were lysed with RIPA buffer supplemented with 1X complete protease inhibitor (Roche) incubated 30 min on ice. After incubation, lysed cells were centrifuged at 13,500 x g for 20 min at 4°C and the soluble fraction was collected. The protein concentration of the soluble fraction was determined with the BCA protein assays (Thermo Fisher Scientific) as recommended by the manufacturer.

Quantification of intracellular reactive oxygen species. To quantify reactive oxygen species (ROS) in infected cells the CellROX Green Reagent from Invitrogen was used. Human alveolar A549 cells were seeded in an 8 well chamber slide,

and once confluent, cells were infected with Spn or mutant derivatives and incubated for 6 h at 37°C in a 5% CO_2 atmosphere. After incubation, planktonic pneumococci were removed and infected cells were incubated for 30 min with fresh infection medium containing the CellROX Green Reagent at a concentration of 5 μM. Cells were then washed three times with PBS and fixed with 2% PFA for 15 min after which the cells were washed two times with PBS, then air-dried, and mounted with ProLong Diamond Antifade mountant containing DAPI (50 μg/ml). Cells were immediately imaged by confocal microscopy. Quantification of intracellular ROS from confocal micrographs was performed using ImageJ version 1.3t (National Institutes of Health, NIH) and done by taking intensity spectrum measurements of a region of interest in the green channel (GFP) and obtaining area under the curve. Values were expressed by creating a ratio of ROS (GFP): DAPI intensity within the same samples.

Bacterial cell fractionation. To investigate heme or hemoglobin uptake, the subcellular fractions of TIGR4, TIGR4*ΔspxBΔlctO*, and TIGR4Δ*glnP* without or with hemoglobin, heme growth conditions were prepared by the method as previously described[4,5] with minor modification. Briefly, grown bacterial cells were pelleted by centrifugation at 7,500 x g for 10 min at room temperature. The supernatant was discarded, cells were washed once with ice-cold PBS to remove cell debris, and resuspended in 1 ml protoplast buffer (1X protease inhibitor cocktail [Roche], 200 U/μl mutanolysin, 2 mg/ml lysozyme in a 20% sucrose-10 mM Tris [pH 7.5]- 50 mM MgCl2 buffer) and incubated at 37°C for 2 h with shaking. The bacterial endogenous autolytic enzymes hydrolyze the peptidoglycan layer of Spn activated by MgCl2, and the sucrose maintains the protoplasts intact. After incubation, the suspension was centrifuged at 21,130 x g for 10 min at 4°C, and the supernatant containing cell wall extract fraction was collected and kept at -80°C. The pellet protoplasts were resuspended in a 20% sucrose-10 mM Tris [pH 7.5]- 50 mM $MgCl_2$ buffer supplemented with 1X protease inhibitor cocktail [Roche] and lysed by sonication. The lysed cell suspension was centrifuged at 6000 x *g* for 10 min at 4°C to remove any particulate material. The supernatant-contained cytoplasmatic membrane and cytoplasmatic proteins were separated by ultracentrifugation at 25,000 x g for 3 h at 4°C. After centrifugation, the supernatant was kept as cytoplasmatic fraction, and the pellet cytoplasmatic membrane fraction resuspended in TN buffer and stored for further processing.

Western blotting. Equivalent amounts of cellular or subcellular fractions, as specified in the appropriate section, from bacteria, infected cells, or lung specimens were combined with 4x reducing sample buffer and boiled for 5 min at 100°C. The mixture was loaded into a 12% Mini-Protean TGX precast gels (Bio-Rad), which were run for 2 h at 90 V. Gels were

transferred to nitrocellulose membranes using the recommended transfer buffer supplemented with 20% ethanol and the Trans-Blot Turbo transfer system. Transferred membranes were blocked for 1 h at room temperature in a solution of Tris-buffered saline supplemented with 0.1% Tween 20 (TBST) and 5% non-fat dry milk. The membrane was then incubated overnight at 4°C with a primary antibody diluted in TBST containing 5% non-fat dry milk. The following primary antibodies were used: anti-β tubulin at 1.6 µg/µl (Proteintech, 10068-1-AP), anti-β actin at 1.6 µg/µl (Proteintech, 66009-1-Ig), anti-GAPDH at 2 µg/µl (Proteintech, 60004-1-Ig), anti-catalase at 1.2 µg/µl (Proteintech, 21260-1-AP), anti-hemoglobin α chain mAb at 2 µg/µl, anti-hemoglobin β chain mAb at 2 µg/µl or an anti-hemoglobin polyclonal antibody at 10 µg/µl (Invitrogen).

The next day, the membrane was washed three times for 5 min each with TBST, in a rocking platform, and incubated for 1 h at room temperature with Starbright Blue 520 (Bio-Rad) anti-mouse, or anti-rabbit; this secondary antibody was diluted 1:2500 in 5% non-fat dry milk in TBST. The membrane was then washed six times for 5 min each with TBST. Blots were then imaged on a ChemiDoc MP imager (Bio-Rad) using Image Lab 5.0 software, with automatic exposure settings for chemiluminescence and high specificity, optimizing for bright bands. Densitometric analysis of the bands was performed with ImageLab software (Bio-Rad), normalizing to a selected target protein.

Bacterial growth curves and studies of the minimum inhibitory concentration (MIC). Bacteria were grown in 24-well plates poured with 1 ml fresh THY (with or without supplements) at 37°C in a 5% CO_2 atmosphere. The medium was then inoculated with fresh Spn inoculum, and the OD_{600} was monitored every 20 minutes for 24 h using a BioTek Synergy H1 Multimode Reader (Agilent Technologies, Inc). Uninfected THY was always used as the blank and negative control. To assess the inhibition of growth by heme, a 2 mM stock solution of heme prepared in dimethyl sulfoxide (DMSO), was diluted in THY broth. This stock solution was used same day. Non-heme supplemented THY broth was used as a control. Pneumococci were inoculated and the OD_{600} was monitored as above. Two technical replicates and three biological replicates were performed in these experiments.

The minimum inhibitory concentration (MIC) of heme was determined using a slightly modified broth microdilution method, as recommended by the Clinical Laboratory Standards Institute (CLSI)[6]. Briefly, a 2 mM stock solution of heme was diluted in THY broth and added in 96-well plates; note that we cannot use lysed horse blood, as recommended by the CLSI, because the lysate contains hemoglobin and heme. The 96-well plates were inoculated with pneumococci at ~10×10^8 cfu/ml and incubated at 37°C in a 5% CO_2 atmosphere for 24 h. The MIC was recorded as the

heme concentration of the well with no visible growth. MIC assays were performed with technical triplicates and two biological replicates.

To assess the viability of pneumococci challenged with heme, Spn was inoculated in 6-well plates that had been added with THY, as a control, or THY supplemented with heme. The samples were incubated for 2, 4, or 6 h at 37°C in a 5% CO_2 atmosphere. After incubation, bacteria were collected, diluted, and plated on BAP to obtain the density (cfu).

Spectroscopic analysis of heme, or hemoglobin, when incubated with pneumococci. Spn was inoculated in THY broth or THY supplemented with heme (0.62, 1.25, 2.5, 5, 10, or 20 µM) or hemoglobin (10 µM), and incubated for the indicated time at 37°C in a 5% CO_2 atmosphere. The culture supernatants were collected, and then centrifuged at 4°C for 5 min at 21,130 x g and transferred to a 96-well plate and analyzed by spectroscopy spanning 200 nm through 1000 nm using an BMG LabTech FLUOstar Omega spectrophotometer.

Qualitative assessment and quantification of hydrogen peroxide. Spn hydrogen peroxide production was determined with qualitative and quantitate methods. Qualitative detection of H_2O_2 production by Spn was performed as previously described[3,7] using the Prussian blue agar assay. Shortly, Spn strains or culture supernatants (10 µl), obtained as described above, were inoculated or spotted, respectively, onto Prussian blue agar plates and these plates were incubated at 37°C in a 5% CO_2 and ~20% O_2 atmosphere overnight (Spn) or for 4 h (supernatants). The plates were then photographed with a Canon Rebel EOS T5 camera system, and digital pictures were analyzed.

H_2O_2 was quantified from supernatants of Spn cultures that had been infected in THY (with or without supplements) or in cell culture medium (DMEM) and incubated at 37°C in a 5% CO_2 and ~20% O_2 atmosphere for the indicated time. At the end of the incubation, culture supernatants were collected and centrifuged at 4°C for 5 min at 21,130 x g, and then transferred to new tubes that were placed on ice. Some supernatants were filter sterilized using a 0.22-µm syringe filter (Genesee Scientific) and kept on ice. Collected supernatants were processed within 30 min by dilution with 1X reaction buffer from the Amplex Red H_2O_2 assay kit (Molecular Probes), and H_2O_2 levels were quantified according to the manufacturer's instructions using an BMG LabTech FLUOstar Omega spectrophotometer.

H_2O_2 was quantified from lungs removed 24 h post-infection with pneumococci or mock-infected. Lungs were homogenized within 20 minutes after removal using a LabGen Series 7 Homogenizer (Cole-Parmer) and H_2O_2 was quantified within 30 min. H_2O_2 concentration was measured using the Amplex Red (10 µM) which is converted to resorufin (highly fluorescent) by the reaction of H_2O_2 and horseradish peroxidase (HRP, 1U/ml). Superoxide dismutase

(SOD, 5U/ml) was also added to convert superoxide (SO) to H_2O_2. The rate of H_2O_2 production was obtained by calibrating the fluorescence response of known concentrations of H_2O_2 in the Oroboros O2k FluoRespirometer. Additionally, the end point absorbance was measured using a SpectraMax M5 plate reader at 570 nm with a separate calibration curve for the absorbance.

In-gel heme detection assay. Bacterial cytosolic or membrane fractions, or supernatants harvested from experiments incubating pneumococci with hemoglobin were combined with nonreducing loading buffer. Samples were not heated. The mixtures were loaded into a nondenaturing 12% Mini-Protean TGX precast gel (Bio-Rad), which was run for 2 h at 100 V in running buffer lacking sodium dodecyl sulfate (SDS). The gel was then stained using a published protocol[8]. Briefly, after electrophoresis, gels were immersed in a methanol-sodium acetate solution (pH 5) and incubated at room temperature on a rocking platform (VWR) at a speed of 1 for 2 min. After incubation, a solution of o-dianisidine-sodium acetate (pH 5) was added to the gel, which was incubated for 20 min in the dark. To visualize heme in the gel, 3% hydrogen peroxide was added, and the reaction was stopped by washing with distilled water. The gel was then photographed with a Canon Rebel EOS T5 camera system, and digital pictures analyzed.

Quantification of hemoglobin and heme. The concentration of heme or hemoglobin, was determined by using the QuantiChrom™ Heme Assay Kit or the QuantiChrom™ Hemoglobin Assay Kit (BioAssay), respectively. Heme and Hemoglobin levels were determined using manufacturer's instructions, calibration standards provided in each kit and using a BMG LabTech FLUOstar Omega spectrophotometer.

Mouse model of pneumococcal disease. Female 4-5week old Balb/c mice (Charles River Laboratories) were infected intranasally with 10^7 cfu/ml Spn resuspended in 50 µl PBS. The mock infection control group received 50 µl of PBS. Some mice were infected intraperitoneally with 10^7 CFU/ ml Spn resuspended in 100 µl PBS, while the control group received 100 µl PBS. Prior to the infection, the animals were anesthetized via inhalation of 5% isoflurane. Survival was monitored for up to four days. To avoid cross bacterial infection, mice with the same strain where housed within the same box. Animals were weighted daily whereas their behavior and appearance were monitored two times per day. Mice were euthanized when they lost ≥15% of their body weight, compared to their body weight before infection, or when mice were non-responsive to manual stimulation, and/or if they show signs of illness such as ruffled fur, intermittent hunching, and exhibiting respiratory distress. Blood was collected under anesthesia, and the nasopharyngeal tissue, and lungs, were excised post-euthanasia.

An aliquot of blood was immediately added with THY broth added with 10% glycerol and used for dilution and plating onto BAP containing gentamicin. Another aliquot of blood was left untreated and kept at 4°C for 20 min after which serum was separated by centrifugation at 1000 x g for 20 min. Serum was frozen at -80°C until used. Nasopharyngeal tissue, or the lungs, was split in two aliquots, one of them was fixed with 4% paraformaldehyde (PFA) and immediately stored at -80°C for histological analysis and confocal microscopy. The second aliquot was placed in THY added with 10% glycerol (THY-G) and a cocktail of 1X protease inhibitors and immediately homogenized after which the specimens were stored at -80°C. This aliquot was utilized for bacterial counts and for Western blot.

Histological analysis. The PFA-fixed lungs were paraffin-embedded, sectioned (~5 µm) and stained with hematoxylin and eosin (H&E) at the UMMC histology core facility. Micrographs of the tissues were captured with an Olympus BX63 inverted fluorescence microscope. The evaluation of cytotoxicity in various cellular compartments of the lung was conducted blindly by a certified Pathologist. Inflammatory cellular infiltration, bronchiolar hypertrophy, and the extent of bronchiolar exudate and cellular infiltration were assessed using a five-point severity scoring method.[9]

Quantification of immunofluorescence images. Confocal z-stacks micrographs were analyzed using the NIS Elements Basic Research software, version 4.30.01 build 1021. For quantifying encapsulated and non-encapsulated bacteria in lung of infected mice, a similar method was used as detailed above for the quantification of encapsulated bacteria in inocula. Region of interest (ROI) was selected to quantify bacteria in the different compartments of the lung.

Whole-genome sequencing. Genomic DNA was purified using the Qiagen QIAamp DNA Mini Kit as instructed by the manufacturer. The DNA was sequenced at the SeqCenter (Before known as MiGS Microbial Genome Sequencing Center) using the NextSeq 2000 platform. The paired-end read data were assembled and annotated using tools available on RAPT NCBI using g reference strain TIGR4 (AE005672). The sequences were deposited on NCBI GenBank (PRJNA1018957).

Construction of a *glnP* mutant and complemented strain. To prepare a TIGR4 isogenic Δ*glnP* mutant, we PCR amplified upstream and downstream sequences of SP1241 (TIGR4 nomenclature) and the erythromycin resistance gene (*ermB*) from pJIR750[1]. All three fragments were sowed by PCR and the construct was purified using the QIAquick PCR Purification Kit (QIAGEN) and then transformed into TIGR4 or D39 using a standard transformation procedure (79). Transformants were harvested in BAP containing erythromycin (1 µg/ml), and the deletion of *glnP* was confirmed by PCR and sequencing (GenBank accession will be provided during revision).

The TIGR4Δ*spd1098* complemented strain was generated by return the gene back into same location. Firstly, the upstream and downstream parts of *spd1097* gene were amplified and merged with chloramphenicol gene which was amplified from pJIR750 plasmid. The fragment was inserted into TIGR4, and transformants were harvested in BAP with chloramphenicol (3.5 μg/ml) then, the DNA was extracted. Amplified around 8 kb fragment from it and transformed into TIGR4*Δspd1098*. The chloramphenicol resistance and erythromycin susceptible colonies were selected. The insertion was confirmed by PCR and sequencing.

Preparation of a TIGR4Δ*spxB*Δ*lctO* expressing the green fluorescence protein (GFP). The gene encoding GFP, including a downstream chloramphenicol resistant cassette (*cat*), was amplified from a strain MK147[11], and the fragment was transformed into competent cells of TIGR4Δ*spxB*Δ*lctO*. Chloramphenicol resistant colonies were selected in BAP containing 3.5 μg/ml of the antibiotic. The insertion of the *gfp-cat* fragment was confirmed by PCR and sequencing and the expression of the GFP was verified by fluorescence microscopy.

RNA extraction and qRT-PCR analysis. Cells infected with Spn in 6-well plate collected after 4, 8, 12, and 16 h. Then cells were harvested, and the total RNA was extracted using the RNeasy Plus Mini Kit (QIAGEN) following the manufacturer's instructions. DNA was removed using the Turbo DNA-free Kit (Ambion by Life Technologies). The RNA concentration was obtained using a NanoDrop spectrophotometer (Thermo Fisher Scientific), and 1000 ng of RNA was cDNA transcribed using the iScript cDNA Synthesis Kit (Bio-Rad). Gene expression analysis was carried out using PerfeCTa qPCR ToughMix (QuantaBio) with ready to use mixture of primers with FAM probe (TaqMan® Gene Expression Assays, Thermo Fisher Scientific) and a CFX96 Touch real-time PCR system (Bio-Rad). The primers used for the qRT-PCR analysis were GAPDH, Cat, Nrf1, SOD1, and HO-1. The following conditions were utilized: 1 cycle at 95°C for 3 min and 40 cycles of 95°C for 15 s, 60°C for 30 s and 72°C for 30 s. Melting curves were generated to confirm the absence of primer dimers. The relative quantitation of mRNA expression was normalized to the constitutive expression of the housekeeping GAPDH gene and calculated by the comparative cycle threshold (2−ΔΔCT) method.

Statistical analysis. We performed one-way analysis of variance (ANOVA) followed by Dunnett's multiple-comparison test when more than two groups were compared or Student's t test to compare two groups, as indicated. All statistical analysis was performed using the software GraphPad Prism (version 8.3.1).

Transposon insertion site sequencing analysis of transposon mutant libraries. In brief, replicate starter cultures of a *S. pneumoniae* mariner transposon library in the D39 background containing sufficient cells to represent the mutant library by at least 100-fold were thawed, grown to log phase in THY, a sample taken for gDNA isolation (**t1**), and an aliquot used to inoculate fresh THY with and without Hb (10 μM) for growth in microtiter plates. Samples from planktonic (non-adherent) and biofilm cultures (adherent) were collected separately after 8 h and gDNA isolated (**t2**). The HITS variation of transposon insertion site sequencing was then conducted, essentially as previously described with some modifications, to specifically identify and quantitate transposon insertions throughout the genome within each selected library at t1 vs t2 [12,13]. Briefly, genomic DNA was sheared, ends repaired via T4 polymerase, 3' ends tailed with adenosine via Klenow polymerase, and custom adaptors[12] added via DNA ligase. After quantitation with a NanoDrop™ spectrophotometer and quality control by gel electrophoresis, transposon junctions were enriched via PCR with primers specific to the adaptor and to the mariner transposon arm[12], repurified, verified by gel electrophoresis and reamplified for barcode addition by PCR with a nested mariner transposon primer and Illumina 'BC' primers containing unique barcodes for each sample. Sample quality was validated via Agilent™ analysis prior to single-end Illumina HiSeq analysis. After sequencing, reads adjacent to transposon insertions were mapped to the genome and changes in mutant frequency (i.e., the number of reads per insertion) from **t1** to **t2** determined with the Burrows-Wheeler aligner[14,15]. The TRANSIT analysis pipeline implementing normalization (non-zero means at each site) and a resampling (permutation) test was used to statistically evaluate fitness of each mutant in the library under each experimental condition[15]. Sequencing yield was greater than 10 million reads per sample and after filtering to obtain only the genomic matches adjacent to the transposon ~7 million pseudoreads were obtained per sample. Input samples contained insertions within 46,417 unique genomic TA sites (*mariner* inserts only into the dinucleotide TA) of the total genomic 133,753 TA positions indicating a ~37% saturation of sites within the input library. Output samples all exceeded 34% saturation. Overall, these data indicated that library complexity was maintained throughout the experiment and sequencing coverage of transposon insertions was >150-fold. HITS raw sequences were deposited on NCBI GenBank (PRJNA1029615).

Sequence- and structure-based screening for potential heme-binding motifs (HBMs) in the amino acid ABC transporter. The sequence of the amino acid ABC transporter (*S. pneumoniae* serotype 2; UniProt: A0A0H2ZPN9) was screened for potential HBMs by using the web application HeMoQuest (http://131.220.139.55/SeqDHBM/)[16]. In total 13

potential HBMs were shortlisted, which were further subjected to manual refinement, combining overlapping motifs (around Y^{395} and Y^{397}) and excluding less suitable motifs (e.g., with acidic residues as in case of Y216). In order to gain insights into the accessibility of the predicted coordinating sites in the remaining nine motifs, a homology model of the ABC transporter monomer was generated by use of the structure prediction tool C-I-Tasser[17]. After manual inspection of the motifs within the homology model, motifs with sterically inaccessible coordinating residues (Y^{125}, Y^{269}, and Y^{635}) were excluded from selection, finally revealing six potential HBMs in the ABC transporter.

Synthesis and analytical characterization of ABC transporter-derived peptides. As described earlier[18,19], the six predicted HBMs (TTKSHKISK (**1**), IKDKYGFTI (**2**), NQSKYGYKIKT (**3**), LQNNYKQLL (**4**), SPYKSLR (**5**), IARNYQSFK (**6**)) were subjected to automated solid-phase peptide synthesis (SPPS; Economy Peptide Synthesizer EPS 221, Intavis). In brief, synthesis of peptides **1** – **6** was performed following standard 9-fluorenylmethyloxycarbonyl/*tert*-butyl (Fmoc/tBu) strategy on Rink amide MBHA resin (0.67 mmol/g loading). 2-(1H-benzotriazol-1-yl)-1,1,3,3-tetramethyluronium hexafluorophosphate (HBTU) served as the coupling agent. Side-chain deprotection and cleavage of the peptide from resin was achieved by adding reagent K (0.75 g phenol, 0.25 ml ethandithiol, 0.5 ml thioanisol) in 95% trifluoroacetic acid (1 ml per 100 mg resin) for a reaction time of 3 h at room temperature. The crude products were precipitated in cold diethyl ether and several times washed with the same. Afterwards, the crude products were purified by semipreparative reverse-phase high-performance liquid chromatography (RP-HPLC; LC-8A, Shimadzu) on a C18 reversed phase Eurospher 100 column. Subsequently, purity and identity of the peptides was proven by analytical RP-HPLC (LC10AT, Shimadzu, equipped with C18 reversed phase Vydac 218TP54 column), thin-layer chromatography (TLC), and electrospray ionization mass spectrometry (ESI-MS; micrOTOF-Q III, Bruker Daltonics GmbH), respectively (Table S4). The peptide content was determined by analytical RP-HPLC through comparison to an internal peptide standard and considered for further usage.

UV/vis spectroscopic binding studies of heme with the ABC transporter-derived peptides. Using an established experimental setup[18-20], the heme-binding capacity of peptide **1** – **6** was determined by UV/vis spectroscopy. In brief, heme (0.4 – 40 µM) was preincubated with each peptide in a constant concentration (5 – 20 µM) in 4-(2-hydroxyethyl)-1-piperazineethanesulfonic acid (HEPES) buffer (100 mM, pH 7.0) for 30 min at room temperature. Absorbance spectra (300 – 600 nm) were recorded using a Multiskan GO spectrophotometer (Thermo Fisher Scientific). Difference spectra were obtained by substraction of the spectra from heme and peptide only from the spectra from the heme-peptide

complexes. Dissociation constants (KD) were determined by usage of the earlier established equation of Pîrnău and Bogdan in GraphPad Prism 8.0[20].

Molecular docking of heme to the amino acid ABC transporter. For HBMs **1**, **3**, and **5**, molecular docking studies were conducted in YASARA (version 21.8.27[21]), as described earlier[19]. In brief, for each motif, a cubic simulation cell of 10 Å x 10 Å x 10 Å was built around the predicted coordinating residue in the by C-I-Tasser produced homology model (Zheng et al., 2021). Focused docking was performed by using the heme ligand as downloaded from the ChemSpider database (ID: 16739951[22]) and applying the Autodock Vina algorithm as implemented in YASARA[21,23]. Force Field calculations were done according to AMBER14 force field[24].

Primary metabolism analysis of pneumococcal cultures containing oxidized hemoglobin. THY or THY containing 10 µM hemoglobin (Hb-Fe^{3+}), was infected with either TIGR4 or TIGR4Δ*sxB*Δ*lctO,* in a 6-well microplate, and the cultures were incubated for 2 or 4 h at 37°C in a 5% CO_2 atmosphere. The culture supernatant was removed, filter sterilized with a 0.22 µm syringe filter and immediately frozen at -80°C. Aliquots of these frozen supernatants were analyzed by spectroscopy to investigate the oxidation of hemoglobin. Primary metabolism by gas chromatography-time of flight mass spectrometry (GC-TOF MS) was performed at the West Coast Metabolomics Center, UC Davis. Briefly, samples extracted using 1ml of 3:3:2 ACN:IPA:H_2O (v/v/v). Half of the sample was dried to completeness and then derivatized using 10 µl of 40 mg/ml of methoxyamine in pyridine. They were shaken at 30°C for 1.5 h. Then 91 µl of MSTFA + FAMEs to each sample and they were shaken at 37°C for 0.5 h to finish derivatization. Samples were then vialed, capped, and injected onto the instrument. We use a 7890A GC coupled with a LECO TOF. 0.5 µl of derivatized sample is injected using a splitless method onto a RESTEK RTX-5SIL MS column with an Intergra-Guard at 275°C with a helium flow of 1 ml/min. The GC oven is set to hold at 50°C for 1 min then ramp to 20°C/min to 330°C and then hold for 5 min. The transferline was set to 280°C while the EI ion source was set to 250°C. The Mass spec parameters collect data from 85m/z to 500m/z at an acquisition rate of 17 spectra/sec. Raw data were processed by LECO ChromaTOF version 4.5 for baseline subtraction, deconvolution and peak detection, while BinBase was used for annotation and reporting.[25]

Quantification of metals in lung tissue. Elemental images of lung sections were collected via laser ablation inductively coupled plasma time of flight mass spectroscopy (LA-ICP-TOF-MS) at the Biomedical National Elemental Imaging Resource (BNEIR) at Dartmouth College (NIGMS R24GM141194) in April 2023. Instrumentation consisted of an

imageBIO266 laser ablation unit (Elemental Scientific Lasers,) and a Vitesse ICP-TOF-MS detection system (Nu Instruments,).

Laser ablation used the imaging cup, a 10 µm spot size, 150 Hz repetition rate, with He gas flow through both imaging cup and sample chamber at 225 L/min, a scan speed of 1500 µm/sec and a fluence of 3 J/cm^2. The LA unit was connected to the Vitesse via a Dual Concentric Injection (DCI) connection unit, with a nebulizer argon flow of 1150 L/min, and the Vitesse was operated in H_2 gas mode. The mass range scanned was 22 to 260, omitting masses 27.5 to 40.5 to prevent over-saturation of the Vitesse detector. The LA-ICP-TOF-MS was tuned daily using the NIST 612 glass standard to optimize performance.

Quantification of detector counts into parts per million used analysis of a custom-made micro-spotted gel standard calibration series[26] consisting of 5 concentration levels, collected before and after analysis of each sample. Data reduction was conducted using the Iolite application package[27], which conducts background subtraction and quantification using the Howell method [28] as part of the 3D Trace Elements data reduction scheme.

References

1. Vidal, J.E., Ludewick, H.P., Kunkel, R.M., Zahner, D., and Klugman, K.P. (2011). The LuxS-dependent quorum-sensing system regulates early biofilm formation by Streptococcus pneumoniae strain D39. Infect Immun *79*, 4050-4060. 10.1128/IAI.05186-11.
2. Wu, X., Jacobs, N.T., Bozio, C., Palm, P., Lattar, S.M., Hanke, C.R., Watson, D.M., Sakai, F., Levin, B.R., Klugman, K.P., and Vidal, J.E. (2017). Competitive Dominance within Biofilm Consortia Regulates the Relative Distribution of Pneumococcal Nasopharyngeal Density. Appl Environ Microbiol *83*. 10.1128/AEM.00953-17.
3. Alibayov, B., Scasny, A., Khan, F., Creel, A., Smith, P., Vidal, A.G.J., Fitisemanu, F.M., Padilla-Benavides, T., Weiser, J.N., and Vidal, J.E. (2022). Oxidative Reactions Catalyzed by Hydrogen Peroxide Produced by Streptococcus pneumoniae and Other Streptococci Cause the Release and Degradation of Heme from Hemoglobin. Infect Immun *90*, e0047122. 10.1128/iai.00471-22.
4. Tai, S.S., Wang, T.R., and Lee, C.J. (1997). Characterization of hemin binding activity of Streptococcus pneumoniae. Infect Immun *65*, 1083-1087. 10.1128/IAI.65.3.1083-1087.1997.
5. Rowe, H.M., Karlsson, E., Echlin, H., Chang, T.C., Wang, L., van Opijnen, T., Pounds, S.B., Schultz-Cherry, S., and Rosch, J.W. (2019). Bacterial Factors Required for Transmission of Streptococcus pneumoniae in Mammalian Hosts. Cell Host Microbe *25*, 884-891 e886. 10.1016/j.chom.2019.04.012.
6. Clinical and Laboratory Standards Institute. (2016). Methods for antimicrobial dilution and disk susceptibility testing of infrequently isolated or fastidious bacteria, 3rd edition. Edition (Clinical and Laboratory Standards Institute).
7. Saito, M., Seki, M., Iida, K., Nakayama, H., and Yoshida, S. (2007). A novel agar medium to detect hydrogen peroxide-producing bacteria based on the prussian blue-forming reaction. Microbiol Immunol *51*, 889-892. 10.1111/j.1348-0421.2007.tb03971.x.
8. Maitra, D., Byun, J., Andreana, P.R., Abdulhamid, I., Diamond, M.P., Saed, G.M., Pennathur, S., and Abu-Soud, H.M. (2011). Reaction of hemoglobin with HOCl: mechanism of heme destruction and free iron release. Free Radic Biol Med *51*, 374-386. 10.1016/j.freeradbiomed.2011.04.011.
9. Gingles, N.A., Alexander, J.E., Kadioglu, A., Andrew, P.W., Kerr, A., Mitchell, T.J., Hopes, E., Denny, P., Brown, S., Jones, H.B., et al. (2001). Role of genetic resistance in invasive pneumococcal infection: identification and study of susceptibility and resistance in inbred mouse strains. Infect Immun *69*, 426-434. 10.1128/IAI.69.1.426-434.2001.
10. Wang, H., Hou, L., Kwak, D., Fassett, J., Xu, X., Chen, A., Chen, W., Blazar, B.R., Xu, Y., Hall, J.L., et al. (2016). Increasing Regulatory T Cells With Interleukin-2 and Interleukin-2 Antibody Complexes Attenuates Lung Inflammation and Heart Failure Progression. Hypertension *68*, 114-122. 10.1161/HYPERTENSIONAHA.116.07084.
11. Kjos, M., Aprianto, R., Fernandes, V.E., Andrew, P.W., van Strijp, J.A., Nijland, R., and Veening, J.W. (2015). Bright fluorescent Streptococcus pneumoniae for live-cell imaging of host-pathogen interactions. J Bacteriol *197*, 807-818. 10.1128/JB.02221-14.
12. Wong, S.M., Gawronski, J.D., Lapointe, D., and Akerley, B.J. (2011). High-throughput insertion tracking by deep sequencing for the analysis of bacterial pathogens. Methods Mol Biol *733*, 209-222. 10.1007/978-1-61779-089-8_15.
13. Gawronski, J.D., Wong, S.M., Giannoukos, G., Ward, D.V., and Akerley, B.J. (2009). Tracking insertion mutants within libraries by deep sequencing and a genome-wide screen for Haemophilus genes required in the lung. Proc Natl Acad Sci U S A *106*, 16422-16427. 10.1073/pnas.0906627106.
14. Li, H., and Durbin, R. (2009). Fast and accurate short read alignment with Burrows-Wheeler transform. Bioinformatics *25*, 1754-1760. 10.1093/bioinformatics/btp324.
15. DeJesus, M.A., Ambadipudi, C., Baker, R., Sassetti, C., and Ioerger, T.R. (2015). TRANSIT--A Software Tool for Himar1 TnSeq Analysis. PLoS Comput Biol *11*, e1004401. 10.1371/journal.pcbi.1004401.

16. Paul George, A.A., Lacerda, M., Syllwasschy, B.F., Hopp, M.T., Wissbrock, A., and Imhof, D. (2020). HeMoQuest: a webserver for qualitative prediction of transient heme binding to protein motifs. BMC Bioinformatics *21*, 124. 10.1186/s12859-020-3420-2.
17. Zheng, W., Zhang, C., Li, Y., Pearce, R., Bell, E.W., and Zhang, Y. (2021). Folding non-homologous proteins by coupling deep-learning contact maps with I-TASSER assembly simulations. Cell Rep Methods *1*. 10.1016/j.crmeth.2021.100014.
18. Kuhl, T., Sahoo, N., Nikolajski, M., Schlott, B., Heinemann, S.H., and Imhof, D. (2011). Determination of hemin-binding characteristics of proteins by a combinatorial peptide library approach. Chembiochem *12*, 2846-2855. 10.1002/cbic.201100556.
19. Hopp, M.T., Alhanafi, N., Paul George, A.A., Hamedani, N.S., Biswas, A., Oldenburg, J., Potzsch, B., and Imhof, D. (2021). Molecular Insights and Functional Consequences of the Interaction of Heme with Activated Protein C. Antioxid Redox Signal *34*, 32-48. 10.1089/ars.2019.7992.
20. Kuhl, T., Wissbrock, A., Goradia, N., Sahoo, N., Galler, K., Neugebauer, U., Popp, J., Heinemann, S.H., Ohlenschlager, O., and Imhof, D. (2013). Analysis of Fe(III) heme binding to cysteine-containing heme-regulatory motifs in proteins. ACS Chem Biol *8*, 1785-1793. 10.1021/cb400317x.
21. Krieger, E., and Vriend, G. (2014). YASARA View - molecular graphics for all devices - from smartphones to workstations. Bioinformatics *30*, 2981-2982. 10.1093/bioinformatics/btu426.
22. Pence, H.E., and Williams, A. (2010). ChemSpider: An Online Chemical Information Resource. J Chem Educ *87*, 1123-1124. 10.1021/ed100697w.
23. Krieger, E., and Vriend, G. (2015). New ways to boost molecular dynamics simulations. J Comput Chem *36*, 996-1007. 10.1002/jcc.23899.
24. Duan, Y., Wu, C., Chowdhury, S., Lee, M.C., Xiong, G., Zhang, W., Yang, R., Cieplak, P., Luo, R., Lee, T., et al. (2003). A point-charge force field for molecular mechanics simulations of proteins based on condensed-phase quantum mechanical calculations. J Comput Chem *24*, 1999-2012. 10.1002/jcc.10349.
25. Skogerson, K., Wohlgemuth, G., Barupal, D.K., and Fiehn, O. (2011). The volatile compound BinBase mass spectral database. BMC Bioinformatics *12*, 321. 10.1186/1471-2105-12-321.
26. Theiner, S., Egger, A., Keppler, B., Heffeter, P., Kornauth, C., Theiner, S., Heffeter, P., and Keppler, B. (2014). Bioimaging and quantification of metal-based anticancer drugs using LA-ICP-MS. Journal of Biological Inorganic Chemistry *19*, S681-S681.
27. Paton, C., Hellstrom, J., Paul, B., Woodhead, J., and Hergt, J. (2011). Iolite: Freeware for the visualisation and processing of mass spectrometric data. Journal of Analytical Atomic Spectrometry *26*, 2508-2518. 10.1039/c1ja10172b.
28. Howell, D., Griffin, W.L., Pearson, N.J., Powell, W., Wieland, P., and O'Reilly, S.Y. (2013). Trace element partitioning in mixed-habit diamonds. Chem Geol *355*, 134-143. 10.1016/j.chemgeo.2013.07.013.